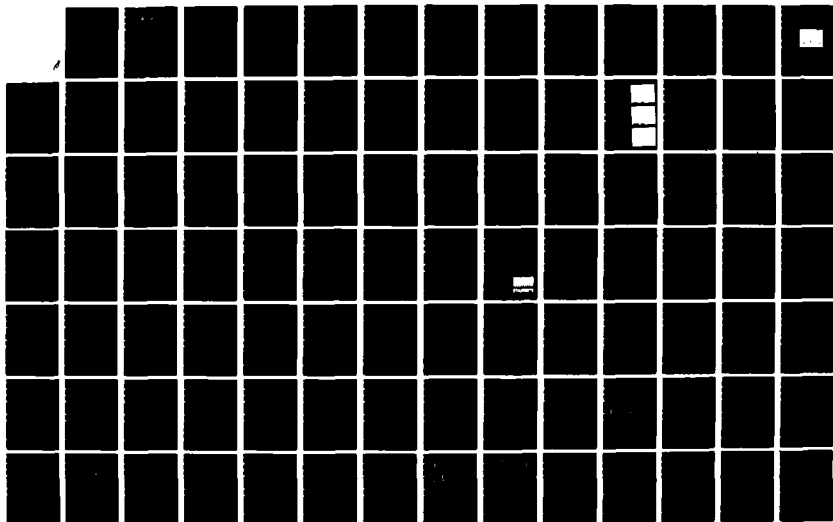AD-A187 417   OPTICALLY CONTROLLED DEVICES AND ULTRAFAST LASER   1/2
               SOURCES FOR SIGNAL PROCE (U) MARYLAND UNIV COLLEGE
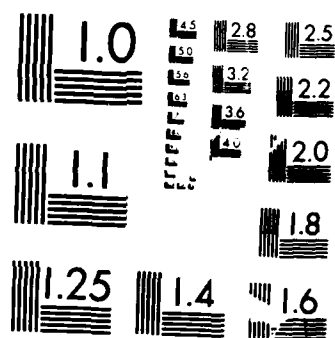   PARK DEPT OF ELECTRICAL ENGINEERING C H LEE ET AL
UNCLASSIFIED   30 JUN 87 AFOSR-TR-87-1583 AFOSR-84-0238   F/G 9/3   NL

MICROCOPY RESOLUTION TEST CHART
NATIONAL BUREAU OF STANDARDS 1963 A

$\mathcal{A}\mathcal{W}$ ②

AD-A187 417

UMENTATION PAGE

1a. REPORT SEC Unclass		1b. RESTRICTIVE MARKINGS			
2a. SECURITY Cl		3. DISTRIBUTION / AVAILABILITY OF REPORT			
2b. DECLASSIFICATION / DOWNGRADING SCHEDULE JUL 1 7 1987		Unlimited			
4. PERFORMING ORGANIZATION REPORT NUMBER(S)		5. MONITORING ORGANIZATION REPORT NUMBER(S) AFOSR. TR. 87 1583			
6a. NAME OF PERFORMING ORGANIZATION University of Maryland	6b. OFFICE SYMBOL (If applicable)	7a. NAME OF MONITORING ORGANIZATION AFOSR			
6c. ADDRESS (City, State, and ZIP Code) The University of Maryland College Park Campus Department of Electrical Engineering		7b. ADDRESS (City, State, and ZIP Code) Building 410 Bolling AFB, DC 20332-6448			
8a. NAME OF FUNDING / SPONSORING ORGANIZATION AFOSR	8b. OFFICE SYMBOL (If applicable) NP	9. PROCUREMENT INSTRUMENT IDENTIFICATION NUMBER AFOSR-84-0238			

8c. ADDRESS (City, State, and ZIP Code) Building 410 Bolling AFB, DC 20332-6448	10. SOURCE OF FUNDING NUMBERS			
	PROGRAM ELEMENT NO. 61102F	PROJECT NO. 2301	TASK NO. A1	WORK UNIT ACCESSION NO.

11. TITLE (Include Security Classification)

"OPTICALLY CONTROLLED DEVICES AND ULTRAFAST LASER SOURCES FOR SIGNAL PROCESSING" (U)

12. PERSONAL AUTHOR(S)
Dr. Chi H. Lee, Dr. P. -T. Ho

13a. TYPE OF REPORT FINAL	13b. TIME COVERED FROM 84/07/01 TO 87/06/30	14. DATE OF REPORT (Year, Month, Day)	15 PAGE COUNT 107

16. SUPPLEMENTARY NOTATION

17	COSATI CODES		18 SUBJECT TERMS (Continue on reverse if necessary and identify by block number)
FIELD	GROUP	SUB-GROUP	Modelocked, Saturable, Diode-arrays

19 ABSTRACT (Continue on reverse if necessary and identify by block number)

The progress to date is summarized as follows:
1. Experimental confimation has been made of the pulse formation mechanism in a laser modelocked by a slow saturable absorber as proposed by New and Haus.
2. We have shown analytically and experimentally that the degree of coherence is the same in a diode laser whether modelocked or singlemode at the same power.
3. The continuously operating phosphate Nd:glass laser has been modelocked for the first time ever to generate 7 ps pulses. We have also successfully amplified these pulses to μJ/pulse at 500 Hz rate.

20 DISTRIBUTION / AVAILABILITY OF ABSTRACT ☒ UNCLASSIFIED/UNLIMITED ☒ SAME AS RPT ☐ DTIC USERS	21 ABSTRACT SECURITY CLASSIFICATION UNCLASSIFIED	
22a NAME OF RESPONSIBLE INDIVIDUAL DR. HOWARD R. SCHLOSSBERG	22b. TELEPHONE (Include Area Code) 202/767-4906	22c OFFICE SYMBOL NP

DD FORM 1473, 84 MAR 83 APR edition may be used until exhausted. All other editions are obsolete.

SECURITY CLASSIFICATION OF THIS PAGE

UNCLASSIFIED

Final Technical Report

to

Air Force Office of Scientific Research

Project Title: OPTICALLY CONTROLLED DEVICES AND ULTRAFAST LASER
                 SOURCES FOR SIGNAL PROCESSING

Grant No.:   AFOSR-84-0238

University No.:   015-28137

Period: 1 July 1984 to 30 June 1987

Submitted by

Dr. Chi H. Lee
Co-Principal Investigator
(301) 454-6852

Dr. P.-T. Ho
Co-Principal Investigator
(301) 454-7441

Electrical Engineering Department
University of Maryland
College Park, MD 20742

DTIC
COPY
INSPECTED
6

Accesion For

NTIS CRA&I	☑
DTIC TAB	☐
Unannounced	☐
Justification	

By

Distribution /

Availability Codes

| Dist | Avail and / or Special |

A-1

87   ﾉ7 0

Summary of the Project

The research objectives are:

1. To develop and study modelocked lasers as sources for fast optical
   signal processing.

2. To assess all aspects of picosecond optoelectronic devices based on
   transient photoconductivity effect as signal processors.

Within these general and broad objectives, we have undertaken the following
areas of research tasks:

1. Measure the time evolution of the active media in a modelocked laser to
   understand the fundamental pulse generation mechanism.

2. Develop compact, high-power sources of short pulses using semiconductor
   laser diode arrays and neodymium:phosphate glass for signal processing.

3. Generate electric pulses which are in complete synchronization with the
   optical pulses both in pulsed and cw modes.

The progress to date is summarized as follows:

1. Experimental confirmation has been made of the pulse formation
   mechanism in a laser modelocked by a slow saturable absorber as pro-
   posed by New and Haus.

2. We have shown analytically and experimentally that the degree of
   coherence is the same in a diode laser whether modelocked or single-
   mode at the same power.

3. The continuously operating phosphate Nd:glass laser has been modelocked
   for the first time ever to generate 7 ps pulses. We have also success-
   fully amplified these pulses to 5 μJ/pulse at 500 Hz rate.

4. A new optoelectronic cw microwave source up to 20 GHz which can be completely phase-controlled by picosecond optical pulses has been demonstrated.

5. Two composite picosecond photoconductors, GaAs on SOS (silicon-on-sapphire) and InGaAs, have been developed in collaboration with MIT Lincoln Lab.

6. GaAs picosecond switches have been used as analog-to-digital converter with over 30 db dynamic range achieved.

7. Pulsed RF signals down to one cycle have been optically generated.

8. A diode laser array has been injection-locked with a single diode laser. Modelocking of the array by injection locking to generate high power picosecond pulses is expected shortly.

9. A diamond optoelectronic switch has been fabricated which can be activated by a simple, low-energy nitrogen laser.

Since most of the results have been published in scientific journals, we shall describe each project very briefly on the following pages. The list of publications for each project is included as part of the project description while the reprints and/or preprints of the published works are enclosed as appendices which should be regarded as an integral part of this final technical report.

2

Project Descriptions

1. The Coherence Property of a Modelocked Laser.

A coherence property of a modelocked laser was predicted and experimentally verified. A modelocked laser's coherence is not degraded despite its broad bandwidth; in fact, at the same average power, a laser has exactly the same degree of coherence whether operating single-mode or modelocked. This is an extension of the Schawlow-Townes formula to a multimode case. For the semiconductor laser used in the experiment, the electric fields of over 1,000 pulses were correlated.

Publications:

1. P.-T. Ho, "Amplitudes and Phase Fluctuations in a Modelocked Laser," IEEE J. Quan. Elec., QE-21, 1806 (1985) (Appendix 1).

2. D. W. Rush, G. L. Burdge and P.-T. Ho, "The Linewidth of a Modelocked Semiconductor Laser Caused by Spontaneous Emission: Experimental Comparison to Single-Mode Operation," IEEE J. Quan. Elec., QE-22, 2088 (1986) (Appendix 2).

3. D. W. Rush, P.-T. Ho, G. L. Burdge, "The Linewidth of a Modelocked Semiconductor Laser Caused by Spontaneous Emission: Experimental Comparison with Single Mode Operation," 10th IEEE International Semiconductor Laser Conference, Oct. 14-17, 1986, Kanazawa, Japan.

2. Pulse Formation Dynamics in a Dye Laser Modelocked by a Slow Saturable Absorber.

Experimental data have been obtained which support the pulse formation mechanism in a femtosecond pulse dye laser proposed by New and Haus. This is the first experimental study of the pulse formation in this laser and should facilitate the design of other short-pulse lasers on the same principle.

3

Publications:

1. Y. X. Wu, L. A. Vitoria, T. N. Ding, X. H. Shyy, and P.-T. Ho, "Experimental Verification of New's and Haus's Theories of Modelocking by a Slow Saturable Absorber," 1987 International Conference on Lasers, Nov. 15-19, 1987, Xiamen, P.R. China (Appendix 3).

2. Y. X. Wu, P.-T. Ho, "Pulse Formation Dynamics in a Dye Laser Modelocked by a Slow Saturable Absorber," in preparation.

3. Diamond Optoelectronic Switch.

An optoelectronic switch was fabricated of diamond, which could be efficiently activated by a simple nitrogen laser or an excimer laser. The switch, made of inexpensive type IIa industrial diamond, is specially well-suited for high voltage and high power applications [1]. Our switch measured 0.1 mm x 5 mm x 5 mm, with gold sputtered on 2 mm diameter spots on the 2 larger surfaces for electrical contact. High voltage was applied via a transmission line, and an ultraviolet laser beam was focused on one side for switching (Fig. 1). Fig. 2 shows some typical data. Note that in Fig. 2a, the lowest resistivity achieved is 7×10^{-4} Ω cm, at least 10^{19} lower than the lower limit of the dark resistivity (10^{16} Ω cm); and in Fig. 2b, the theoretical switch-out fraction is 50 percent.

Further development in the switch is underway.

4. High-Power Diode Laser Arrays.

A high-power laser diode array system has been designed and constructed in a compact and rugged package of Selfoc lenses (Fig. 3). The resonator was made up of two Selfoc lenses (glass rods whose refractive index decreases radially from the axis). The end surfaces of the lenses were reflection-coated so that with the cleaved faces of the diode, the resonator had four reflective surfaces
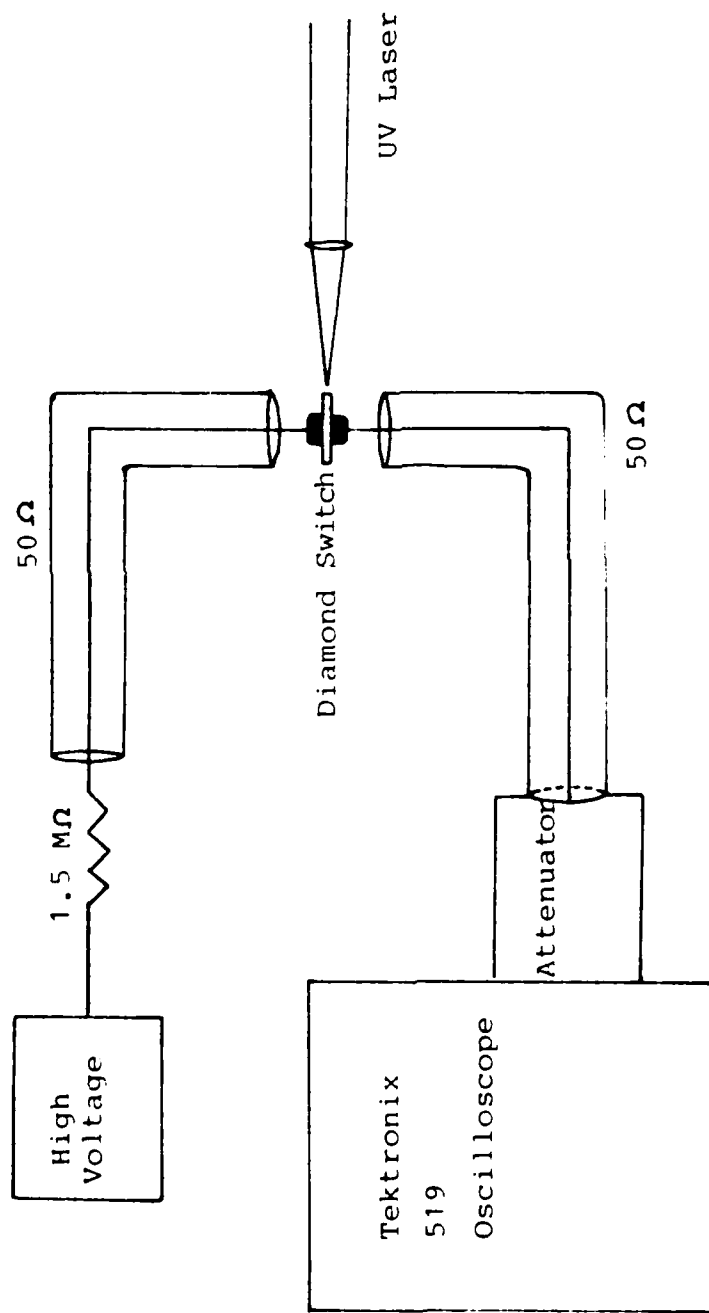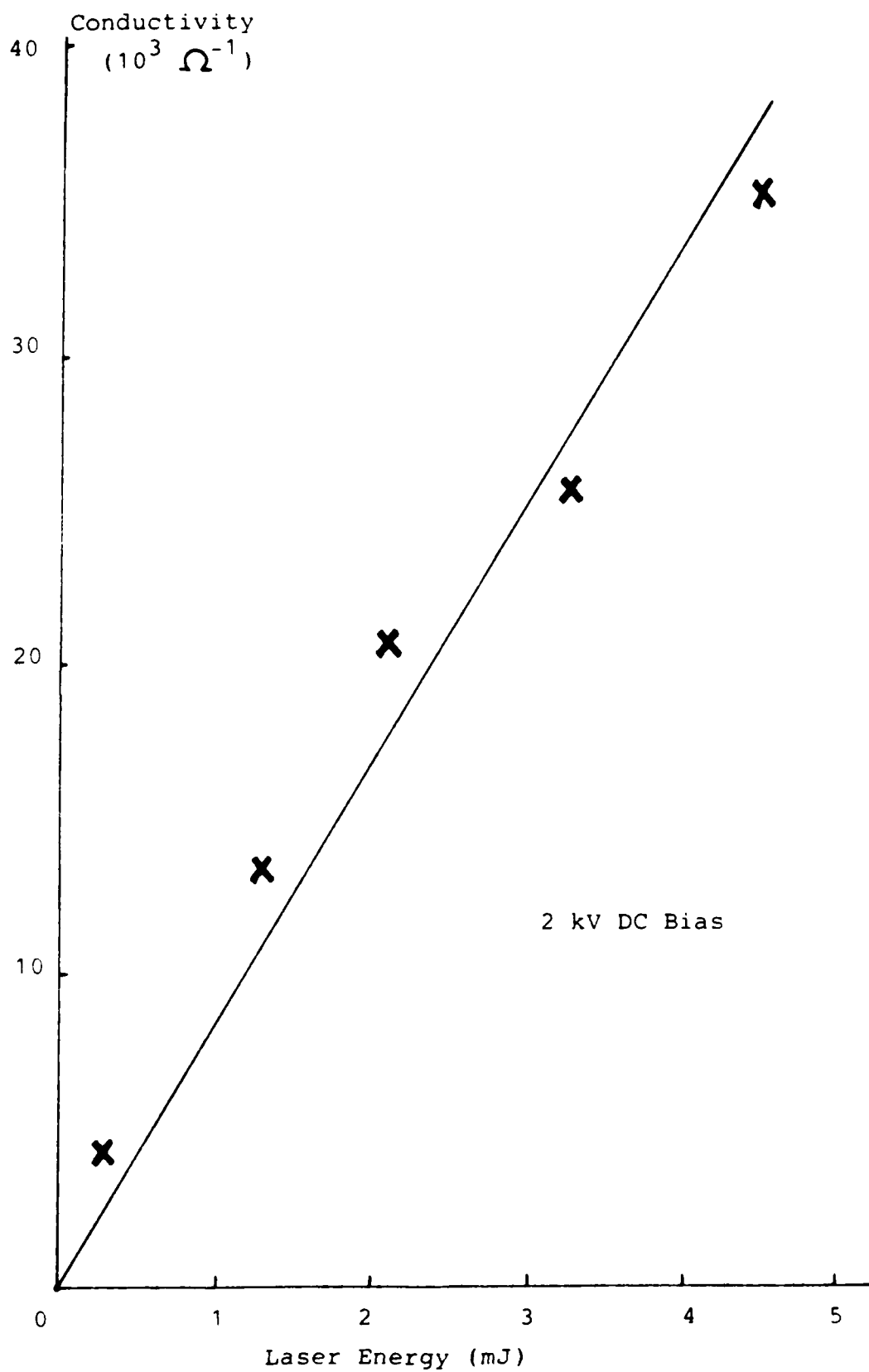
4

FIGURE 1   Diamond Opto-electronic Switch

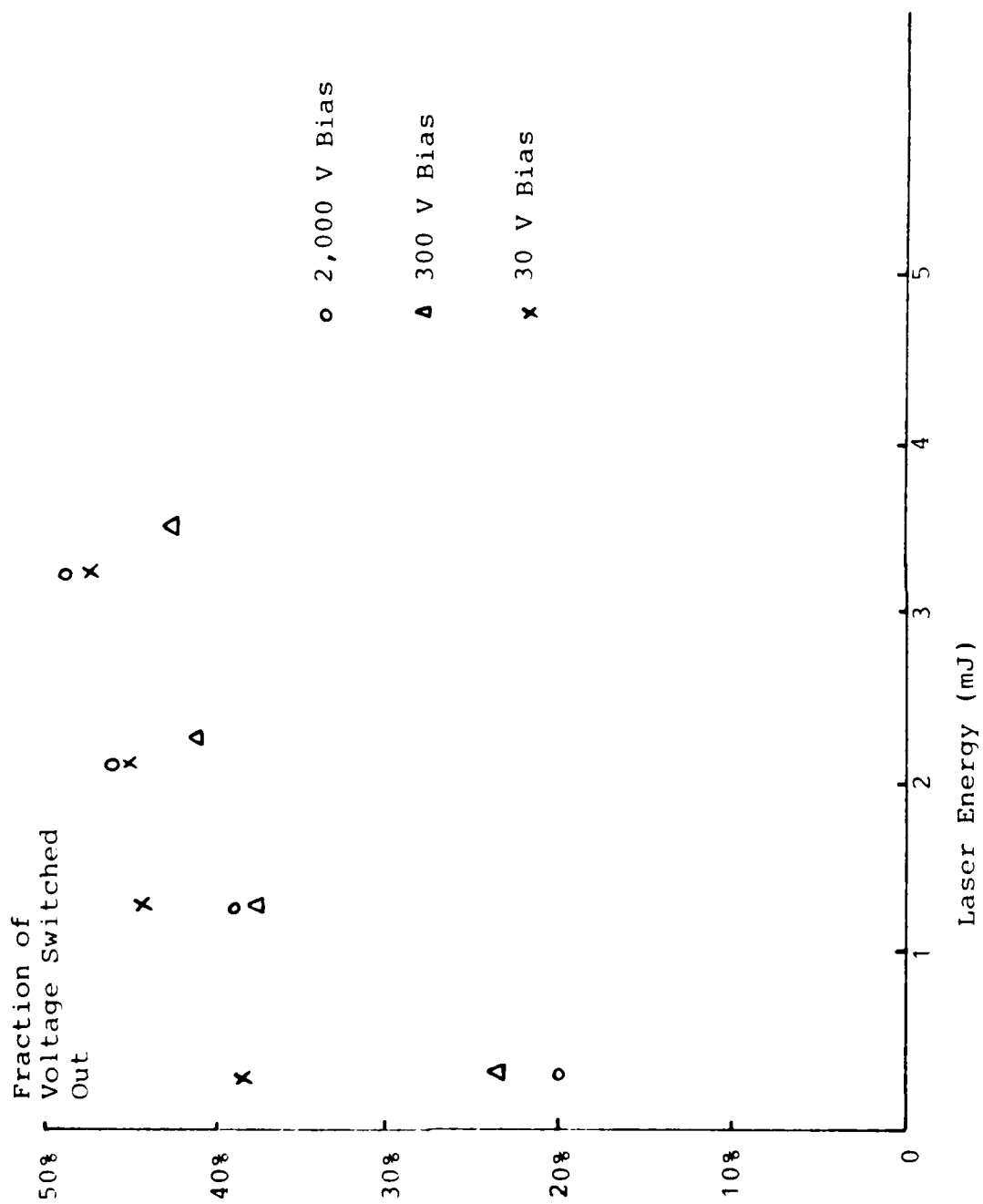FIGURE 2(a)   Diamond conductivity vs. Laser Power

Fraction of
Voltage Switched
Out

50%
40%
30%
20%
10%
0

o 2,000 V Bias

△ 300 V Bias

✗ 30 V Bias

Laser Energy (mJ)

FIGURE 2(b)   Fraction of Voltage Switched Out Vs. Laser Energy

diode array

AR coated

1/4 pitch

1/2 pitch
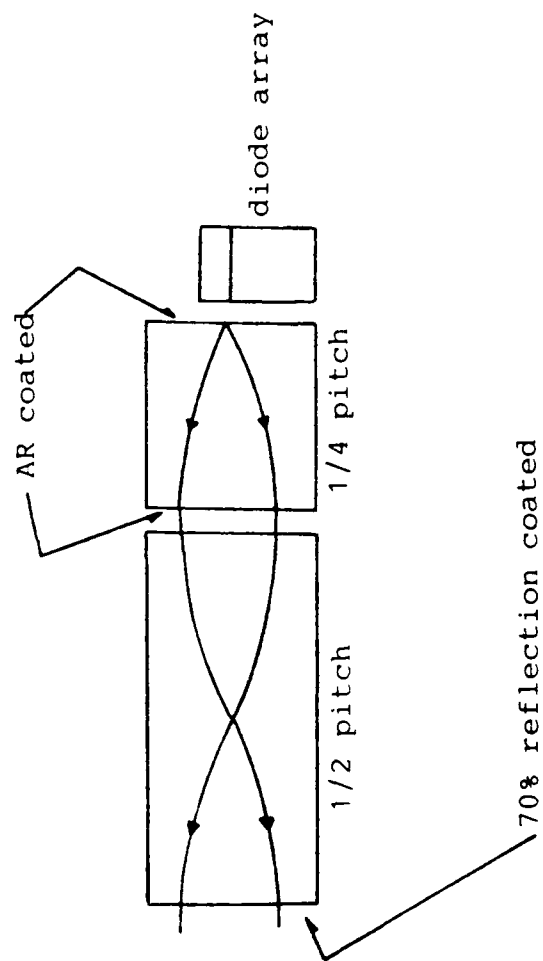
70% reflection coated

FIGURE 3   Single-Frequency Diode Array in
Selfoc Lens External Cavity

(Fig. 3). This kind of resonator is very frequency-selective and has very high Q. The output from the system was monitored with both a grating spectrometer and a Fabry-Perot to ensure single-frequency operation. The linewidth of the output was measured with a fiber interferometer [2]. The difference of optical paths in the fiber interferometer determines its resolution, which in our case was 70 kHz. Figure 4 shws a spectrum; the sidebands at 70 kHz are in accordance with theory when the linewidth is much smaller than the resolution of 70 kHz. More accurate measurements are underway.

In another experiment, a cw array was injection-locked by a cw single-diode laser. Modelocking of the injection-locked array is underway.

Publication:

J.-S. Wey and P.-T. Ho, "Narrow-linewidth, single-mode diode-array laser with a compact resonator," in preparation.

5. Theory of Modelocking in Extended Media.

Existing theories of modelocking are either numerical in nature or ignore propagating effects in the active media in an effort to obtain analytical results. The former tend to lose physical insight, and the latter are not realistic. We have developed a theory of passive modelocking with a saturable absorber, including propagation in the active media. The functional form of the pulses generated was found to be hyperbolic secant, and stability conditions, worse than in the limit of thin media, were also obtained in close forms.

Publication:

P.-T. Ho, "A theory of passive modelocking with extended media," in preparation.

6. High Repetition Rate Nd:phosphate Glass Oscillator and Regenerative Amplifier System.

The continuously operating phosphate Nd:glass laser has been modelocked

5

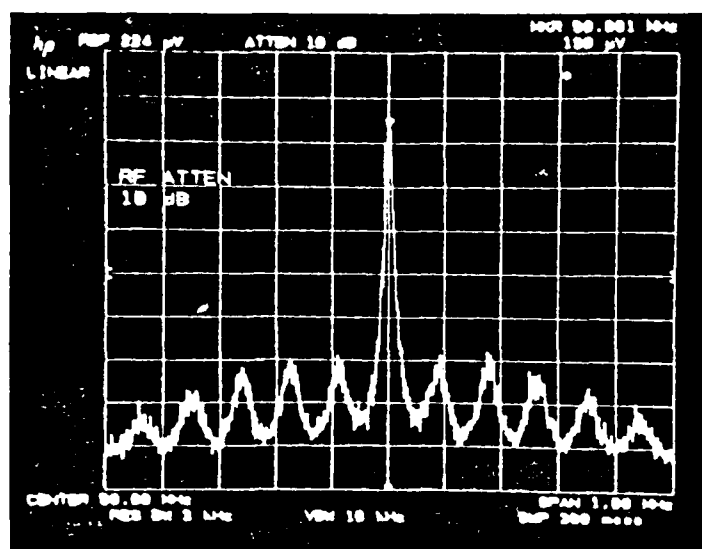FIGURE 4   Photocurrent spectrum of single
            frequency diode array. Sidebands
            are 70 KHz apart, the inverse
            of the fiber delay (see text)

for the first time ever; 7 ps pulses have been generated. The potential of this laser to generate subpicosecond pulses is obvious by using optical pulse compression technique.

We have succeeded in amplifying the pulse by using a regenerative amplifier. A regenerative amplifier of similar construction as the oscillator can provide ten microjoules of energy per pulse at kilohertz repetition rate. Furthermore, pulses can be compressed by an optical fiber and a grating pair down to the femtosecond region. Such a laser system should have many applications in science and technology.

We have demonstrated the first operation of a cw-pumped Nd:phosphate glass regenerative amplifier which amplifies the output from a cw modelocked Nd:phosphate glass laser [3]. Because of the broad spectral bandwidth, the Nd:phosphate glass regenerative amplifier is ideal for the generation of short laser pulses. Similar work with a Nd:YAG regenerative amplifier has been reported earlier [4,5]. In that work, the authors amplified 100 picosecond pulses. Although similar in design, the amplifier investigated in our laboratory has both broad spectral bandwidths and high repetition rates.

By injecting the 20 pJ, 20 picosecond pulses from a cw modelocked Nd:phosphate glass laser into a cw-pumped Nd:phosphate glass regenerative amplifier, we have amplified these pulses 4×10^5 times to 10 µJ at a 500 Hz repetition rate.

Figure 5 shows a schematic of the regenerative amplifier. A $2 \times 15 \times 20$ mm Nd:phosphate glass slab (Schott LG 760) provides the gain. To ensure performance at high repetition rates, the Nd:phosphate glass slab is pumped longitudinally by the cw output at 514 nm from an argon ion laser. We focus the pump beam to about 0.13 mm diameter in the slab. The regenerative amplifier cavity is constructed from two high-reflection coated plane parallel mirrors and an
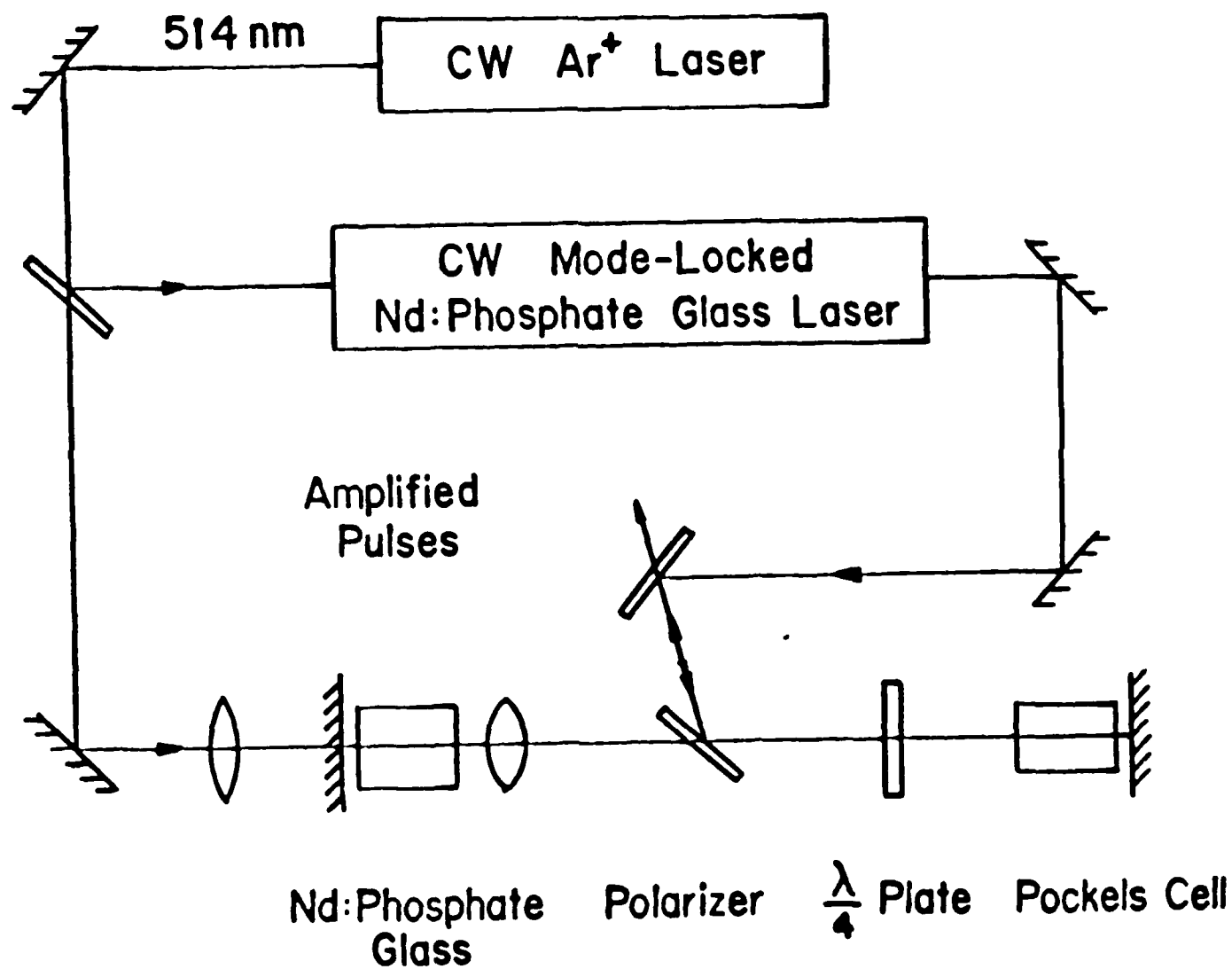
514 nm

CW Ar⁺ Laser

CW Mode-Locked
Nd:Phosphate Glass Laser

Amplified
Pulses

Nd:Phosphate   Polarizer $\frac{\lambda}{4}$ Plate   Pockels Cell
Glass

Fig. 5   Schematic of the regenerative amplifier for the
                CW mode-locked Nd:glass laser.

f = 85 mm focusing lens. The intracavity IR beam size in the gain medium matches the pump beam size to maximize pumping efficiency. Such a cavity design also gives a large stability range for flexibility in adjusting cavity parameters such as beam sizes and cavity length. A single intracavity Packels cell serves to trap the injected pulse and later dump it out of the regenerative amplifier. Phase locking of the regenerative amplifier and the injected mode-locked pulse is maintained by driving the Pockels cell at a frequency of 500 Hz downshifted from the 50 MHz frequency of the intracavity acousto-optic modulator of the cw modelocked Nd:phosphate glass laser.

The beam waist of the oscillator is imaged by a lens to match the larger amplifier waist. This maintains a high energy contrast ratio of the initial injected pulse to the spontaneous emission from the amplifier and minimizes the amplified spontaneous emission.

Measurements with a streak camera of the width of the amplified pulses yield 50 ps. Although the 500 Hz repetition rate is presently limited by the Pockels cell, the cw pump scheme should allow a 2 KHz repetition rate. The detailed description of the research findings can be found in the following publications.

Publications:

1. S. A. Strobel, P.-T. Ho, Chi H. Lee, and G. L. Burdge, "Continuous Wave Mode-Locked Neodymium Phosphate Glass Laser," Appl. Phys. Letts. 45, pp. 1171-11712, 1984. (Appendix 4).

2. L. Yan, J. D. Ling, P.-T. Ho, and Chi H. Lee, "Picosecond Pulse Generation from a CW Nd:Phosphate Glass Laser," Ultrafast Phenomena V, Eds.: G. R. Fleming and A. E. Siegman, Springer-Verlag, pp. 30-32, June 1986.

3. L. Yan, J. D. Ling, P.-T. Ho, and Chi H. Lee, "Picosecond-pulse generation from a continuous-wave neodymium:phosphate glass laser," Optics Lett. Vol. 11, pp. 502-503, Aug. 1986. (Appendix 5)

4. L. Yan, J. D. Ling, P.-T. Ho, Chi H. Lee, and G. L. Burdge, "High Repetition Rate Nd:Phosphate Glass Regenerative Amplifier," presented at CLEO '87, June 1987.

5. L. Yan, J. D. Ling, P.-T. Ho, Chi H. Lee, and G. L. Burdge, "An Actively Mode-Locked Continuous-Wave Nd:Phosphate Glass Laser Oscillator and Regenerative Amplifier," accepted for publication in a special issue of the IEEE J. of Quan. Elec. on Ultrafast Optics and Electronics. (Appendix 6)

7. A/D Converter and Parallel Processing Using GaAs Photoconductive Switches.

Figure 6 shows the basic arrangement of a multi-channel A/D array to carry out parallel processing. The key element is the track and hold sampling device based on the picosecond optoelectronic switch. The signal to be sampled (V_a) is distributed to M channels and time multiplexed sampling is performed by illuminating the individual photoconductive gap with time multiplexed picosecond light pulses. The output of each switch is proportional to $V_a(t)$, where t corresponds to the instant time of sampling. This signal is stored by the holding capacitor C_h and will be processed electronically by a slower quantizer. In order to use such a type of device for the multi-channel processor, the fundamental device parameters must be measured. The efficiency and the bandwidth of the switch are two of the most important parameters. The dynamic range of the switch must also be established by experimental measurements. We have performed such measurements.

The output signals from the switch were measured by both a sampling scope (Tektronix 7834 with 7S11 and S-4 sampling head) and an HP 8569B spectrum analyzer. Various GaAs switches have been characterized. Among these, we selected one non-ion-implanted GaAs 20 μm switch because it has the best figure of merit. It is found that the output voltage varies linearly with bias voltage

8

TIME-DELAYED
LASER PULSES

SWITCH C_H

QUANTIZER

VIDEO
AMPLIFIER

OUTPUT

$h\nu$

microstrip line

Output

C_H
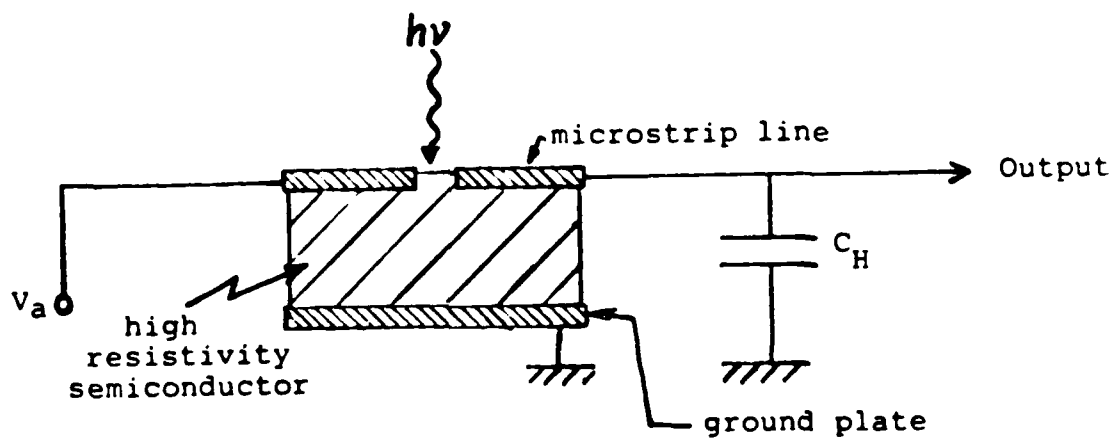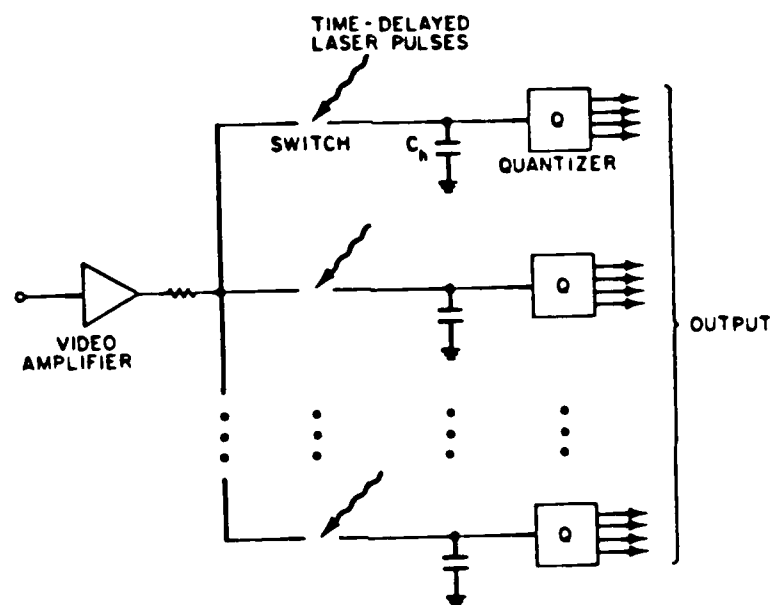
V_a

high
resistivity
semiconductor

ground plate

Fig. 6   Parallel arrangement of ADC array with
track and hold sampling devices.

over 3 orders of magnitude for a constant laser power (Fig. 7). For a given bias voltage, the output voltage saturates as a function of the laser intensity with $I_s = 1.8$ kw/cm^2.

The switch characteristics were tested at 0.58 µm from a Quantronix dye laser (Rodamine 6G) which was pumped by a frequency doubled Nd:YAG laser. The pulse width from the dye laser was 3 ps, as measured by an Inrad auto-correlator. Here, the switch out efficiency did not change significantly, but the switch response width showed a larger broadening as a function of the DC bias voltage for a given laser power.

To use this switch, we apply a 50 MHz synchronized AC signal with 180 mV amplitude on the switch as the test signal. When a 100 MHz green light irradiates on the switch, we observe one positive and one negative sampled signal. By adjusting the optical delay, we sampled the 50 MHz signal (10 cm of optical delay correspond to a change of 0.66 ns in sampling time) (Fig. 8). By using the HP 8569B spectrum analyzer, a laser power of less than a millivatt was needed to sample the signal. Because the Fourier component at 100 MHz is canceled from both positive and negative signals, the output Fourier component at 150 MHz was utilized for measurement.

This technique can be used to sample a waveform in the multigigahertz frequency range. The testing waveform has to be in complete time synchronization with the optical pulses. This has been accomplished in our laboratory. We are able to generate both a multigigahertz pulsed and cw signal by using only a single picosecond optoelectronic switch. To sample such a high frequency wave-form, a fast switch with a response time of 10 ps or less is needed. Currently, we are developing such a switch with high sensitivity under a joint contract with COMSAT awarded by MIT Lincoln Laboratory investigating a high performance photomixer at 10 GHz. These mixers are also based on photoconductive switch
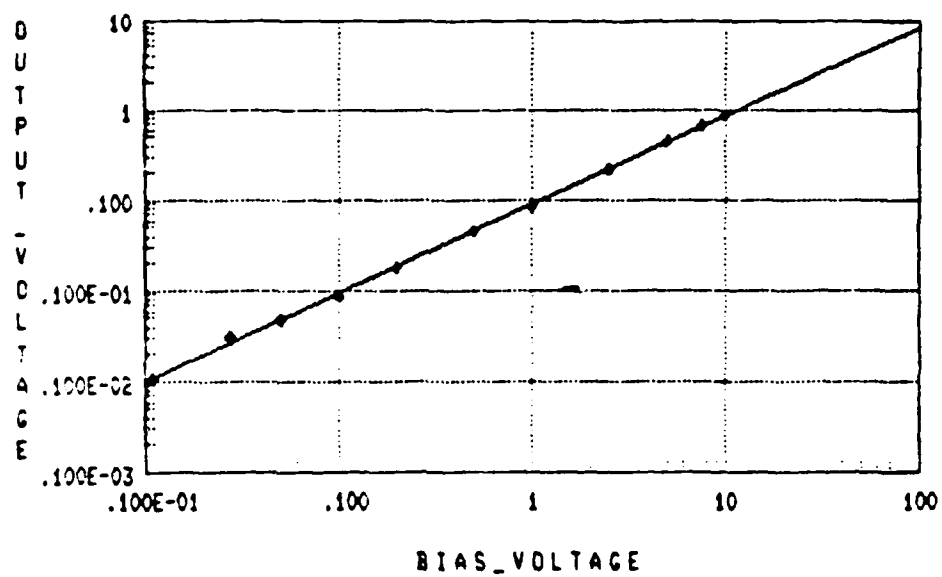
9

Fig. 7   Linear dependence of the output voltage
vs. bias voltage of an optoelectronic
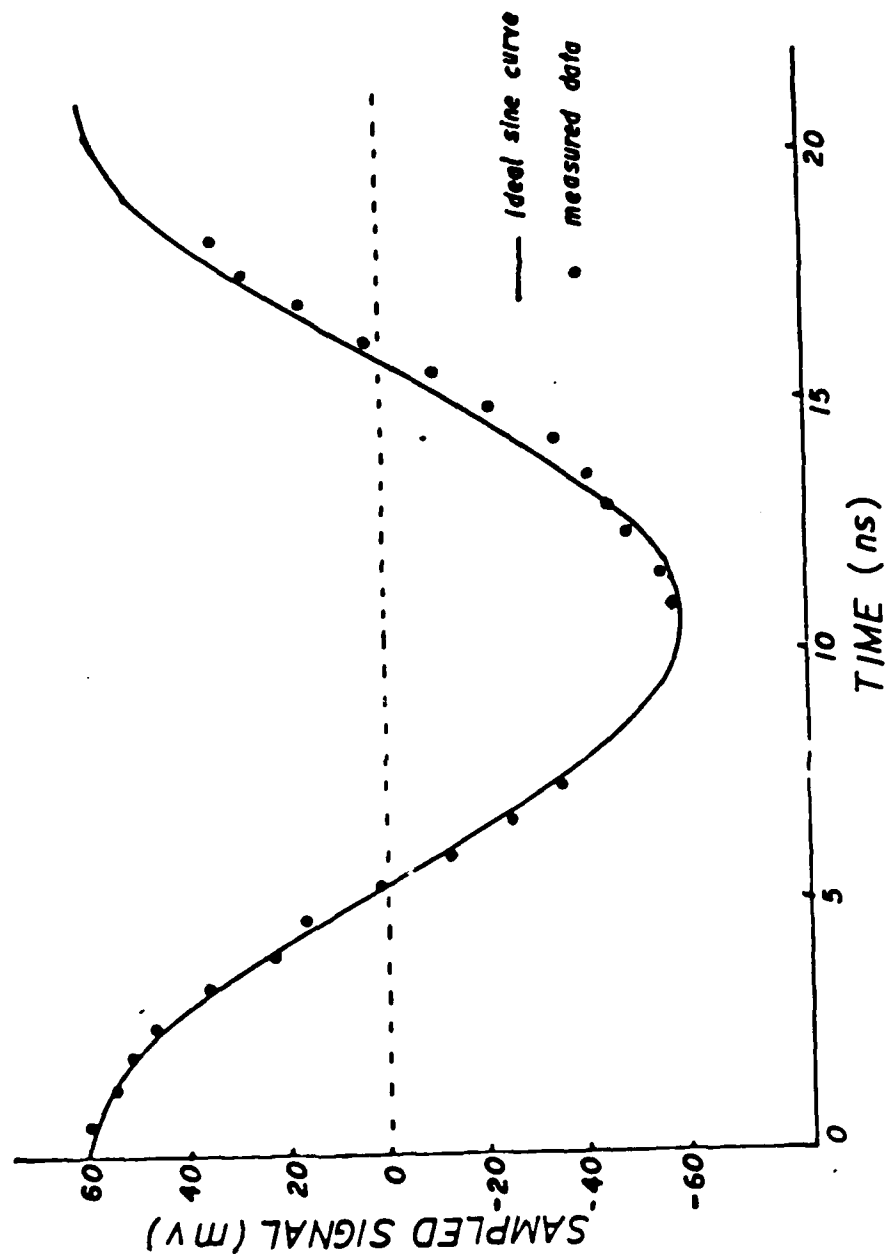ADC at constant laser intensity.

Fig. 8   Comparison plot between the applied (solid line) sine wave and the measured datas (dot) through the optical delay measurement. The laser power is 500 mW at wavelength of 0.53 mW.

technology. The technology developed under the Lincoln Laboratory contract can be applied directly to fabricate a multi-channel device for testing the idea of the time multiplexing signal processing scheme using ADC's.

In addition, a modelocked laser diode array can be used as the light source to perform the optically activated sampling since it has been found that the sampling can be carried out with less than one milliwatt of laser power.

8. A New Optoelectronic CW Microwave and Millimeter-Wave Source.

Ultrafast switching utilizing picosecond photoconductors finds many applications, including optoelectronic sampling and characterization of high speed electronic devices [6]. One of the major areas of application that has not been explored is in microwave and millimeter-wave generation and control. The jitter-free switching characteristic of these devices is very promising since the microwave or millimeter-wave signals can be generated in complete time synchronization with the exciting optical pulses. The time synchronization opens the way to unique applications. For example, it becomes possible to use optoelectronic techniques to modulate the cw microwave allowing it to carry information at a very high rate (up to 20 GHz). Another potentially powerful application is in phased array antennas, where the central issue is to provide the correct phase and amplitude at each element of the array in a manner which allows rapid scanning.

We were able to generate a low-noise 19.76 GHz signal at -19 dbm that was in phase synchronization with a 100 MHz laser. This signal was visible on a Tektronix sampling scope. We used light from a frequency-doubled 100 MHz YAG laser on a voltage-biased, 5 micron, silicon damaged, silicon-on-sapphire photoconductive switch to create a 100 MHz voltage pulse train. This voltage waveform acts as something of a comb generator with frequency components occurring at every harmonic of 100 MHz, starting at 100 MHz and extending beyond 40 GHz.

10

The highest power is in the lowest frequencies, and the power slowly tails off in the higher frequency ranges. At 19.76 GHz, this switch can produce a -36 dbm signal.

For the purposes of this experiment, the signal is only useful if it can be used to produce a relatively noise-free voltage sine wave. Therefore, the 40%-plus other harmonics must be eliminated. This was done in two ways. First, an elliptical bandpass filter centered around 19.76 GHz was placed after the photo-conductive switch. This yielded a minimum of 33 db attenuation for all the frequencies less than 22 GHz while only attenuating 19.76 GHz by 1.236 db. Of special value is its ability to suppress the two closest harmonics, 19.66 and 19.86 GHz, by 35 db. Between 22 and 40 GHz, this filter has two unwanted pass-bands centered around 22.84 and 31.24 GHz. The oscillogram of the spectral component of the 20 GHz signal is shown in Fig. 9.

COMSAT supplied a three-stage amplifier with a gain of 21 db at 19.76 GHz. It was also designed to attenuate 22.84 GHz by 12.6 db and 31.24 GHz by 30 db. This effectively eliminated all the remaining unwanted frequencies.

The detailed technical description can be found in Appendix 7.

Publications:

1. C. J. Clark, E. A. Chauchard, K. Webb, K. Zaki, Chi H. Lee, P. Polak-Dingels, H.-L. A. Huang, and Ho C. Huang, "Generation of CW Microwaves by an Optoelectronic Technique," the 11th International Conference on Infrared and Millimeter Waves, pp. 605-608, Pisa, Italy, Oct. 20-24, 1986.

2. C. J. Clark, E. A. Chauchard, K. Webb, K. Zaki, Chi H. Lee, P. Polak-Dingels, H. A. Hung, and Ho W. Huang, "A New Optoelectronic CW Microwave Source," the Topical Meeting on Picosecond Electronics and Opto-electronics, Tech. Digest, pp. 176-178, Jan. 1987.
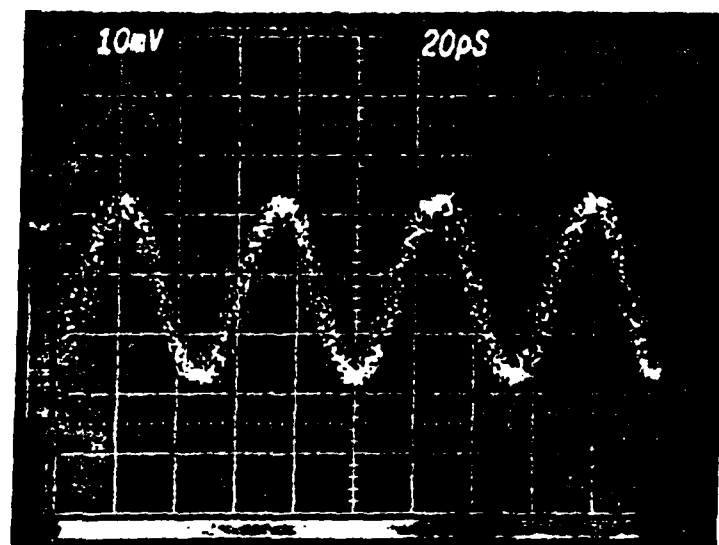
11

FIGURE 9   20 GHz Signal
The oscillograms in (a)
and (b) show the 20 GHz
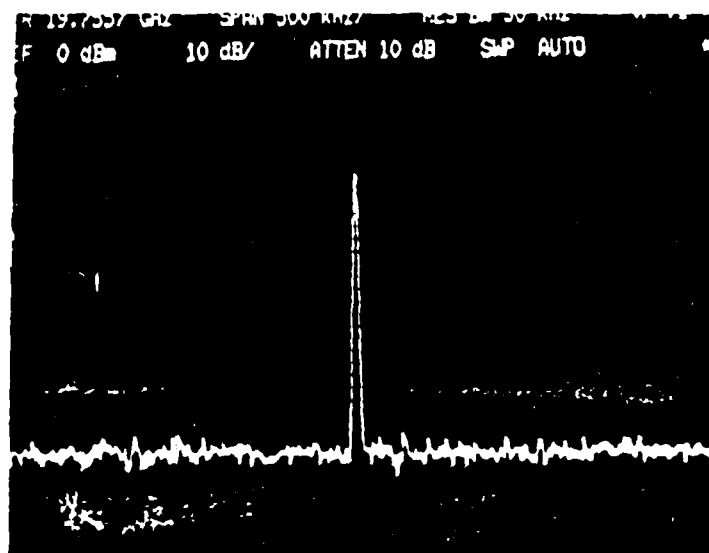waveform, and the spectral
component is displayed
in (c)

(a)

(b)

(c)

11a
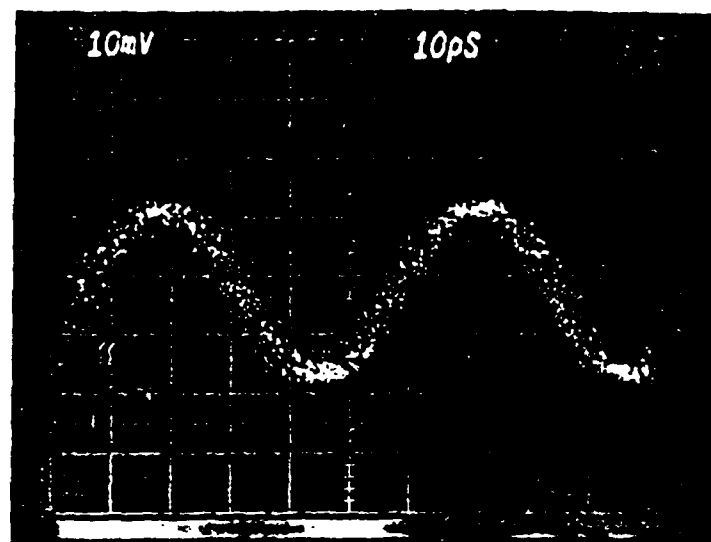
3. C. J. Clark, E. A. Chauchard, K. J. Webb, K. Zaki, Chi H. Lee,
    P. Polak-Dingels, H.-L. A. Hung, and H. C. Huang, "Investigation of a
    New Optoelectronic CW Microwave Source," IEEE/OSA J. of Lightwave
    Technology, Vol. LT-5, pp. 388-39?, March 1987. (Appendix 7)

9. Picosecond Optoelectronic Switches Using Composite Electronic Materials.

Since the discovery of picosecond photoconductivity, optoelectronic switches made from a variety of materials have been studied. A great number of applications have already been recognized and many new techniques depend on the availability of ultrafast (picosecond) devices. In collaboration with MIT Lincoln Laboratory, we have investigated the use of artificially structured electronic materials for picosecond optoelectronic switches. The two switches using composite electronic materials studied in this work are Fe-doped InGaAs grown in InP substrates and GaAs on a silicon-on-sapphire (SOS) substrate. The semi-insulating character of the Fe:InGaAs epilayer makes it very attractive for fabrication of integrated devices such as PIN photodetectors and FETs. This material also exhibits a very high mobility ($10000 \ cm^2$/Vs) and a photosensitivity extending up to 1.65 μm. The GaAs on SOS is of interest for the monolithic integration of GaAs and silicon devices where, for example, a GaAs FET could be integrated on a silicon wafer. This process takes advantage of the mature Si technology and the availability of low cost high quality silicon wafers. There is also an interest in using SOS as substrate because it provides better isolation and it is transparent. The silicon-sapphire interface exhibits a high density of defects, allowing faster devices to be fabricated. In our experiment, the sapphire substrate was used for mechanical strength. Whatever the material, the fabrication of a switch by deposition of metallic electrodes makes it possible to determine the switch characteristics and possible applications as well as to test the material's optical properties.

12

The study of device speed often reveals several phenomena which can appear as distinct time constants in the observed time waveform. The attribution of each of these different time constants to a particular cause is difficult and often inaccurate. One can classify the phenomena contributing to the speed of the device in two main categories: carier recombination times (bulk recombination, surface recombination, Auger recombination, etc.) and effects related to the applied electric field (carrier sweep-out). In addition, two other effects can contribute to the observed time waveform: contact fabrication plays a role because of the formation of a Schottky barrier at the metal-semiconductor interface, and optical intensity which can saturate the switch and lead to slower response times.

We present a study of the effect of applied electric field on the speed of the device. We point out the distintion between the true carrier recombination time, which is independent of the field, and the so-called "carrier sweep-out effect" due to the field-induced movement of the carriers. Measurement of the sweep-out time allows us to calculate the effective field in the material. Because of the carrier screening of the field, the effective field is much smaller than the field expected from the applied voltage. The detailed technical description is contained in Appendix 8.

Publications:

1. E. A. Chauchard, Chi H. Lee, V. Diadiuk, and G. W. Turner, "Picosecond Optoelectronic Switches Using Composite Electronic Materials," Digest and Proceedings of OSA Topical Meeting on Picosecond Electronics and Optoelectronics, Lake Tahoe, Jan. 1987.

2. E. A. Chauchard, Chi H. Lee, V. Diadiuk, and G. W. Turner, "Fe:InGaAs Picosecond Optoelectronic Switches," submitted to the J. of Applied Physics. (Appendix 8)

13

10. <u>Generation and Forming of Ultrashort High Voltage Pulses</u>.

High voltage pulse-forming utilizing spark gaps is a mature field.
However, problems associated with synchronizing spark gap switching in the pico-
second regime limit its application. A new approach, developed over the past
few years, is to use laser controlled photoconductive switches in generating
ultrashort high voltage pulses [7]. The use of photoconductive switches
achieves picosecond synchronization and very long lifetimes. Furthermore, such
switches can be readily incorporated into various types of pulse generating and
forming structures. We report here on an investigation of the performance of
various types of high voltage generating structures with photoconductive
switches. These include Blumleins (with multiple switches), Marx banks, stacked
lines, and L.C. generators in coaxial, microstrip, and coplanar geometries.
High voltage pulses with picosecond rise and fall times were generated and moni-
tored using Pockels cells monolithically integrated with the pulse-forming
structures. Using dc charged voltage multiplication circuits, up to 5 kv was
generated in nanosecond pulses. Also, 5 kv peak to peak RF single cycle pulses
were generated using a similar multiplication circuit. This type of RF pulses
has important applications in high resolution radar systems [8].

Representative data are shown in Fig. 10. The pulse generator consisted of
a 5 mm microstrip structure, with composite GaAs-glass dielectric with GaAs as
the switch whose effective round trip length is 100 picoseconds. The microstrip
is biased to 2 kv dc. The observation of the electrical pulse was made using a
miniature homemade longitudinal Pockels electro-optic modulator. The electro-
optic material used was $KD^{*}P$. An active-passive modelocked Nd:YAG laser was
used to general 200 μJ of 0.53 μm radiation with 35 picoseconds pulsewidth.
Each optical pulse was split into two pulses, one going through the Pockels cell
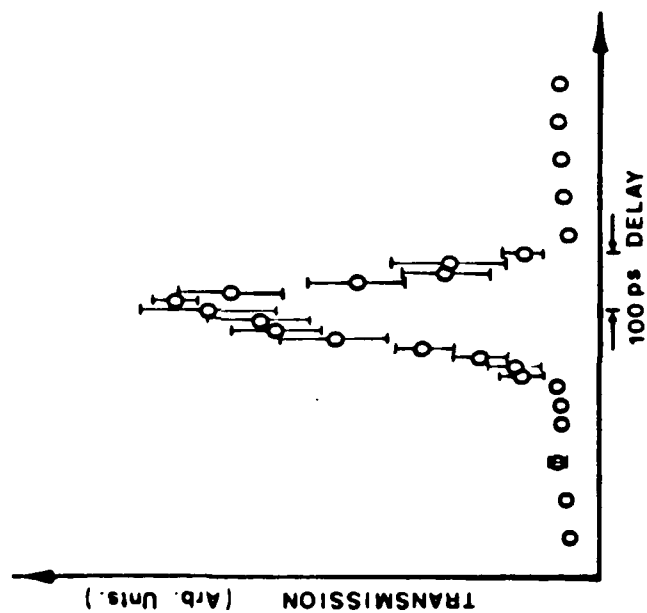so as to probe the electrical pulse, the other optical pulse was used to trigger

14

Fig. 10   Transmission of 35 ps 0.53 μm radiation through
KD*P, corresponding to a 1 kv pulse of 100 ps width.
Maximum of transmission is ~ 10%.

the GaAs photoconductive switch. By varying the optical delay between the probing and switching pulses, we have monitored the generated electrical pulses. In Fig. 10, we show the transmission of the 0.53 μm radiation through the Pockels cell as a function of delay between the probe and switch pulses. The maximum transmission is 10 percent, corresponding to ~1kv pulse. This is consistent with the bias on the microstrip. Note that the full width at half maximum is 100 picoseconds corresponding to the electrical pulse width.

A problem inherent in dc voltage holding switches is the necessity for gap separation to increase with the magnitude of the voltage held off. Photo-conductive switches are prone to the same problem. On the other hand, practical design considerations, e.g., maintaining a matched impedance throughout the switch area and minimizing stray inductance and capacitance effects, become more difficult as the gap length increases. Furthermore, the energy in the optical pulse required to trigger the photoconductive switch increases as the gap length squared. Hence, there are practical limitations on the charging voltage when dc biased. We are examining multistage schemes of HV generation, where a high voltage of relatively short pulsewidth, ~10 nanoseconds, is used to charge the pulse generating and forming structures. Since the bias voltage remains for a short time, overbiasing the photoconductive switches can be maintained without breakdown, thus avoiding the problems mentioned above. A single optical pulse, split into two, can be used to trigger the voltage pulse so as to charge the HV generating structure, which in turn is triggered by the optical pulse generating high voltage picosecond pulses. This technique will also allow us to examine breakdown phenomena, as the photoconductive switches are biased to higher voltages.

The voltage multiplication structures use the principle of parallel charging and series discharging of pulse-forming lines [9]. Marx banks require

15

a switch per stage, whereas only one switch may be used for the entire stacked line structure. We have constructed 3-stage coaxial stacked line structures capable of generating 5 nanosecond pulses with GaAs as the photoconductive switch. With 2.5 kv dc bias, pulses up to 5 kv were obtained. The efficiency is limited by the laser energy and the short carrier lifetime of the GaAs switch (~1 nanosecond). A modified version of this circuit generates single-cycle RF pulses with peak to peak voltage of 5 kv.

In summary, we have discussed the generation, shaping, and monitoring of high voltage picosecond pulses using pulse-forming techniques in conjunction with photoconductive switches integrated with electro-optical probes.

Publications:

1. H. A. Sayadian, S. T.Feng, J. Goldhar,and Chi H. Lee, "Generation and Forming of Ultrafast High Voltage Pulses," Digest of the Second Topical Meeting on Picosecond Electronics and Optoelectronics, pp. 57-59, Lake Tahoe, Jan. 1987.

2. H. A. Sayadian, M. G. Li, and Chi H. Lee, "Generation of Kilowatt/ Kilovolt Broadband Microwave Bursts with a Single Picosecond Photo-conductive Switch," IEEE MTT-S International Microwave Symposium Digest, pp. 649-652, June 1987. (Appendix 9)

3. Chi H. Lee, "Optical Generation and Control of Microwaves and Millimeter-Waves," invited paper at the IEEE MTT-S International Microwave Symposium Digest, pp. 811-814, June 1987.

16

References

1. P.-T. Ho, C. H. Lee, J. C. Stephenson, and R. R. Cavanagh, Opt. Comm. 46, 202 (1983).

2. T. Okoshi, K. Kikuchi, and A. Nakajima, Elec. Lett. 16, 630 (1980).

3. L. Yan, J. D. Ling, P.-T. Ho, and Chi H. Lee, "Picosecond pulse generation from a cw Nd:phosphate glass laser," Opt. Lett. 11, 502 (1986).

4. J. N. Duling III, T. Norris, T. Sizer II, P. Bado, and G. Mourou, J. Opt. Soc. Am. B2, 617 (1985).

5. P. Bado and M. Bouvier, Rev. Sci. Instrum 56, 1744 (1985).

6. Chi H. Lee, Editor, Picosecond Optoelectronic Devices, Academic Press, Orlando, 1984.

7. G. Mourou, W. H. Knox, and S. Williamson, Chapter 7 of Picosecond Optoelectronic Devices, edited by Chi H. Lee, Academic Press, 1984.

8. E. Brokner, Radar Technology, Artech House, 1977.

9. R. A. Fitch and V. T. S. Howell, Proc. IEE, Vol. III, 849 (1964).

APPENDICES

1. "Amplitude and Phase Fluctuations in a Modelocked Laser," P.-T. Ho, IEEE J. Quan. Elec. QE-21, 1806 (1985).

2. "The Linewidth of a Modelocked Semiconductor Laser Caused by Spontaneous Emission: Experimental Comparison to Single-Mode Operation," D. W. Rush, G. L. Burdge, and P.-T. Ho, IEEE J. Quan. Elec. QE-22, 2088 (1986).

3. "Experimental Verification of New's and Haus's Theories of Modelocking by a Slow Saturable Absorber," Y. X. Wu, L. A. Victoria, T. N. Ding, X. H. Shyy, and P.-T. Ho, 1987 International Conference on Lasers, Nov. 15-19, 1987, Xiamen, P.R. China.

4. "Continuous Wave Mode-Locked Neodymium Phosphate Glass Laser," S. A. Strobel, P.-T. Ho, Chi H. Lee, and G. L. Burdge, Appl. Phys. Lett. 45, 1171-72, Dec. 1984.

5. "Picosecond Pulse Generation from a Continuous-Wave Neodymium:Phosphate Glass Laser," L. Yan, J. D. Ling, P.-T. Ho, and Chi H. Lee, Optics Letters, Vol. 11, 502, Aug. 1986.

6. "An Actively Mode-Locked Continuous-Wave Nd:Phosphate Glass Laser Oscillator and Regenerative Amplifier," L. Yan, J. D. Ling, P.-T. Ho, Chi H. Lee, and G. L. Burdge, accepted for publication in a special issue on Ultrafast Optics and Electronics, IEEE J. of Quan. Elec.

7. "Investigation of a New Optoelectronic CW Microwave Source," C. J. Clark, E. A. Chauchard, K. J. Webb, K. A. Zaki, Chi H. Lee, P. Polak-Dingels, H.-L. A. Hung, and H. C. Huang, J. of Lightwave Tech. Vol. LT-5, pp. 388-397, Mar. 1987.

8. "Fe:InGaAs Picosecond Optoelectronic Switches," E. A. Chauchard, Chi H. Lee, V. Diadiuk, and G. W. Turner, submitted to J. of Appl. Physics.

9. "Generation of Kilowatt/Kilovolt Broadband Microwave Bursts with a Single Picosecond Photoconductive Switch," H. A. Sayadian, M. G. Li, and Chi H. Lee, IEEE MTT-S International Microwave Symposium Digest, pp. 649-652, June 1987.

Phase and Amplitude Fluctuations in a Mode-Locked Laser

P. T. HO

Abstract — Comparisons are made of the phase and amplitude fluctuations of a laser when it operates single mode and when it is mode locked with the same total average power. Despite the much lower signal-to-spontaneous emission noise ratio of the mode-locked laser, the linewidth of each of the locked modes is the same as that of the single mode. The fluctuation of the total intensity of the mode-locked laser, and the linewidth enhancement factor due to intensity fluctuation as recently analyzed by Henry, are the same in both cases.

I. INTRODUCTION

RECENTLY, interest in laser linewidths has been resurgent, especially in semiconductor lasers. One obvious reason is the application of semiconductor lasers in communication. Another reason is the relative ease of observing the linewidth due to spontaneous emission, which affords an opportunity to study a fundamental process in a laser. Most work to date, however, has been on either single mode or multimode free-running lasers [1]–[10]. One exception is [11], in which the first- and second-order correlations of a picosecond pulse train were measured. This work deals with the linewidth of each of the modes of a mode-locked laser. When a laser changes its operation from single mode to N modes locked in phase, the total spontaneous emission noise is increased N times, and the power per mode is decreased N times. One result of this study is that, despite the N-fold decrease in signal-to-noise ratio in each mode, the linewidth in each mode remains the same as in single mode operation. As the finite linewidth of a mode determines the coherence length over which the electric field of the mode-locked pulses interfere (Section III-C), this result can be reworded: a laser has the same coherence length operating single mode as mode locked at the same total average power. Preliminary experimental data confirmed this prediction [12]. Chirping effects due to carrier density changes can be neglected due to the effects of external cavities and small modulation depth in the diode laser mode locking considered in this paper. Whether two pulses interfere is important in coherent applications using the high peak power of a mode-locked laser, for example, coherent detection, signal processing. As phase and amplitude fluctuations in a single mode laser are well understood, we shall refer to them for comparisons.

We are mainly interested in the semiconductor laser, but the treatment is general enough to apply to other lasers. For much of the paper, we shall assume homogeneous broadening and active mode locking. Inhomogeneous broadening and mode locking by saturable absorbers will be discussed in Section IV.

The plan of this paper is as follows: the main results are summarized in Section II. The actual derivations are in Section III, which may be skipped to Section IV for physical explanations and discussions.

II. RESULTS

In a mode-locked laser, we have found the following.

1) Random fluctuations such as spontaneous emission or cavity length jitter are ineffective in causing changes in the relative phases among the modes; fluctuations in the relative phases are damped. This is to be compared to the phase of a single mode oscillator which undergoes undamped diffusion [15], [16].

2) The phases of the locked modes, however, can diffuse as a collective unit without any damping, as in the single mode case. In other words, despite deleterious perturbations which try to break up the locking of modes, any deviation from the locked phases is quickly damped, perturbations only succeed in causing the modes to fluctuate together as a unit. This collective fluctuation causes the same finite linewidth in each of the modes, irrespective of the power in that mode. If the perturbation is spontaneous emission, then the familiar Schawlow-Townes formula for the linewidth of a mode [13] is modified to take an inverse dependence on the *total* power of all the modes instead of just the power in the mode under consideration. Furthermore, the linewidth enhancement factor due to power fluctuation as recently analyzed [3], [4] for the single mode laser turns out to be exactly the same in each of the locked modes and is independent of the gain length. In the case of laser resonator length variations, all modes are affected in the same way, and the linewidth thus caused is independent of power.

3) As in the single mode laser, amplitude (power) fluctuations are damped. The fluctuation of the *total* power in the mode-locked laser is damped by exactly the same time constant as the single mode laser, with an inverse dependence on the total power of all modes. Fluctuations in individual mode amplitudes are also damped, in a way of no analog in the single mode laser.

The derivations of these results are given in the following section.

III. THE PERTURBED MODE-LOCKED OSCILLATOR

We shall follow the frequency domain approach of McDuff and Harris [17], adding random polarizations to account for

spontaneous emission. As is standard in oscillator linewidth calculations [15], [16], the noise-free amplitudes and phases are subjected to the added perturbations in linearized equations. The approach taken here is mathematically equivalent to the "supermode" analysis of Haken and Pauthier [17] and of Haus [18], [19], but we feel that in treating the more familiar individual cavity mode amplitudes and phases, the underlying mechanisms responsible for linewidth become clearer.

A. The Basic Equations

We start with the mode-locking equations derived by McDuff and Harris [14], applicable to our model laser which has a short loss modulator at one end of the cavity (Fig. 1). The modulator locks the cavity modes in phase by sideband generation, and its action is represented by a quadrature component of susceptibility:

$$\Delta\chi''(z,t) \quad \Delta\chi''(z)[1 - \cos \nu_M t]$$

where z is the distance along the cavity length and the modulation frequency ν_M is approximately equal to the roundtrip frequency $\Delta\Omega \quad c/2L$ of the empty cavity. The time origin is chosen so that the loss is minimum at $t \quad 0$. The cavity electric field is

$$E(z,t) \quad \sum_n E_n(t) \cos[\nu_n t + \phi_n(t)]U_n(z)$$

where

$$U_n(z) \quad \sin \frac{(n_o + n)\pi z}{L}$$

and

$$\nu_n \quad (n + n_o)\nu_M.$$

n_o denotes the center mode. The modulator mixes adjacent modes, and the amplitudes E_n and phases ϕ_n satisfy the following equations [14]:

$$\dot{E}_n + \frac{\nu}{2}\left[\frac{1}{Q} + \chi_n''\right]E_n \quad -\frac{2\alpha}{T_R}E_n$$
$$+ \frac{\alpha}{T_R}\{E_{n+1}\cos(\phi_{n+1} - \phi_n)$$
$$+ E_{n-1}\cos(\phi_n - \phi_{n-1})\}$$
$$- \frac{\nu}{2E_n}S_n(t) \tag{1}$$

$$\left[\dot{\phi}_n - (\Omega_n - \nu_n) + \frac{\nu}{2}\chi_n'\right]E_n \quad \frac{\alpha}{T_R}\{E_{n+1}\sin(\phi_{n+1} - \phi_n)$$
$$- E_{n-1}\sin(\phi_n - \phi_{n-1})\}$$
$$- \frac{\nu}{2E_n}C_n(t) \tag{2}$$

where
$\Omega_n \quad (n + n_o)c/2L$ empty cavity resonance frequency
$\nu \quad n_o\nu_M$ center frequency
χ_n' in-phase component of the laser gain susceptibility at ν_n
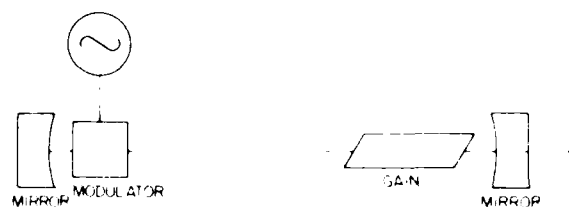

Fig. 1. Actively mode-locked laser

χ_n'' in-quadrature component of the laser gain susceptibility at ν_n
T_R empty cavity roundtrip time
$1/Q$ inverse empty cavity Q
$\alpha \quad (\nu/c)\int^L \Delta\chi''(Z)U_{n+1}(Z)U_n(Z)dZ$
coupling coefficient between two adjacent modes due to the modulator
$2\alpha \quad (\nu/c)\int^L \Delta\chi''(Z)U_n^2(Z)dZ$ average loss of the modulator

We have added random polarizations S_n and C_n to represent spontaneous emission. A physical interpretation of the above equations in the time domain can be found in [20]. The following noise sources will be considered here: 1) spontaneous emission; 2) cavity optical length variations due to amplitude fluctuations caused by spontaneous emission, as recently analyzed by Henry [3]; and 3) mechanical fluctuations in the cavity length.

If the number of modes is large, then the mode number n can be treated approximately as a continuous variable [17]. For a homogeneously broadened gain whose frequency width ω_l is broader than the bandwidth $\Delta\omega$ of the mode-locked pulse, χ_n'' can be approximated by [17]

$$\chi_n'' \quad \frac{\chi_o''}{1 + P/P_l}\left[1 - \left(\frac{\nu_n - \nu}{\omega_l}\right)^2\right]$$

where P_l is the saturation power of the gain, $\chi_o''(< 0)$ is the unsaturated χ'' of the center mode, and P is the average optical power. For simplicity, we have assumed that the gain has a long recovery time, and it responds only to the average power. If this restriction were relaxed, the resulting oscillation in the gain would generate noise sidebands [4]. The real part of the susceptibility χ' gives rise to a refractive index. We shall only consider its frequency dependence to the first order of frequency.

With these assumptions, the steady-state solution $(C = S = 0)$ of (1) and (2) has been found [17]:

$$\phi_n \quad 0 \tag{3a}$$

$$E_n \quad E_o e^{-n^2} \tag{3b}$$

$$\frac{2\alpha}{T_R}\frac{1}{N^2} \quad -\frac{\nu}{2}\frac{\chi_o''}{1 + P/P_l} \quad \frac{\nu}{2Q} \tag{3c}$$

$$\nu_n \quad \Omega_n - \frac{1}{2}\nu\chi_n' \tag{3d}$$

$$\frac{4\alpha}{T_R}\frac{1}{N^3} \quad \frac{\nu}{2}\frac{\chi_o''}{1 + P/P_l}\left(\frac{\nu_M}{\omega_l}\right) \tag{3e}$$

In (3c), the left-hand side is the additional loss due to the modulator, which in many circumstances is smaller than the

cavity loss $\nu = 2Q$, then

$$\frac{\nu}{2Q} = \frac{\nu}{2}\frac{\chi''}{1 + P/P_t}$$

and the number of modes locked is, from (3e),

$$N = \left[\frac{\nu}{2Q}\left(\frac{\nu_M}{\omega_t}\right)\frac{T_k}{4\alpha}\right]^{1/2} \tag{3g}$$

The average power P is given by

$$P = \sum_n E_n^2 \quad E_n^2 = \int dn\, e^{-2n^2\sigma^2} = \sqrt{\frac{\pi}{2}}\, NE_0^2 \tag{3h}$$

Now when noise is added to the system, the definite phase relationship among the modes, as well the amplitude of each mode, is perturbed. Following standard methods in calculating oscillator linewidths [15], [16], we assume that the noise sources are not strong enough to disrupt mode locking completely, and that the phase and amplitude of each mode only deviate slightly from the steady state, and we linearize (1) and (2) to obtain equations for the perturbed phases $\Delta\phi_n(t)$ and amplitudes $\Delta E_n(t)$.

$$\Delta\dot E_n = \left(\frac{\nu}{2}\Delta\chi''\right)E_n + \frac{\nu}{2}\left(\frac{1}{Q} + \chi''\right)\Delta E_n$$

$$\qquad \frac{2\alpha}{T_k}\Delta E_n + \frac{\alpha}{T_k}\{\Delta E_{n+1} + \Delta E_{n-1}\} + \frac{\nu}{2\epsilon_0}S_n(t) \tag{4}$$

$$\left|\Delta\dot\phi_n = \Delta\Omega_n + \frac{\nu}{2}\Delta\chi'\right|E_n + \frac{\alpha}{T_k}\{E_{n+1}(\Delta\phi_{n+1} - \Delta\phi_n)$$

$$\qquad\qquad - E_{n-1}(\Delta\phi_n - \Delta\phi_{n-1})\}$$

$$\qquad\qquad\qquad + \frac{\nu}{2\epsilon_0}C_n(t) \tag{5}$$

$\Delta\chi''$ and $\Delta\chi'$ are the changes in χ'' and χ' due to power fluctuation ΔP:

$$\Delta\chi'' = \frac{\partial\chi''}{\partial P}\Delta P = -\frac{\chi''}{(1 + P/P_t)}\frac{\Delta P}{P_t}\left[1 + \left(\frac{\nu_s}{\omega_t}\right)\right]$$

$$\qquad = -\frac{\chi''}{(1 + P/P_t)}\frac{\Delta P}{P_t} \tag{6a}$$

$$\Delta\chi' = \frac{\partial\chi'}{\partial P}\Delta P \tag{6b}$$

The frequency dependence of $\Delta\chi''$ in (6a) is ignored as it is a second-order effect. Mechanical vibrations cause a random change ΔL in the cavity length, and therefore a random change in the cavity resonance frequency $\Delta\Omega_n$:

$$\Delta\Omega_n = (n + m)\frac{c}{2(L + \Delta L)} - (n + m)\frac{c}{2L}$$

$$\qquad\qquad = (n + m)\frac{c}{2L}\frac{\Delta L}{L}$$

$$\qquad\qquad = \frac{n\,c\,\Delta L}{2L\cdot L}$$

$$\qquad\qquad = \nu\frac{\Delta L}{L} \tag{7}$$

Since spontaneous emission is equally likely to be in phase or in quadrature with the cavity field, $C_n(t)$ and $S_n(t)$ have the same average value but are uncorrelated with each other. Spontaneous emission noise is modulated by the modulator, and consequently, some correlation exists among the noise from different modes. But in most cases in practice, the modulation is weak, and therefore the modulated part of the noise is much smaller than the unmodulated, uncorrelated part. We therefore assume

$$\frac{\nu^2}{4\epsilon_0^2}\langle C_n(t)C_{n'}(t')\rangle = D\delta_{nn'}\delta(t - t') \tag{8a}$$

$$\frac{\nu^2}{4\epsilon_0^2}\langle S_n(t)S_{n'}(t')\rangle = D\delta_{nn'}\delta(t - t') \tag{8b}$$

$$\frac{\nu^2}{4\epsilon_0^2}\langle C_n(t)S_{n'}(t')\rangle = 0. \tag{8c}$$

D, the power per unit frequency, is approximately independent of n since the spontaneous emission width ω_t is much wider than the pulse bandwidth $\Delta\omega = N\nu_M$.

B. Solutions

The linearized equations (4) and (5) can be solved by treating, once again, n as a continuous variable and differences in $\Delta\phi_n$ and in ΔE_n by derivatives with respect to n. This requires justification since $\Delta\phi_n$ and ΔE_n, driven by random sources uncorrelated in n, may not be smooth functions of n. As will be shown immediately below, $\Delta\phi_n$ and ΔE_n are expanded in complete functions of n so that rapid changes can also be accounted for. Furthermore, components of $\Delta\phi_n$ and ΔE_n which change rapidly in n are small, being heavily damped. Even when $\Delta\phi_n$ and ΔE_n are smooth functions of n, they are still random functions in time. In particular, at two different times, $\Delta\phi_n$ may be completely different functions of n, which means a phase fluctuation among the modes. To convert the difference equations (4) and (5) into differential equations, we make the approximations

$$\Delta E_{n\pm1} = \Delta E_n \pm \frac{\partial}{\partial n}\Delta E_n + \frac{1}{2}\frac{\partial^2\Delta E_n}{\partial n^2}$$

$$\Delta\phi_{n\pm1} = \Delta\phi_n \pm \frac{\partial}{\partial n}\Delta\phi_n + \frac{1}{2}\frac{\partial^2}{\partial n^2}\Delta\phi_n$$

We also normalize n to the number of locked modes N to introduce a new variable ε:

$$\varepsilon = \frac{\sqrt{2}}{N}n \tag{9}$$

with which we replace the subscript n. Equations (4) and (5) then become

$$\frac{\partial}{\partial t}\Delta E(\varepsilon, t) = \left(\frac{\nu}{2}\frac{\partial\chi''}{\partial P}\right)\Delta P(t)E(\varepsilon)$$

$$\qquad + \frac{2\alpha}{T_k N}\left[\frac{\partial^2}{\partial\varepsilon^2} + 1 + \varepsilon\right]\Delta E + \frac{\nu}{2\epsilon_0}S(\varepsilon, t) \tag{10}$$

$$\frac{d}{dt}\Delta\phi(\xi,t) = \frac{2a}{I_s N}\left[\frac{d}{d\xi} - 2\xi\frac{d}{d\xi}\right]\Delta\phi + \Delta\Omega(\xi t)$$

$$+ \frac{v}{2}\frac{\partial\Delta\chi}{\partial P}\Delta P(t) + \frac{v}{2F}\frac{C(\xi,t)}{F(\xi)} \tag{11}$$

The operators within the square brackets suggest expansions in Hermite polynomials $H(\xi)$ and Hermite-Gaussians

$$\Delta F(\xi,t) = \sum B(t)H(\xi) \tag{12}$$

$$\Delta\phi(\xi,t) = \sum A(t)H(\xi) \tag{13}$$

The eigenequations for $H(\xi)$ and $H(\xi)$ are [21]

$$\left[\frac{d}{d\xi} + 1 - \xi\right]H(\xi) = 2pH(\xi) \tag{14}$$

$$\left[\frac{d}{d\xi} - 2\xi\frac{d}{d\xi}\right]H(\xi) = 2pH(\xi) \tag{15}$$

The operators on the left-hand side are the same as those in (10) and (11). The unperturbed fields are

$$F = F e^{\cdots} = F_0 e \qquad F = H(\xi) = F(\xi) \tag{16}$$

and the change in total power is

$$\Delta P(t) = 2\sum F_i \Delta F_i$$

$$= 2\sum\sum\int d\xi F H(\xi) \quad B(t)H(\xi)$$

$$= \sqrt{2\pi} N F_{\cdot} B(t) \tag{17}$$

where (12), (16), and the orthogonality condition [21]

$$\int d\xi H(\xi)H(\xi) = \delta \, 2^{p} p'\sqrt{\pi} \tag{18}$$

have been used. Substituting the expansions (12) and (13) into (10) and (11), using (18), $H(\xi) = 1$, we have

$$\frac{dB}{dt} = \frac{4pa}{I_s N}B + \left(\frac{v}{2}F\sqrt{2\pi}N\frac{\partial\chi}{\partial P}\right)\delta B$$

$$+ \frac{1}{2F}(t) \tag{19}$$

$$\frac{dA}{dt} = \frac{4pa}{I_s N}A \qquad \frac{\Delta F(t)}{F} \qquad \delta$$

$$+ \left(\frac{v}{2}F\sqrt{2\pi}N\frac{\partial\chi}{\partial P}\right)B(t) \tag{20}$$

with

$$\frac{1}{2^{p}p'\sqrt{\pi}}\int d\xi H(\xi) \quad N(\xi,t) \tag{21}$$

$$\frac{1}{2^{p}p'\sqrt{\pi}}\int d\xi H(\xi) \quad C(\xi,t) \tag{22}$$

The correlations of F and C are, from (8) and the definition of

$$\frac{1}{4\epsilon}(t)(t) = \sqrt{\frac{2}{\pi}}D\delta\quad \frac{1}{2p'\sqrt{\pi}}\delta \tag{23a}$$

$$(t)C(t) = 0 \tag{23b}$$

We first find the amplitude fluctuations $B(t)$ for $p = 0$,

$$\frac{dB}{dt} = \left[\frac{v}{2}F\sqrt{N}2\pi\frac{\partial\chi}{\partial P}\right]B \qquad \frac{1}{2F}(t)$$

which, with standard methods in stationary processes [22], can be solved to yield

$$B(t) = \frac{v}{2F}e \int e^{\cdots}(\cdots)dx$$

and

$$B(t)B(t') = e \qquad \int dx\int dx'(\cdots)$$

$$= \sqrt{\frac{2}{\pi}}\frac{D}{N}\frac{e}{2\Gamma} \tag{24}$$

where

$$\Gamma = \frac{v}{2}N\sqrt{N}2\pi\left(\frac{\partial\chi}{\partial P}\right)F \tag{25}$$

Similarly, for $p, q = 0$,

$$\frac{dB}{dt} + p\gamma B = \frac{v}{2F}(t)$$

$$B(t) = e \int e^{\cdots}(\cdots)dx$$

and

$$B(t)B(t') = \delta\frac{1}{2^{p}p'}\sqrt{\frac{2}{\pi}}\frac{D}{N}\frac{e}{2p\gamma} \tag{26}$$

with

$$\gamma = \frac{4a}{I_s N} \tag{27}$$

Thus, all amplitude fluctuations are damped, as in the case of a single-mode laser [16]. Since the *total* power fluctuation ΔP only depends on $B(t)$, the damping constant Γ determines the power fluctuation linewidth. We shall show below that Γ is exactly the damping constant for a single-mode laser of the same power. For phase fluctuations, we first look at $p = 0$ in (20)

$$\frac{dA}{dt} + p\gamma A = \frac{v}{2F}\frac{(t)}{F}$$

or

$$A(t)A(t') = \delta\frac{1}{p^{2}}\sqrt{\frac{2}{\pi}}\frac{D}{N}\frac{1}{F}\frac{e}{2p\gamma}$$

$$p,q \tag{28}$$

For $p \neq 0$,

$$\frac{dA_n}{dt} = v \frac{\Delta L(t)}{L} - \frac{v}{2\varepsilon} \frac{G_n(t)}{E_n}$$

$$- \left(\frac{v}{2} E_n \sqrt{2\pi} N \frac{\partial \chi'}{\partial P} \right) B_n(t)$$

The last term is the additional phase jitter caused by power fluctuation $B_n(t)$. It can be rewritten as

$$\left(\frac{v}{2} E_n \sqrt{2\pi} N \frac{\partial \chi'}{\partial P} \right) B_n(t) = - \Gamma_n \alpha \frac{B_n(t)}{E_n}$$

where Γ_n is defined in (25) and

$$\alpha = \frac{\partial \chi' / \partial P}{\partial \chi'' / \partial P} = \frac{\Delta \chi'}{\Delta \chi''}$$

is the enhancement factor defined by Henry [13]. It should be noted that this factor is independent of the length of the gain. The equation for A_n can be integrated to yield

$$A_n(t) - A_n(t')^2$$

$$= \frac{1}{E} \int dx \int dx \left[\frac{v}{4\varepsilon} G_n(t)(t - t') + \alpha \Gamma_n^2 \langle B_n(x) B_n(x') \rangle \right]$$

$$+ \frac{v}{L} \int dx \int dx \, \Delta L(t) \Delta L(t')$$

$$= (1 + \alpha^2) \sqrt{\frac{2}{\pi}} \frac{D}{N} \left[\frac{t}{E} + \frac{t'}{L} \right] b(t - t')$$

$$+ \sqrt{\frac{2}{\pi}} \frac{D}{N} [1 - e^{-t-t'}]$$

The parameter b is defined by

$$\Delta L(t) \Delta L(t') = b \delta(t - t')$$

and (24) has been used. The last term is exponentially damped and will be ignored [4]. Then

$$A_n(t) = A_n(t') = (1 + \alpha^2) \frac{D}{\sqrt{\pi}} \frac{t - t'}{2 N E_n} + \frac{v^2}{L} b(t - t') \tag{29}$$

The first term on the right hand side is the phase diffusion caused by spontaneous emission, including the enhancement factor α. It gives a linewidth exactly the same as a single mode laser with the same power $P = \sqrt{\pi} 2 N E_n$, as shown in Section III-D.

C. Spectra and Linewidths

The spectrum and linewidth of the laser output can now be calculated. The output field is proportional to

$$\varepsilon(t) = \sum_n (E_n + \Delta E_n) e^{...}$$

where we have reverted to the subscript n. The field correlation function is defined by [23]

$$\varepsilon^*(t) \varepsilon(t + \tau) = \langle \sum_n E_n E_{n+...} \rangle$$

where linear terms in ΔE_n average to zero, and the quadratic terms are too small and are therefore ignored. Since the phase $\Delta \phi_n$ changes very little in one cavity roundtrip $T_R = 2\pi/(\nu_n - \nu_{n-1})$, the field correlation becomes

$$\langle \varepsilon^*(t) \varepsilon(t + \tau) \rangle = \sum_n E_n^2 e^{-i\omega_n \tau} \langle e^{i(\Delta \phi_n + \Delta \phi_{n+...})} \rangle \tag{30}$$

For Gaussian processes [22],

$$\langle e^{i(\Delta \phi_n + \Delta \phi_{n+...})} \rangle = e^{-1/2 \langle (\Delta \phi_n + \Delta \phi_{n+...})^2 \rangle} \tag{31}$$

From (13), (28), and (29),

$$\langle (\Delta \phi_n(t) - \Delta \phi_n(t + \tau))^2 \rangle$$

$$= \sum_{pq} \left\{ H_p^2 \left(\frac{\sqrt{2} n}{N} \right) \langle A_p^2(t) \rangle + H_q^2 \left(\frac{\sqrt{2} n}{N} \right) \langle A_q^2(t + \tau) \rangle \right.$$

$$\left. - 2 H_p \left(\frac{\sqrt{2} n}{N} \right) H_q \left(\frac{\sqrt{2} n}{N} \right) \langle A_p(t) A_q(t + \tau) \rangle \right\}$$

$$= \langle (A_0(t) - A_0(t + \tau))^2 \rangle$$

$$+ \sum_{p=1} 2 \langle A_p^2 \rangle H_p^2 \left(\frac{\sqrt{2} n}{N} \right) [1 - e^{-\gamma \tau}].$$

The series in the last line is much smaller than unity:

$$\sum_{p=1} 2 \langle A_p^2 \rangle H_p^2 \left(\frac{\sqrt{2} n}{N} \right) [1 - e^{-\gamma \tau}]$$

$$< \sum_{p=1} 2 \langle A_p^2 \rangle H_p^2 \left(\frac{\sqrt{2} n}{N} \right)$$

$$= \sum_{p=1} 2 \sqrt{\frac{2}{\pi}} \frac{D}{N} \frac{1}{p^2 2^p} \frac{1}{2 p \gamma} \frac{1}{E_n} H_p^2 \left(\frac{\sqrt{2} n}{N} \right)$$

$$= \frac{1}{E_n} \sum_p \langle B_p^2(t) \rangle H_p^2 \left(\frac{\sqrt{2} n}{N} \right) = 2 \frac{\langle \Delta E_n^2 \rangle}{E_n^2} \ll 1.$$

Equations (26) and (28) have been used to relate the phase fluctuation A_p to amplitude fluctuations B_p.

Thus, from (31),

$$\langle e^{i(\Delta \phi_n + \Delta \phi_{n+...})} \rangle = e^{-1/2 \langle (A_0 + A_{0+...})^2 \rangle} \tag{32}$$

and, substituting into (30), we obtain

$$\langle \varepsilon^*(t) \varepsilon(t + \tau) \rangle = e^{-1/2 \langle (A_0 + A_{0+...})^2 \rangle}$$

$$\cdot \sum_n E_n^2 e^{-i\omega_n \tau} = e^{-1/2 \langle ... \rangle}$$

$$\sqrt{\frac{\pi}{2}} N E_n e^{-...} \sum_m$$

$$\cdot \exp \left[-\frac{v^2 N}{8} (\tau - m T_R)^2 \right]$$

Recalling that $\langle (A_0(t) - A_0(t + \tau))^2 \rangle$ is proportional to τ, (29), we define a correlation time τ_c such that

$$\langle (A_0(t) - A_0(t + \tau))^2 \rangle = 2 \frac{\tau}{\tau_c} \tag{33}$$

or

$$\frac{1}{\tau_c} = (1 + \alpha^2) \sqrt{\frac{8}{\pi}} \frac{D}{N} \frac{1}{E_n} + \frac{2 v^2}{L} b$$

Then

$$\gamma(\tau) = \frac{\langle E^*(t)E(t+\tau)\rangle}{\langle E^2\rangle} \quad \cdots \quad \sum_n \cdots$$

A plot of $\gamma(\tau)$ is shown in Fig. 2(a). It consists of spikes, each of width $2N/2 = N\tau_0$, which is just the mode-locked pulse width τ. The height of these spikes decreases exponentially with τ at a rate $1/\tau$. A spike occurs when two pulses overlap, therefore, τ determines the delay over which two pulses correlate. The power spectrum is given by the Fourier transform of $\gamma(\tau)$

$$P(\omega) = \int \gamma(\tau)e^{\cdots}d\tau$$

$$= \sqrt{\frac{2}{\pi}}\frac{1}{N}\int e^{\cdots}\cdots d\tau$$

$$= \frac{2}{\pi}\frac{1}{N}\sum_n e^{\cdots}\frac{2\tau}{(1+\tau^2)\cdots+(\omega-\nu_n)^2}$$

Thus, each mode n has the same linewidth $(1/\tau)$. A plot of $P(\omega)$ is shown in Fig. 2(b). It is obvious that the total bandwidth $N\omega_0$ determines the width of the spikes in $\gamma(\tau)$, but the correlation time as measured by the height of the spikes is determined by the width in a single mode $1/\tau$.

The intensity (power) fluctuation spectrum can also be calculated easily. The fluctuation in the total power is

$$\frac{\langle\Delta P(t)\Delta P(t+\tau)\rangle}{\langle\Delta P^2\rangle} = e^{\cdots}$$

from (17) and (24). The damping constant determines the spectral width of the intensity spectrum:

$$P_I(\omega) = \int d\tau e^{\cdots}\frac{\langle\Delta P(t)\Delta P(t+\tau)\rangle}{\langle\Delta P^2\rangle} = \frac{2\Gamma_0}{\Gamma_0^2+\omega^2}$$

This spectral width

$$\Gamma = \nu\frac{\partial\chi''}{\partial P}P \tag{34}$$

is proportional to power near threshold $(P \to P_t)$ as in the single mode case [16]

The amplitude fluctuation in one mode has a more complicated expression

$$\langle\Delta E_n(t)\Delta E_n(t+\tau)\rangle = e^{\cdots}\left\{\sqrt{\frac{2}{\pi}}\frac{D}{N}\frac{e^{\cdots}}{2\Gamma_0}\right.$$

$$\left. + \sum_n H\left(\frac{N-2n}{N}\right)\frac{1}{2^n p^1}\sqrt{\frac{2}{\pi}}\frac{D}{\pi}\frac{e^{\cdots}}{2p\gamma}\right\}$$

and has no analog in the single mode laser

D. Comparisons to the Single Mode Laser

It is interesting to compare the mode-locked laser to the single mode laser. In many respects, the locked modes behave collectively similar to the single mode. First, despite noise, which disrupts phase coherence among the modes, the phases of the modes fluctuate as a unit while maintaining the relative phase relationship among themselves. More pre-
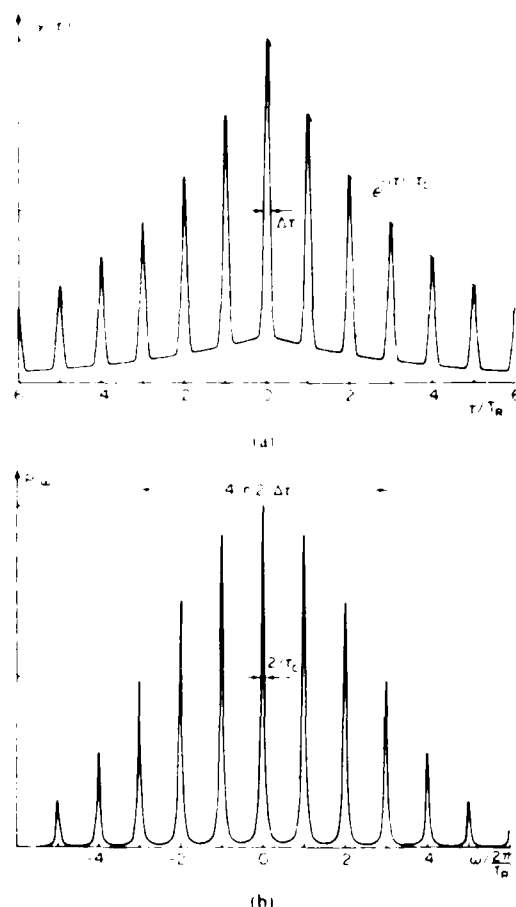

Fig. 2   (a) Magnitude of field correlation function (b) Power spectrum corresponding to (a)

cisely, in the presence of random noise,

$$\Delta\phi_n(t) = A_0(t) + \cdots .$$

The omitted terms contribute little to the linewidth; therefore, all modes approximately have the same random phase $A_0(t)$. Furthermore, the spectrum and linewidth in each mode are the same as those of the single mode oscillator operating at the same power. This is readily demonstrated using (1) and (2) with the modulator turned off $(\alpha_c = 0)$. Suppose the center mode oscillates with power $\mathcal{P} = E^2$:

$$\dot{E} + \frac{\nu}{2}\left[\frac{1}{Q} + \chi''\right]E = -\frac{\nu}{2\varepsilon_0}S_{n,0}(t)$$

$$\left[\dot{\phi} - (\Omega_0 - \nu_0) + \frac{\nu}{2}\chi'\right]E = -\frac{\nu}{2\varepsilon_0}C_{n,0}(t)$$

where the subscripts on E and ϕ are omitted to avoid confusion with the mode-locked case. The steady-state solutions and linearized equations are

$$\frac{1}{Q} = \frac{\chi_0''}{1 + E^2/P_t}, \qquad \dot{\phi} + \nu_0 = \Omega_0 - \frac{\nu}{2}\chi'$$

$$\delta\dot{E} + \frac{\nu}{2}E\frac{\partial\chi''}{\partial P}\delta P = \frac{\nu}{2\varepsilon_0}S_{n,0}(t)$$

$$\delta\dot{\phi} = \delta\Omega_0 + \frac{\nu}{2}\frac{\partial\chi'}{\partial P}\delta P = \frac{\nu}{2\varepsilon_0}\frac{C_{n,0}(t)}{E}$$

when δ denotes perturbed quantities and

$$\delta P = 2E \,\delta E .$$

The linearized equations are then solved in the same manner. In fact, if we identify P with $P = N \sqrt{\pi/2} E$ (that is, if the total average powers are the same in both cases), then the equations for δE and B, and those for $\delta\phi$ and A, are identical. The linewidth for the single mode laser is given by its phase jitter:

$$\langle \delta\phi(t) - \delta\phi(t')^2 \rangle = (1 + \alpha^2)\frac{D}{E^2}|t - t'| + \frac{v^2}{L^2}b|t - t'|$$

which is to be compared to (29). Again, α^2 is the linewidth enhancement factor. The amplitude damping constant is $v(\partial\chi''/\partial P)/P$, the same as Γ_a (25), (34).

IV. PHYSICAL EXPLANATIONS AND DISCUSSIONS

Very simple physical explanations can be given to the remarkable phase properties of the mode-locked laser. When the random phases are not the same for every mode [$p > 0$ terms in (13)], the modulator, through its action of sideband generation, "diffuses" these phases throughout the whole bandwidth (the "diffusion" is represented mathematically by the operator within the square brackets in (11); [24] gives good physical interpretations of the operator). Since these phases are random with one another, they cancel out when added together. An alternative explanation can be given in the time domain. Random phases will alter the pulse shape from its unperturbed Gaussian. In the part of the pulse where the intensity is decreased, for example, a net gain appears to amplify it, thus tending to restore the pulse to its original shape. Of course, when the random phases are identical in every mode [equal to $A_0(t)$], the pulse shape is not changed at all, and the gain will do nothing to the pulse and the common phase A_0 diffuses without being damped.

The linewidth of the mode-locked spectrum can also be explained simply in the time domain. In the single mode laser, the random phase angle due to in quadrature spontaneous emission is

$$\theta(t) = \frac{\delta E_s(t)}{E}$$

where δE_s is the spontaneous emission field and E is the steady-state field [Fig. 3(a)]. The linewidth is determined by

$$\frac{1}{2}\langle|\theta(t + \tau) - \theta(t)|^2\rangle = \frac{1}{E^2}[\langle\delta E_s^2\rangle - \langle\delta E_s(t + \tau)\delta E_s(t)\rangle].$$

Now, when the same power E^2 is distributed over N modes by mode locking, pulses appear and the pulse field has a peak value of $\sqrt{N}E$. Since there are N modes, the spontaneous emission noise from N modes contributes to the total noise, so that the average noise power is now N times higher than in the single mode case. If the noise field is ΔE_s, then the random phase angle is [Fig. 3(b)]

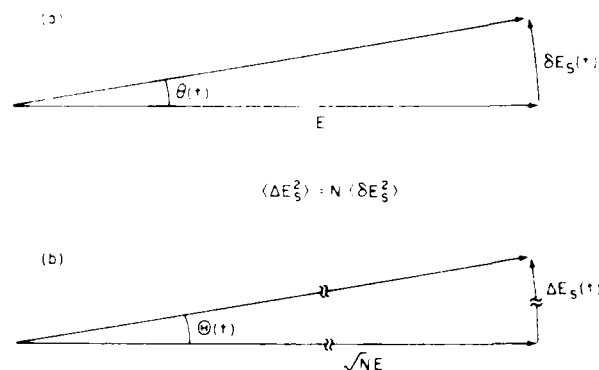$$\Theta(t) = \frac{\Delta E_s(t)}{\sqrt{N}E}$$

Fig. 3. Random phase angle of the electric field. (a) Single mode. (b) Mode locked.

so that

$$\frac{1}{2}\langle|\Theta(t + \tau) - \Theta(t)|^2\rangle = \frac{1}{NE^2}[\langle\Delta E_s^2\rangle$$
$$- \langle\Delta E_s(t + \tau)\Delta E_s(t)\rangle]$$
$$= \frac{1}{NE^2}\cdot N[\langle\delta E_s^2\rangle$$
$$- \langle\delta E_s(t + \tau)\delta E_s(t)\rangle]$$
$$= \frac{1}{2}\langle|\theta(t + \tau) - \theta(t)|^2\rangle,$$

the same as in the single mode case. Noise appearing between pulses is damped since the net gain is negative between pulses [18].

Our analysis is based on an actively mode-locked laser whose gain is homogeneously broadened. Relaxing these conditions will not change the results substantially. First, an inhomogeneously broadened laser, when properly mode locked, behaves similarly to a homogeneously mode-locked laser: the sidebands of one single mode quench the mode oscillations which, under free-running conditions, are independent of one another [14]. Using saturable absorbers for mode locking usually produces pulses whose width is at least as short as the response times (T_1) of absorbers and gain; otherwise, shorter pulses would be produced. Fluctuations in the phase relationship among the modes create rapid intensity fluctuations, to which the net gain window cannot respond fast enough; therefore, the fluctuations will be damped. There is, however, a situation where mode locking by absorber differs from active mode locking: jitters in pulse repetition rates are not damped [25].

Finally, in semiconductor lasers, the refractive index is a sensitive function of carrier density. In a mode-locked laser, the density may change periodically owing to either gain modulation or saturation by the circulating pulse inside the resonator, so the index of refraction may also change periodically ("chirp"). Additional broadening of the width of each mode due to this change is actually small because periodic index variation is just mode locking by frequency modulation: the chirping only broadens the total bandwidth [26] instead of the individual mode. In any case, when the active medium (semiconductor) occupies only a small fraction of the total

resonator length or when the gain modulation depth is small, or when the pulse repetition period is shorter than the gain response time, as assumed throughout this paper, frequency chirps can be ignored.

V. CONCLUSIONS

We have analyzed the mode-locked laser under noise perturbation and have found that instead of a different random phase for each mode, all the modes acquire the same random phase. This common random phase gives an identical finite width in each mode, irrespective of the power in each mode. When the noise source is spontaneous emission, this common width is the same as in a single mode laser operating at a power equal to the total average power of the mode-locked laser. Amplitude fluctuations are damped as in the single mode laser. Preliminary experimental data have already been obtained which verify our results [12].

Thus, the mode-locked laser has the advantages of high peak power, broad bandwidth, and long coherence length.

REFERENCES

[1] E. D. Hinkley and C. Freed, "Direct observation of the Lorentzian as quantum phase noise in a laser above threshold," *Phys. Rev. Lett.*, vol. 23, pp. 277–280, 1969.

[2] M. W. Fleming and A. Mooradian, "Fundamental line broadening of single mode (GaAl)As diode lasers," *Appl. Phys. Lett.*, vol. 38, pp. 511–513, 1981.

[3] C. H. Henry, "Theory of the linewidth of semiconductor lasers," *IEEE J. Quantum Electron.*, vol. QE-18, pp. 259–264, 1982.

[4] K. Vahala and A. Yariv, "Semiclassical theory of noise in semiconductor lasers, Part I and Part II," *IEEE J. Quantum Electron.*, vol. QE-19, pp. 1096–1109, 1983.

[5] A. R. Reisinger, C. D. David, Jr., K. L. Lawley, and A. Yariv, "Coherence of a room-temperature CW GaAs/GaAlAs injection laser," *IEEE J. Quantum Electron.*, vol. QE-15, pp. 1382–1387, 1979.

[6] K. Petermann and E. Weidel, "Semiconductor laser noise in an interferometer system," *IEEE J. Quantum Electron.*, vol. QE-17, pp. 1251–1256, 1981.

[7] A. Dandridge and A. B. Tveten, "Phase noise of single-mode diode lasers in interferometer systems," *Appl. Phys. Lett.*, vol. 39, pp. 530–532, 1981.

[8] T. Okoshi, K. Kikuchi, and A. Nakayama, "Novel method for high resolution measurement of laser output spectrum," *Electron. Lett.*, vol. 16, pp. 630–631, 1980.

[9] P. B. Gallion and G. Debarge, "Quantum phase noise and field correlation in single frequency semiconductor laser systems," *IEEE J. Quantum Electron.*, vol. QE-20, pp. 343–349, 1984.

[10] T. P. Lee, C. A. Burrus, K. Y. Liou, N. A. Olsson, R. A. Logan, and D. P. Wilt, "Measured spectral linewidth of single-frequency 1.3 and 1.5 μm injection lasers," *Electron. Lett.*, vol. 20, pp. 1011–1012, 1984.

[11] P. Andersson, T. Anderson, S. Lundquist, and S. T. Eng, "Temporal coherence properties of picosecond pulses generated by GaAlAs semiconductor lasers for directly modulated and frequency stabilized optical communication systems," *IEEE J. Quantum Electron.*, vol. QE-12, pp. 146–154, 1984.

[12] D. W. Rush, P. T. Ho, and G. L. Burdge, "The coherence time of a modelocked pulse train," *Opt. Commun.*, vol. 52, pp. 41–45, 1984.

[13] A. L. Schawlow and C. H. Townes, "Infrared and optical masers," *Phys. Rev.*, vol. 112, pp. 1940–1949, 1958.

[14] O. P. McDuff and S. E. Harris, "Nonlinear theory of the internally loss-modulated laser," *IEEE J. Quantum Electron.*, vol. QE-3, pp. 101–111, 1967.

[15] K. Kurokawa, *An Introduction to the Theory of Microwave Circuits*, ch. 9. New York: Academic, 1969.

[16] J. A. Mullen, "Background noise in nonlinear oscillators," *Proc. IRE*, vol. 48, pp. 1467–1473, 1960.

[17] H. Haken and M. Pauthier, "Nonlinear theory of multimode action in loss modulated lasers," *IEEE J. Quantum Electron.*, vol. QE-4, pp. 454–459, 1968.

[18] H. A. Haus, "A theory of forced modelocking," *IEEE J. Quantum Electron.*, vol. QE-11, pp. 323–330, 1975.

[19] H. A. Haus and P. T. Ho, "Effect of noise on active modelocking of a diode laser," *IEEE J. Quantum Electron.*, vol. QE-15, pp. 1258–1265, 1979.

[20] H. A. Haus, *Waves and Fields in Optoelectronics*, ch. 9. Englewood Cliffs, NJ: Prentice-Hall, 1984.

[21] I. S. Gradshteyn and I. M. Ryzhik, *Table of Integrals, Series, and Products*. New York: Academic, 1980.

[22] H. E. Rowe, *Signals and Noise in Communications Systems*. Princeton, NJ: Van Nostrand, 1965.

[23] M. Born and E. Wolf, *Principles of Optics*, ch. 10. New York: Pergamon, 1975.

[24] M. Sargent III, M. O. Scully, and W. E. Lamb, Jr., *Laser Physics*, ch. 16. Reading, MA: Addison-Wesley, 1974.

[25] H. A. Haus and H. L. Dyckman, "Timing of laser pulses produced by combined passive and active mode-locking," *Int. J. Electron.*, vol. 44, pp. 225–238, 1978.

[26] D. J. Kuizenga and A. E. Siegman, "FM and AM mode locking in the homogeneous laser—Part I: Theory," *IEEE J. Quantum Electron.*, vol. QE-6, pp. 694–708, 1970.

P.-T. Ho, photograph and biography not available at the time of publication.

Appendix 2

The Linewidth of a Mode-Locked Semiconductor Laser Caused by Spontaneous Emission: Experimental Comparison to Single-Mode Operation

D. W. RUSH, G. L. BURDGE, AND P.-T. HO

Abstract—We experimentally compare the linewidth of the individual modes of an extended cavity semiconductor laser when it operates mode locked and when it operates single mode. We find that the linewidths under these two operating conditions have the same inverse dependence on the average power. Therefore, the coherence length of the mode-locked source is the same as that of the single-mode source despite lower power per mode, much broader total bandwidth, and much higher spontaneous emission noise level in the mode-locked source. It can be inferred from our data that the electric fields of over 1000 consecutive mode-locked pulses are correlated.

INTRODUCTION

SEMICONDUCTOR lasers serve as sources in many communication and signal processing applications because they are compact, they can be directly modulated, and they are compatible with optical fibers. For specific applications which involve optical processing or communication at high data rates, the coherence properties of the source are important. In addition to system applications, the coherence properties of semiconductor lasers provide an opportunity to examine the fundamental mechanism of linewidth broadening caused by spontaneous emission. While there have been numerous studies of the coherence properties of semiconductor lasers operating CW [1]-[3] and with various modulation schemes [4]-[8], little attention has been given to the coherence properties of mode-locked semiconductor lasers [4], [9]-[11].

The power spectrum of a mode-locked laser consists of N equally spaced longitudinal modes which are locked in phase. The modes are only locked in phase relative to one another; they can still share a common random phase which determines the width of each mode. The mode spacing determines the repetition rate of the pulse train. The total bandwidth that is locked determines the pulse-width, whereas the width of the individual modes of the mode-locked power spectrum determines the coherence time of the pulse train [11], [12]. If $\Delta\nu$ is the FWHM linewidth of an individual mode of a mode-locked spectrum, then the coherence time

$$\tau_c = \frac{1}{\pi \Delta \nu} \tag{1}$$

is determined by the time when the envelope of the magnitude of the autocorrelation function falls to its $1/e$ value. As can be immediately verified, the number of consecutive pulses whose electric fields correlate is τ_c/T where T is the pulse period.

When a laser is mode locked, the average power P_{avg} is distributed among the N locked modes. The peak power in the mode-locked pulse train is $N \cdot P_{avg}$. We show in this work that the mode-locked semiconductor laser's coherence length is, in fact, the same as the coherence length when the laser is operating in a single mode with the same average power. This is unexpected since, according to the Schawlow–Townes formula [13], the linewidth of a mode in a laser caused by spontaneous emission is inversely proportional to the power P in that mode. Since the total average power is divided among N modes when mode locked, it might be expected as a consequence that the linewidth of each mode would be increased N times. This is not the case. When N modes are locked in phase to generate pulses, the peak power of the pulses is N times higher than the average power. The total spontaneous emission noise is also increased N times over that of single-mode operation since the total bandwidth is increased N times. Therefore, during the pulse, the ratio of signal to spontaneous emission noise is the same as in single-mode operation. In between pulses, the net gain of the laser is negative and the spontaneous emission is suppressed. Consequently, the random phase angle which all the modes share fluctuates the same average amount as in single-mode operation. This physical argument has been substantiated in a recent analysis [11].

In a previous experiment, we compared the fringe visibilities of a semiconductor laser operating mode locked and operating single mode [10]. However, absolute linewidths and inverse power dependence of the linewidth could not be determined. In this paper, we directly compare the linewidth of the individual modes of a mode-locked external cavity semiconductor laser to the linewidth of the same source when operating in a single mode. Our experimental results confirm the theoretical predictions of Ho [11]. The linewidths are measured using the self-delayed heterodyne technique [14].

EXPERIMENTAL DETAILS

The extended cavity semiconductor laser used for this work is constructed with a Hitachi GaAlAs HLP1400 laser diode, a 0.75 pitch self-focusing (Selfoc) lens, and a 0.5 pitch Selfoc lens [15]. The semiconductor laser has a re-
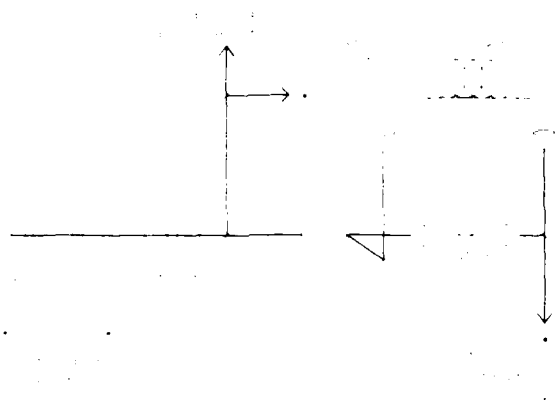
Fig. 1. Experimental arrangement. LD—laser diode. SL1—0.75 pitch Selfoc lens with AR coating on each facet. SL2—0.5 pitch Selfoc lens with AR coating on front facet and 70 percent reflecting coating on back facet. FR—Faraday rotator (optical isolator). ω_{AO}—acoustooptic modulator drive frequency. ω_{ML}—mode-locking frequency

flectivity of 33 percent at each facet. The 0.75 pitch Selfoc lens, which is anti-reflection (AR) coated on both facets, is butted up to the semiconductor laser. The 0.5 pitch Selfoc lens, which is butted up to the 0.75 pitch Selfoc lens, is AR coated on one facet and has a 70 percent reflection coating on the other facet which serves as the output coupler for the extended cavity laser. The extended cavity is formed between the back facet of the semiconductor laser and the 70 percent reflection facet of the 0.5 pitch Selfoc lens. The extended cavity laser has a lasing threshold of 55 mA which is an 18 percent threshold reduction from its nonaligned value of 67 mA. This cavity has a longitudinal mode spacing of 3.12 GHz, corresponding to an optical length of 9.62 cm. The extended resonator laser is not temperature controlled and no electrical feedback stabilization schemes are used.

The extended cavity semiconductor laser is actively mode locked by modulating the drive current to the laser at 3.12 GHz, the frequency equal to the longitudinal mode spacing of the external cavity laser. Autocorrelation traces of the mode-locked output show a well mode-locked train of pulses with a pulse width of 48 ps and a bandwidth-pulsewidth product of 0.7.

Single-mode operation is achieved by simply turning off the microwave modulation.

The experimental arrangement is shown in Fig. 1. Light from the extended cavity laser first passes through two NEC OD8312 optical isolators which provide 60 dB of isolation from the measurement system. A beam splitter picks off 20 percent of the intensity which is used to monitor both the average power and the power spectrum of the laser. An acoustooptic modulator separates the remaining 80 percent of the intensity into two beams, one of which is frequency shifted by 60 MHz. The nonshifted beam is coupled into a 1.0 m length of single-mode fiber. The frequency-shifted beam is coupled into 2.3 km of single-mode fiber which gives an optical delay of 12.3 μs. The outputs of these fibers are combined at a beam splitter and focused onto a RCA C30950G avalanche photodiode.

The signal from the photodiode is amplified and displayed on a Hewlett-Packard 8566B spectrum analyzer.

The power spectrum of the laser is simultaneously monitored by a scanning Fabry–Perot interferometer with a free spectral range of 30 GHz and a finesse of 12. This large free spectral range is required to observe the spectrum when the laser is mode locked. The signal from the scanning Fabry–Perot is displayed on a Tektronix 7854 digital oscilloscope. The average power of the laser is monitored by a photodiode whose output is displayed on a Hewlett-Packard 3437A digital voltmeter. The spectrum analyzer, digital oscilloscope, and digital voltmeter are all interfaced to a Hewlett-Packard 9826 computer for ease of data acquisition and analysis.

The spectrum S of the photocurrent produced in a self-delayed heterodyne experiment such as this has been analyzed by Gallion and DeBarge [16] and can be expressed as

$$S(\omega, \tau) \propto \frac{1}{1 + (\omega \pm \omega_{AO})^2 (\tau_c/2)^2} + \mathcal{O}(e^{-\tau}) \quad (2)$$

where ω_{AO} is the acoustooptic modulator frequency, τ is the fiber delay time, and τ_c is the coherence time of the laser. This formula was derived for a single mode, but as can be easily demonstrated [17], it is the same for each of the modes of a laser when it is mode locked since all the modes share a common random phase. As the ratio of the fiber delay time τ to coherence time τ_c increases, the spectrum of the photocurrent approaches a true Lorentzian signal centered at ω_{AO} with a width equal to twice the width of the laser mode. Using computer simulations, we have found that for coherence times in the neighborhood of 1.0 μs, a delay of six times this coherence time is required for the Lorentzian signal to be within 2 percent of twice the original laser mode width. In our experiment, the fiber delay time is 12.3 μs, which is 20 times the longest coherence time that we measured.

EXPERIMENTAL RESULTS

We have made a direct comparison between the linewidth of the extended cavity laser operating single mode and operating mode locked. Data of linewidth versus inverse power for both the mode-locked and the single-mode case are plotted in Fig. 2. The values shown for inverse power in Fig. 2 correspond to the power coupled out of the 70 percent reflecting end mirror of the extended cavity. This range of measured powers corresponds to a range of drive currents between 1-7 percent above threshold. The linewidth of a given data set is determined by a least squares curve fit of the photocurrent spectrum to (2). A typical data set and its least squares fit to (2) are shown in Fig. 3.

The mode-locked data are obtained by biasing the laser just at threshold and increasing the power of the 3.12 GHz current modulation to increase the average output power. The modulation current is up to 4 mA for the ranges of powers shown in Fig. 2. The mode spectrum, as monitored by the scanning Fabry–Perot, and the pulsewidth are
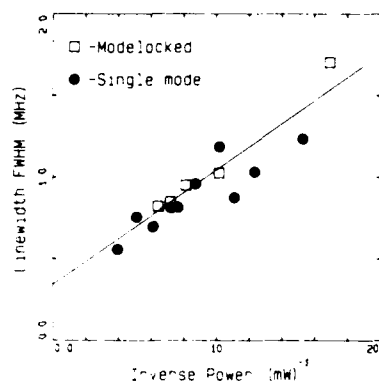
Fig. 2. Laser linewidth versus inverse power for the same source when operating mode locked and when operating single mode.
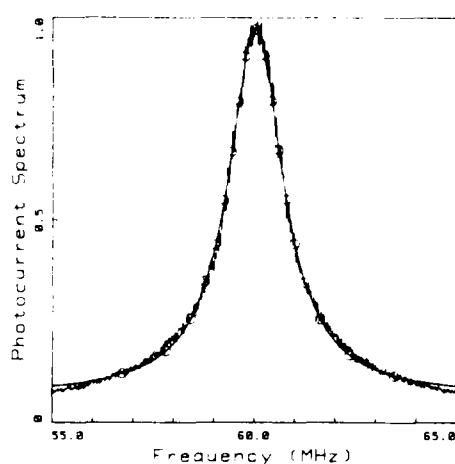

Fig. 3. Typical photocurrent spectrum and its least squares fit to (2).

observed to remain approximately constant over the range of powers shown in Fig. 2. The mode-locking frequency is initially adjusted to get temporal overlap of pulses at the detector from each arm of the interferometer.

Coherence is maintained throughout the pulse, as required of mode locking, and evidenced by two experimental facts: 1) the intensity correlation traces of the pulses have no "coherence spikes," and 2) the width of the photocurrent spectrum as shown in Fig. 3 does not change as the relative delay of the beams is changed. (Of course, the signal disappears completely when the pulses do not overlap.)

For the single-mode case, the output power of the laser is controlled by the dc drive current. As the dc drive current is increased, the laser jumps through different regions of single-mode operation. For the single mode data presented in this paper, the laser is always operating in a single mode, but not necessarily in the same mode. Since the cavity Q is different for the different modes of single-mode operation, we expect each mode to have a slightly different linewidth versus inverse power curve. Nevertheless, the single-mode linewidth clearly shows an inverse power dependence.

Fig. 2 shows that the linewidths of the single-mode source and the linewidths of the individual modes of the

mode-locked source are approximately equal when operating at the same average power. This is in contrast to what would be expected for the mode-locked case if the linewidth of each mode of the mode-locked sources was determined by the power in that mode alone. In addition, the inverse power dependence shown in Fig. 2 indicates that the primary contribution to the linewidth is spontaneous emission noise for both the single-mode and mode-locked cases. The residual linewidth when the laser power is extrapolated to infinity has been observed previously [18], and in our case may be caused by both electron density fluctuations [18] and mechanical instabilities in the cavity.

It should be noted that the above conclusions are independent of the mechanism of mode locking, whether by amplitude or frequency modulation. In this experiment, we mode lock a semiconductor laser by modulating its driving current (and hence its gain) at the cavity roundtrip frequency. However, since the refractive index of the diode is a sensitive function of electron density, current modulation invariably leads to some frequency modulation (chirp). Chirping usually broadens linewidths, but in this case, since the chirping is periodic in the cavity roundtrip frequency, its effect is actually excitation of other modes (i.e., FM mode locking). There should be very little chirping in our laser since the semiconductor diode occupies only a very small portion of the total cavity length.

The narrowest linewidth in our data for mode locking is 0.82 MHz, which corresponds to a coherence time of 0.4 μs (1). Since the pulse repetition rate is 3.12 GHz, there are 1200 pulses within the coherence time, and the electric fields of these pulses correlate.

CONCLUSIONS

We have compared the linewidths of an extended cavity semiconductor laser operating single mode and operating mode locked. We have found that the linewidth of the individual modes of the mode-locked source and the linewidth of the single-mode source have the same inverse dependence on the average power. This experimental result confirms the theoretical result of Ho [11]. A semiconductor laser can therefore be operated as a source of short optical pulses at gigahertz repetition rates without sacrificing the temporal coherence properties of the single-mode semiconductor laser.

REFERENCES

[1] P. T. Ho, "Phase and amplitude fluctuations in a mode-locked laser," IEEE J. Quantum Electron., vol. QE-21, pp. 1806-1813, 1985, refs. [1]-[9].
[2] A. Yariv and W. M. Canton, "Frequency, intensity and field fluctuations in laser oscillators," IEEE J. Quantum Electron., vol. QE-10, pp. 509-517, 1974.

[3] J. A. Armstrong, "Theory of interferometric analysis of laser phase noise," *J. Opt. Soc. Amer.*, vol. 56, pp. 1024-1031, 1966.

[4] P. Andersson, T. Andersson, S. Lundquist, and S. T. Eng, "Temporal coherence properties of picosecond pulses generated by GaAlAs semiconductor lasers for directly modulated and frequency stabilized optical communication systems," *J. Lightwave Technol.*, vol. LT-2, pp. 146-154, Apr. 1984.

[5] H. Olesen and G. Jacobsen, "A theoretical and experimental analysis of modulated laser fields and power spectra," *IEEE J. Quantum Electron.*, vol. QE-18, pp. 2069-2080, 1982.

[6] C. Lin, T. P. Lee, and C. A. Burrus, "Picosecond frequency chirping and dynamic line broadening in InGaAsP injection lasers under fast excitation," *Appl. Phys. Lett.*, vol. 42, pp. 141-143, 1983.

[7] G. Veith, J. Kuhl, and E. O. Gobel, "Temporal and spectral characteristics of rapidly gain switched GaAs-GaAlAs buried heterostructure lasers," *Electron. Lett.*, vol. 19, pp. 385-386, 1983.

[8] K. Kishino, S. Aoki, and Y. Suematsu, "Wavelength variation of 1.6 µm wavelength buried heterostructure GaInAsP-InP lasers due to direct modulation," *IEEE J. Quantum Electron.*, vol. QE-18, pp. 343-351, 1982.

[9] Y. Suzuki and T. Sato, "7 Gbit's coherent pulse generation in an actively mode-locked GaAlAs diode laser," *Electron. Lett.*, vol. 18, pp. 821-822, 1982.

[10] D. W. Rush, P. T. Ho, and G. L. Burdge, "The coherence time of a mode-locked pulse train," *Opt. Commun.*, vol. 52, pp. 41-45, 1984.

[11] P. T. Ho, "Phase and amplitude fluctuations in a mode-locked laser," *IEEE J. Quantum Electron.*, vol. QE-21, pp. 1806-1813, 1985.

[12] L. Mandel and E. Wolf, "The measures of bandwidth and coherence time in optics," *Proc. Phys. Soc.*, vol. 80, pp. 894-897, 1962.

[13] A. L. Schawlow and C. H. Townes, "Infrared and optical masers," *Phys. Rev.*, vol. 112, pp. 1940-1949, 1958.

[14] T. Okoshi, K. Kikuchi, and A. Nakajima, "Novel method for high resolution measurement of laser output spectrum," *Electron. Lett.*, vol. 16, pp. 630-631, 1980.

[15] T. Dimmick, P. T. Ho, and G. L. Burdge, "Coherent pulse generation by active modelocking of a GaAlAs laser in a Selfoc lens extended resonator," *Electron. Lett.*, vol. 20, pp. 831-833, 1984.

[16] P. B. Gallion and G. Debarge, "Quantum phase noise and field correlation in single frequency semiconductor laser systems," *IEEE J. Quantum Electron.*, vol. QE-20, pp. 343-349, 1984.

[17] P. T. Ho, unpublished.

[18] D. Welford and A. Mooradian, "Observation of linewidth broadening in (GaAl)As diode lasers due to electron number fluctuations," *Appl. Phys. Lett.*, vol. 40, pp. 560-562, 1982.

APPENDIX 3

Experimental Verification of New's and Haus's Theories of Modelocking by a Slow Saturable Absorber

Y. X. Wu, L. A. Vitoria, T. N. Ding, Y. H. Shyy and P.-T. Ho

Electrical Engineering Department
University of Maryland
College Park, MD 20742
U. S. A.

Abstract

From a colliding-pulse modelocked dye laser, we have
obtained experimental data which support New's and Haus's
proposal for pulse forming mechanism in a laser modelocked
by a slow saturable absorber.

Experimental Verification of New's and Haus's Theories of Modelocking by a Saturable Absorber

Y. X. Wu, L. A. Vitoria, T. N. Ding, Y. H. Shyy and P.-T. Ho

Electrical Engineering Department
University of Maryland
College Park, MD 20742
U. S. A.

We report experimental investigation of the pulse forming mechanism in a laser modelocked by a slow saturable absorber. Our measurements verify the mechanism proposed by New [1] and Haus [2], which says that both the saturated absorption and saturated gain have to combine together to form a net gain which lasts only as long as the pulses generated, since either medium alone, with a long recovery time, is insufficient for the task.

Although many improvements have been made on the cw modelocked dye laser [3] which originally inspired the theories [1,2], the fundamental pulse forming mechanism has not yet been experimentally investigated. Since the dye laser is still the only system using a slow saturable absorber, it is important to ascertain the mechanism of pulse forming so that other lasers can be designed on the same principle; in particular, the semiconductor laser has many key parameters for modelocking which are close to those of the dye laser.

The experimental set-up consists of a colliding-pulse modelocked laser [4]. No attempt has been made to minimize the pulse width, which is about 1 picosecond . The output pulse train is used to probe the time evolution of the active media in the laser itself when it is modelocked. Transmissions through: (a) the absorber alone; (b) the gain alone; and (c) the absorber and then the gain, are measured as a function of time delay. The delay of the probe pulse is adjusted such that it arrives at

the medium at about the same time as the intracavity laser pulses. Figure 1a and Figure 1b show, respectively, the transmission through the saturable absorber (DODCI) alone, and through the gain (rhodamine 6G) alone. It can be seen that after being saturated by the cavity laser pulses, neither medium recovers immediately. When the proble pulse passes through the absorber and then through the gain, the transmission is entirely different (Fig 1c): the net gain (gain less saturable absorption) shows a peak on the order of the pulse width (1 picosecond). Thus the combined saturable gain and saturable absorption can indeed provide a net gain which lasts only about as long as the pulses, even though either alone cannot. Our results therefore support the pulse forming mechanism proposed by New and Haus.

References:
[1] G.H.C. New, IEEE J. Quan. Elec., QE-10, 115 (1974)
[2] H.A. Haus, ibid., QE-11, 736 (1975)
[3] E.P. Ippen, C.V. Shank, A. Dienes, Appl. Phys. Lett., 21, 348 (1972)
[4] R.L. Fork, B.I. Greene, C.V. Shank, ibid., 38, 671 (1981)

FIGURE CAPTION

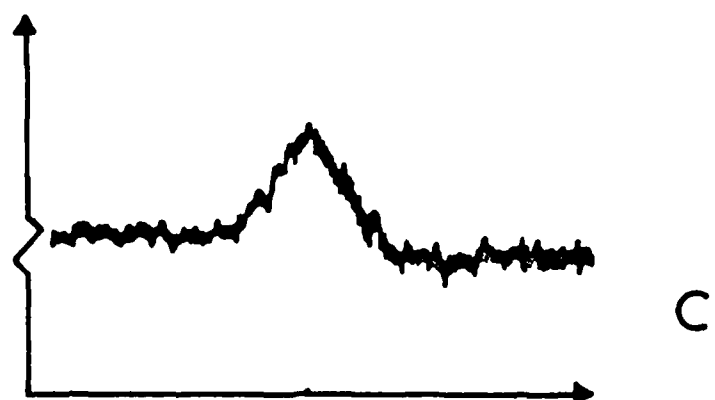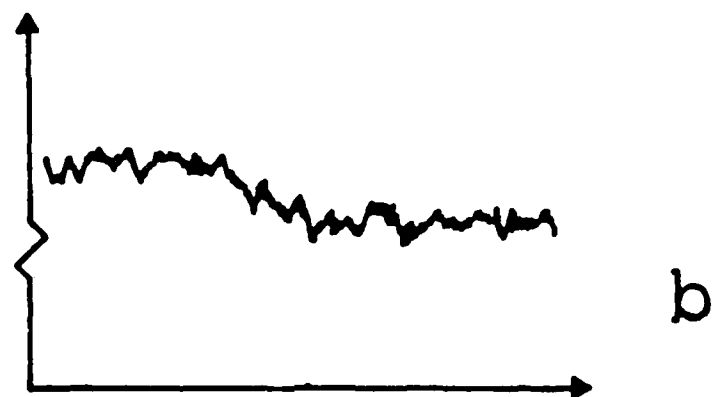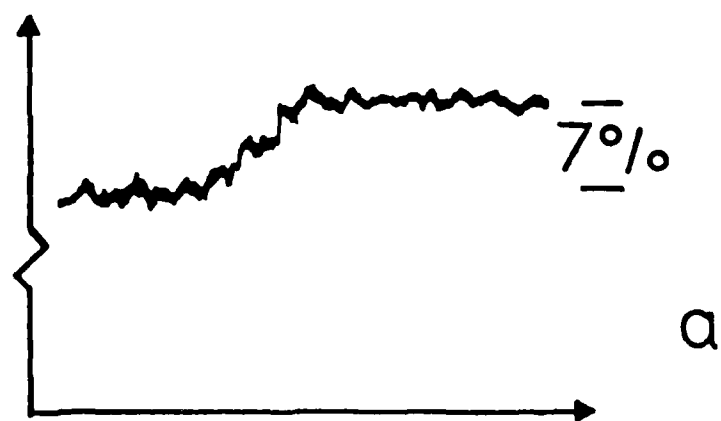FIGURE 1   Transmission of Probe Pulse vs. Time Delay

Horizontal Axis: Time Delay

Vertical Axis: Transmission (arbitary units)

(a) Transmission through Saturable Absorber Alone

(b) Transmission through Gain Alone

(c) Transmission through Absorber and then Gain

7‰

a

b

c

1 ps

Continuous wave mode-locked neodymium: phosphate glass laser

Scott A. Strobel, Ping-Tong Ho, and Chi H. Lee
Department of Electrical Engineering, University of Maryland, College Park, Maryland 20742

Geoffrey L. Burdge
Laboratory for Physical Sciences, College Park, Maryland 20740

We report the first successful mode locking of a cw neodymium phosphate glass laser. Transform-limited, 80-ps pulses were generated at 1 054 μm

We report the first successful mode locking of a cw neodymium glass laser to generate picosecond pulses at 1 054 μm. A cw pulse train offers many advantages over a burst of pulses in some measurements and experiments. Possible applications include ranging and optical communications.

Continuous wave mode locking has been achieved in neodymium yttrium aluminum garnet lasers, but the pulse widths are ultimately limited by the relatively narrow gain linewidth at 1.06 μm $\Delta\nu \simeq 2 \cdot 10^{11}$ s. Fifty times broader gain linewidth is available from neodymium ions in glass hosts. cw mode locking can more efficiently utilize this broad bandwidth to generate subpicosecond pulses. Because pulses can circulate continuously in the laser cavity they can be shortened many times. The experiment reported here is the first successful step towards this goal.

Figure 1 shows the schematic of the mode-locked laser. The lasing gain medium is neodymium in a phosphate glass host. A ring cavity is used in this experiment instead of the linear cavity used earlier for cw operation. The pump source is an argon laser (Spectra Physics 170) operating at 514.5 nm where neodymium has a strong absorption band. An acousto-optical modulator (Intraaction AOM-70R) actively mode locks the laser.

The laser beam is at normal incidence on the phosphate glass to eliminate astigmatic effects, therefore the ends of the glass are optically polished and antireflection coated. To obtain uniform pump absorption we chose a 3% neodymium concentration. The glass is wrapped in indium foil and placed in a copper block which is cooled by temperature-controlled water. Athermal phosphate glass was chosen to avoid thermal lensing effects.

The cavity, designed with a ray tracing program, allows a large stability region with 300-mm curvature mirrors. The chosen radius of curvature is a compromise between the criteria of a large stability region and a low pumping threshold. The 160-mm focal length lens, which focuses the argon pump, matches the pump beam to the laser resonator mode. An end pump geometry was adopted to reduce thermal loading problems, thereby maintaining stable cw operation. The traveling-wave acousto-optic modulator is placed between two AR coated, 85-mm focal length lenses, so that the optical beam size is under one acoustic wavelength in the modulator. The modulator is driven with 6 W of electrical power at the cavity round trip frequency about 85 MHz. An oscillogram exhibiting the 85-MHz pulse train is shown in Fig. 2.

To align the ring cavity the argon laser is tuned to 458 nm where the phosphate glass has little absorption. Once aligned, the cavity round trip frequency and the modulator frequency should be matched to within tens of hertz. The laser output is sampled with a high-speed detector and the cavity length is tuned for maximum pulse peak intensity on the sampling oscilloscope. Experimentally, the polarization of the ring laser followed that of the pump beam. Good beam quality TEM₀₀ was observed even with 2 W of pump power attesting to the good thermal properties of the glass used.

With the setup described above, the laser was mode locked to generate picosecond pulses. Earlier experiments used a Schott LG 760 phosphate glass rod 2 mmD · 20 mm and 30-ps pulses were obtained. More recently, with a glass slab 3 mm · 16 mm · 20 mm and a quartz intracavity etalon (0.2 mm thick, 10% reflectivity) to limit the bandwidth we generated very stable and reproducible pulse trains. Pulse
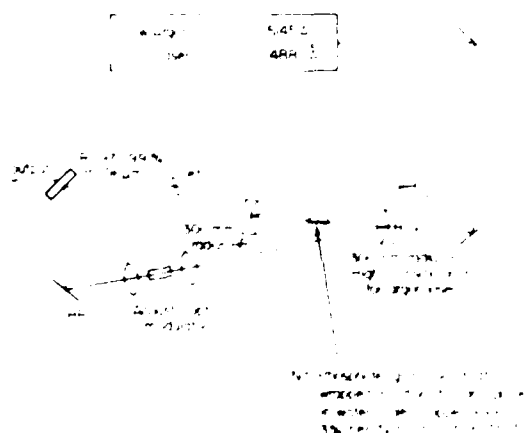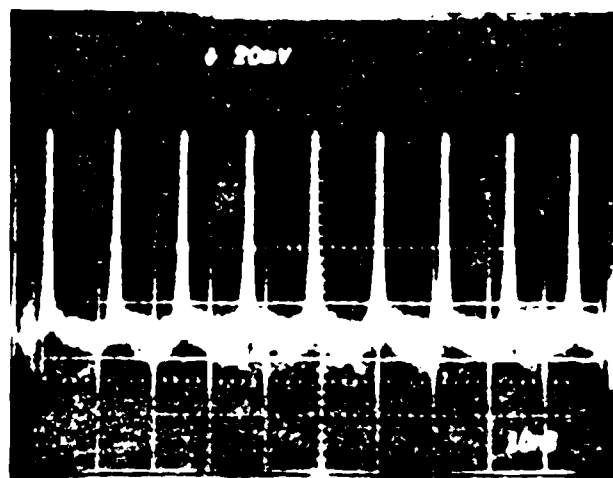

FIG. 1 cw mode-locked Nd phosphate glass laser.

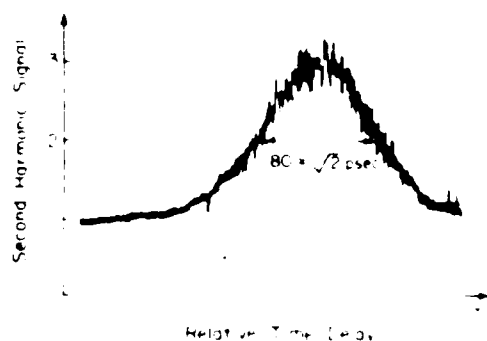FIG. 2 Oscillogram of mode-locked pulse train taken with sampling oscilloscope.

FIG. 3 Second harmonic signal generated by optical pulse intensity autocorrelation.

width is measured by the standard method of second harmonic generation (SHG) in a nonlinear crystal, LiIO, in our case. Figure 3 shows an SHG trace, which can be fit very well with a Gaussian of 80 ps full width at half-maximum. The spectral width of these pulses, ≤ 0.3 Å, was measured with a Morris-McIlrath spectrometer,[4] yielding $\Delta v \Delta t \leq 0.6$. Up to 15 mW power in one beam has been obtained with 2 W of pump power.

In conclusion, we have demonstrated the first mode locking of a cw neodymium glass laser. The success is in part due to the efficiency of the end pump geometry and the excellent optothermal properties of recently developed improved phosphate glasses. End pumping allows the glass to withstand enough pump energy so that lasing can occur even with several intracavity elements. We are presently testing other glasses including Kigre O 98 and working on the generation of even shorter pulses.

[1] S. Kishida, K. Washio, S. Yoshikawa, and Y. Kato, Appl. Phys. Lett. 34, 273 1979.

[2] W. R. Prindle and R. F. Woodcock, Amer Opt Co Tech Summary Rep No 6 1965.

[3] We are grateful to the Shanghai Institute of Optics and Fine Mechanics for the slab antireflection coated on both ends.

[4] M. B. Morris and T. J. McIlrath, Appl Opt 18 4145 1979

Picosecond-pulse generation from a continuous-wave neodymium:phosphate glass laser

L. Yan, J. D. Ling, P.-T. Ho, and Chi H. Lee

Department of Electrical Engineering, University of Maryland, College Park, Maryland 20742

Seven-picosecond pulses at 1054 nm have been generated from a continuous-wave neodymium:phosphate glass laser by active mode locking.

In the past few years, many developments in neodymium (Nd) lasers have been made. The continuous-wave (cw) mode-locked Nd:YAG laser has become an important pump source for the dye-laser system, but its linewidth limits the pulse width. On the other hand, very short (a few picoseconds) pulses have been generated from Nd:glass lasers,[1-3] but only by Q switching at repetition rates of a few hertz. A laser system able to generate picosecond pulses in cw operation will find many applications. In this Letter we report the cw operation of an actively mode-locked Nd:phosphate glass laser that can generate 7-psec pulses at 1054 nm. These pulses are about 14 times shorter than those from a cw mode-locked Nd:YAG laser and 10 times shorter than those previously obtained in our laboratory.[4]

Figure 1 is a schematic of our laser system. A 3 mm × 16 mm × 20 mm slab of Nd:phosphate glass,[5] in a ring resonator, is longitudinally pumped by the cw output of an Ar-ion laser at 514 nm. The Nd laser is mode locked by an acousto-optic loss modulator. Several improvements have been made over our previous system.[4] First, a standing-wave, instead of a traveling-wave,[4] acousto-optic modulator (IntraAction ML505J) is used for active mode locking, driven at about 50 MHz, half of the round-trip frequency of the ring cavity. A standing-wave modulator is believed to give better amplitude modulation of light. Second, use of a standing-wave modulator allows us to remove the two intracavity lenses used previously,[4] resulting in a reduction of the intracavity loss and optical distortion. Third, the water-cooling system of the glass slab has been redesigned. Both the top and bottom surfaces of the slab, wrapped in In foil, are in contact with Cu blocks, which are cooled by temperature-controlled running water. Hence the thermal loading and distortion are reduced, and we can increase the pump power to more than 3 W. The étalon used previously[4] is removed to relieve the spectral-bandwidth constraint.

We have found experimentally that, as the pump power increases, the Nd:phosphate glass laser becomes more stable, and pulses become shorter and coherent. Good laser performance occurs at pump levels well above the mode-locking threshold of ~1.1

W. When the pump power is below 1.6 W, pulses longer than 250 psec are observed by a fast detector and sampling oscilloscope, the combined rise time of which is about 70 psec, and the characteristics of noise bursts[6] are seen in the autocorrelation traces by the standard method of intensity correlation with second-harmonic generation. As the pump power increases to 1.8 to 2 W, the laser becomes more stable; the pulses shorten to under 100 psec and are more coherent. Very short and coherent pulses are generated at pump levels above 2 W. Figure 2 shows the autocorrelation trace of 7-psec pulses generated at 3 W of pump power. The pulse width is comparable with that obtained by a pulsed, passively mode-locked Nd:glass laser, with the advantages of high repetition rate, synchronizibility, and good reproducibility. The average output power of the Nd:glass laser is about 20 mW when the pump power is 3 W.

We have found that, to generate such short pulses, it is important to adjust the resonator for optimum stability and to match the pump-beam profile with the glass-laser beam. For good mode-locking operation, the laser is very sensitive to the tuning of the modulation frequency. A shift by tens of hertz of the modulator driving frequency can change the pulse duration appreciably.
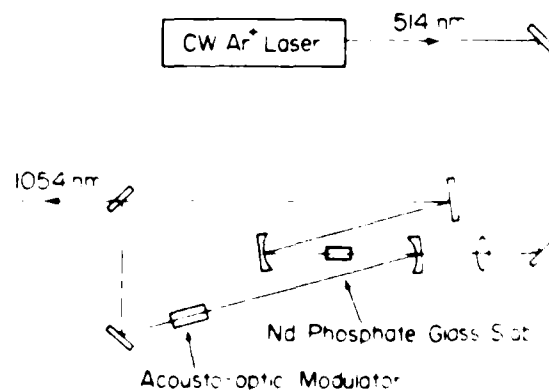
While the main mechanism of mode locking is *am-*

Fig. 1. Schematic of the Nd phosphate glass ring laser. The transmittance of the output mirror is ?
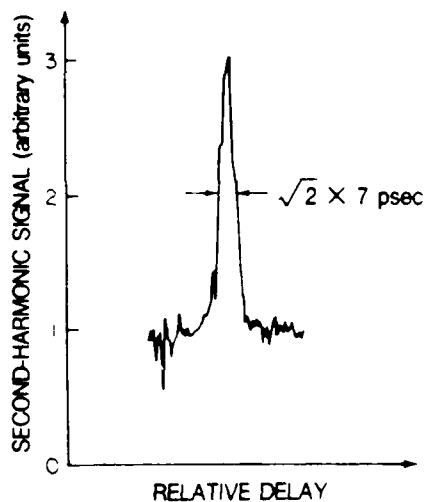
Fig 2. Autocorrelation trace of pulses from the Nd:phosphate glass laser. A Gaussian pulse shape is assumed.

can be increased more than 40 times when the Nd-laser beam is chopped inside the cavity. The expense of the method is the broadening of pulse width to tens of picoseconds.

In conclusion, we have generated 7-psec pulses from a cw actively mode-locked Nd:phosphate glass laser. The laser delivers 20 mW of average power at a 100-MHz pulse repetition rate. We are planning to amplify and compress the pulses. A regenerative amplifier of similar construction can provide microjoules of energy per pulse at kilohertz repetition rates. Fu: .ermore, pulses can be compressed by an optical fiber and grating pairs down to the femtosecond region. Such a laser system should have many applications in science and technology.

plitude modulation. two detailed observations lead us to suspect that there is also some phase modulation: (1) the pulse-width–bandwidth product is 1.1, slightly larger than the transform limit for an AM mode-locked laser; (2) the pulse repetition frequency (twice the modulator driving frequency) is somewhat above the cavity round-trip frequency (by 6–8 kHz) when the shortest pulses are obtained. These two observations are consistent with FM mode-locking theory[7] but not with pure AM mode-locking theory.[7]

We have also introduced a simple method to increase the pulse energy by mechanically chopping the Nd-laser beam inside its cavity or the pump beam outside the cavity. Simultaneous mode locking and relaxation oscillations occur regularly in both cases. The energy of the pulses in the peak of the initial spike

References

1. C. Kolmeder and W. Zinth. Appl. Phys. **24**, 341 (1981)
2. L. S. Goldberg and P. E. Schoen. IEEE J. Quantum Electron. **QE-20**, 628 (1984).
3. T. Tomie and M. Yano. in *Digest of Conference on Lasers and Electro-Optics* (Optical Society of America. Washington. D.C.. 1985). p. 126.
4. S. A. Strobel. P.-T. Ho. C. H. Lee. and G. L. Burdge. Appl Phys. Lett. **45**, 1171 (1984)
5. We are grateful to the Shanghai Institute of Optics and Fine Mechanics for the Nd:phosphate glass slab
6. E. P. Ippen and C. V. Shank. in *Ultrashort Light Pulses*. S. L. Shapiro. ed (Springer-Verlag. Berlin. 1977). pp 83-122.
7. D. J. Kuizenga and A. E. Siegman. IEEE J. Quantum Electron. **QE-6**, 694 (1970)

An Actively Mode-locked Continuous - Wave

Nd. phosphate Glass Laser Oscillator and Regenerative Amplifier

L. Yan, J.D. Ling, P.-T. Ho, And Chi H. Lee
Department Of Electrical Engineering
University Of Maryland
College Park, Maryland 20742

And

G.L. Burdge
Laboratory For Physical Sciences
4928 College Avenue
College Park, Maryland 20740

Abstract

The performance of a continuous wave actively mode-locked Nd phosphate glass laser oscillator and a high repetition rate Nd phosphate glass regenerative amplifier is described. Pulses as short as 7 ps at 1 054 μm have been generated at a 100 MHz repetition rate from the laser oscillator. The oscillator output has been amplified by 2×10^5 to 5 μJ per pulse at a repetition rate of 500 Hz.

Introduction

Mode-locked neodymium (Nd) lasers have become indispensable tools for scientific research. Their high intensity pulses are used to study linear and nonlinear optical phenomena [1,2]. In all applications, high reliability is required. In many applications, electronically synchronized pulses at a high repetition rate are desired for fast data acquisition.

Although a continuous wave (cw) actively mode-locked Nd:YAG laser can be electronically synchronized and can generate optical pulses at a high rate, it cannot produce short pulses reliably. For instance, because of its narrow fluorescence line width (~ 5 cm^{-1}) [3,4], the Nd:YAG pulse width is limited to about 70-100 ps for modulator driving frequencies of about 50 MHz and moderate modulation depths [5,7]. Although passively mode-locked Nd:YAG lasers can produce 25 ps pulses [8,9] and colliding pulse mode-locked lasers can generate 10-12 ps pulses [10], the passive mode-locking process with a saturable dye absorber in these lasers creates a large time jitter which prevents electronic synchronizing.

The Nd glass laser, on the other hand, has a broad linewidth (~ 200 cm^{-1}) and can therefore generate much shorter pulses. Laser pulses of a few picoseconds have been generated from Nd:glass lasers by either passive mode-locking [11,14], or active and passive mode-locking [15], or purely active mode-locking [16]. Short pulses from an active mode-locked Nd glass laser can be synchronized to external equipment. However, these short pulses come with a price. Because of the small stimulated emission cross-section (3.4×10^{20} cm^2), which is an order of magnitude smaller than that of Nd:YAG, a Nd glass laser has a much higher threshold than a Nd:YAG laser. Furthermore, the thermal conductivity of Nd glass is also an order of magnitude smaller than that of Nd:YAG. This makes heat dissipation difficult in Nd glass, and as a result, Nd glass encounters severer thermal distortions [12]

(1)

despite the small thermal-optic coefficient of Nd glass. In fact, Nd glass is more easily fractured by thermally-induced stress than Nd:YAG. The conventional flash lamp pumping of Nd glass generates a lot of useless heat at short wavelengths; therefore, short pulses from these Nd glass lasers are generated by Q-swiching at a few hertz repetition rate [11,16]. And passively mode-locked laser pulses have inherent, stochastic fluctuations, so that stability is poor and synchronizing impossible.

We have developed a c.w. actively mode-locked Nd phosphate glass laser. It combines the advantages of short pulse generation, high repetition rate, and synchronizability. The argon laser longitudinal pump scheme reduces the severe thermal problems thereby allowing cw operation [17,18]. The laser has generated pulses as short as 7 ps at 1.054 μm at a 100 MHz repetition rate with >20 mw of average power [19]. In this paper, we will describe the laser construction and performance. This cw actively mode-locked ring laser also provides a unique opportunity to study the pulse formation in an inhomogeneously broadened solid state laser and to explore some previously unreported properties associated with a ring laser. In the following sections we will discuss the laser characteristics and compare the characteristics of the mode-locked homogeneously broadened laser and other ring lasers with the Nd phosphate glass laser.

Recently, many groups [5,6,20,21] have compressed the pulses from a cw actively mode-locked Nd.YAG laser by using an optical fiber and gratings. Pulses have been compressed to the subpicosecond region [5,21]. However, because of stimulated Raman scattering, the pulse energy after the compression is limited to 1 to 20 nJ [5,6,20,21]. For higher intensity applications, the pulse energy has to be amplified further. A Nd YAG regenerative amplifier can operate at kilohertz

(2)

repetition rates [22], but its narrow linewidth prevents it from amplifying short pulses. However, a high repetition rate Nd glass amplifier system can produce ultrashort pulses at high repetition rates. We will describe the first operation of such a high repetition rate Nd glass regenerative amplifier, which can amplify the pulse energy up to 5 µJ at a 500 Hz repetition rate.

Laser Oscillator

The ring resonator configuration of the laser oscillator is shown in Fig. 1. The spherical mirror M1 through which the pump beam enters has a dichroic coating for maximum transmission at 514 nm. The laser medium is a rectangular Nd phosphate glass slab 3 mm thick, 20 mm long and 15 mm wide [23]. The two 3 x 15 mm surfaces are polished and antireflection coated at 1.054µm. The glass slab is wrapped with indium foil and sandwiched between two copper blocks which are cooled by temperature - controlled running water. The Nd glass slab is longitudinally pumped by the cw output at 514 nm from an argon ion laser, which is focused at the Nd glass medium with a beam waist of 65 µm. A standing wave acousto-optic modulator (IntraAction ML-505J) actively mode-locks the Nd glass laser. Both windows of the modulator are AR-coated at 1.06µm. The modulator is driven with 1.5 watts of RF power at about 50 MHz-half of the round trip frequency of the ring cavity - by a frequency synthesizer with 10 Hz sensitivity and 10^{-9} stability and by a broad band RF power amplifier. The modulator is cooled by temperature - controlled running water.

CW mode-locking of the Nd phosphate glass laser was readily achieved with argon-ion pump power greater than 0.8 watts and with the intra-cavity acousto-optic modulator tuned to a cavity resonance around 50 MHz. Although our cavity design provides a large stability range, we have found that it is important to adjust

(3)

the spacing between the two spherical mirrors to the middle of the stability range. This adjustment results in a cavity which is less sensitive to intracavity elements and more tolerant to the thermal lensing in the glass. Moreover, by operating in the middle of the stable range, the argon-ion pump beam profile has a better match to that of the Nd:glass laser. The argon-ion pump laser power must be held within 0.2 watts; otherwise, lasing will cease.

The mode-locked laser performance is monitored by a fast pin-diode detector and sampling oscilloscope. Tuning sensitivity of the acousto-optic modulator driving frequency depends on the pulse duration itself. For instance, when pulse widths are longer than $\sim$ 120 ps, a few hundred hertz shift in driving frequency will not change the pulse duration appreciably. However, when pulse widths are shorter than $\sim$ 70 ps, even a 10 Hz shift in driving frequency can appreciably change the pulse duration, as monitored on the sampling oscilloscope. In addition to the acousto-optic modulator tuning effects on the pulse width, any etalons created by intracavity elements can also change the pulse width, so extensive care has been taken to avoid these effects.

A TEM_{00} transverse mode is essential for the generation of short pulses. With good alignment, a TEM_{00} transverse mode is achieved without any intracavity aperture because the focused pump beam at the medium forms an effective aperture. However, when the resonator is not aligned well, the laser will produce higher order transverse modes. During operation with higher transverse modes, laser pulses are long (> 150 ps); whereas during TEM_{00} mode operation laser pulse widths are reduced appreciably. Such a broad pulse width for higher transverse modes is primarily caused by non-degeneracy of the mode spacing for the

(4)

fundamental and higher order transverse modes. For a mixture of transverse modes, phase-locking of all the modes becomes difficult.

We have found experimentally that the argon-ion pump level plays an important role in the overall performance of the Nd glass laser. Basically, as the pump power increases, the laser stability and the pulse coherence improve, and the pulse width gets shorter. Fig 2 summarizes the pulse widths observed at different pump powers. When the Nd phosphate glass medium is pumped below 1.1 watts, the laser output is not stable and only $\geqq 100$ ps pulse widths can be attained, as observed on the sampling oscilloscope. When the pump power is increased to 1.2 watts, pulse widths shorter than 100 ps are observed. And when the pump power is increased to above 1.4 watts, pulse widths less than 50 ps are measured. (These short pulse widths were measured by the standard colinear intensity autocorrelation method[24].) When the pump power exceeds 1.8 watts, good stable laser operation is achieved. The sampling oscillogram of laser pulses (Fig 3) shows the good stability and reproducibility of the laser, although the pulse width is shorter than the detection bandwidth limit of 73 ps. The autocorrelation measurements yield pulse widths typically between 20 to 30 ps with good coherence characteristics. At a pump power of ~3.2 watts, we obtained the shortest pulse width of 7 ps (Fig. 4). (To avoid possible damage to the Nd glass slab, we did not use pump powers higher than 3.3 watts.)

The improved performance of the laser as the pump power increases can be explained qualitatively as follows. Although the Nd phosphate glass is nominally inhomogeneously broadened with an effective fluorescence linewidth $\Delta f = 6 \times 10^{12}$ Hz, the homogeneous width of each constituent ion species is about 6×10^{11} Hz [25] This homogeneous width is broad enough to cover many longitudinal modes of the

(5)

resonator (mode spacing = 100 MHz). The laser is neither strictly homogeneously broadened nor strictly inhomogeneously broadened, but rather it is more homogeneously broadened at low pumping levels and increasingly inhomogeneously broadened at higher pumping levels. Mode-locking a homogeneously broadened laser is more difficult as the bandwidth comes from sideband generation. Mode-locking an inhomogeneously broadened laser is easier, since the bandwidth is already there. Only a small injection signal from sideband generation is required to lock in phase the different components within the free-running bandwidth. Thus in our case, at lower pumping levels we can estimate the pulse width τ_p using theories for actively mode-locked homogeneous lasers [26]. As the pumping level increases, the laser becomes more inhomogeneously broadened and the free-running bandwidth increases. We can expect the pulse width to decrease as the longitidinal modes within the increased bandwidth are locked together, which is indeed what we observe experimentally.

The steady state pulse width τ_p expected from active mode-locking a homogeneously broadened laser is [26, 27]:

$$\tau_p = \frac{(2 \ln 2)^{\frac{1}{2}}}{\pi} \left(\frac{g}{\theta^2_m} \right)^{\frac{1}{4}} \left(\frac{1}{f_m \Delta f} \right)^{\frac{1}{2}} \qquad (1)$$

for the single pass amplitude transmission given by

$$m(t) = \cos\left(\theta_m \sin 2\pi f_m t \right) \qquad (2)$$

where Δf is the gain linewidth, f_m is the modulator driving frequency, θ_m is the modulation depth and $g = \frac{1}{2} \ln (1/R_{eff})$ is the saturated round trip amplitude gain R_{eff} is the effective power reflectivity including all cavity losses

(6)

In our experiment, the following parameters are used or estimated: the Nd phosphate glass effective fluorescence linewidth $\Delta f = 6 \times 10^{12}$ Hz, $f_m = 50$ MHz, $\theta_m = 0.4$, and $g = 0.064$. With these parameters, the pulse width expected from Eqn. 1 is $\tau_p = 17$ ps. This value is comparable to the 20 - 25 ps pulse widths observed experimentally at some moderate pumping levels. We do observe quite a large pulse width variation at lower pumping levels (See Fig. 2). However, in this unstable region of operation the Kuizenga-Siegman theory [26] can no longer be applied.

At our highest pump power, the shortest pulse generated (only 7 ps) was about twice as short as that predicted by Eqn. 1. The simultaneous measurement of the pulse spectrum by a spectrometer with a scanning diode array [28] yields a 5.5 A pulse bandwidth (Fig. 5). We think that such short pulse generation reflects the following two facts: 1) the increasing importance of inhomogeneous broadening and 2) the involvement of phase modulation. We note that the bandwidth of the 7 ps pulses, 5.5 A, now approaches the homogeneous linewidth. As the Nd glass behaves more like an inhomogeneously broadened gain medium, the free-running bandwidth increases and mode-locking is facilitated. Although coherent, the shortest pulses we obtained, 7 ps, did have a bandwidth broader than the minimum required by Fourier transform. (The measured product of pulse width - bandwidth is ~ 1.1). A modulated structure can clearly be seen in the pulse spectrum (Fig. 5), this structure indicates that such short pulses are indeed phase modulated. Phase modulation broadens the pulse spectral bandwidth, and under proper conditions, it can generate very short pulses.

Self-phase-modulation (SPM) occurs commonly in high power Nd glass lasers [12,16,29]. In a recent experiment, Tomie [16] generated 4 ps pulses at the second harmonic from an actively mode-locked and Q-switched Nd phosphate glass laser. The mechanism for generating such short pulses is found to be the SPM and

interference through a thin etalon [16]. The intracavity laser intensity in that experiment is 300 MW/cm², which is above the SPM onset intensity of 150 MW/cm² [11]. In our experiment, however, the focused intracavity laser intensity at the Nd glass medium is about 30 MW/cm² (15nJ intracavity pulse energy and beam waist of 58 μm) even for a pulse duration of 10 ps. The laser intensity at the acousto-optic modulator is two orders of magnitude lower than that at the laser gain medium. Furthermore, no thin etalon is inserted inside our laser cavity. The shortest intracavity element is the 2 cm long Nd phosphate glass slab, hence, when the pulse duration is less than 100 ps, any possible interference caused by the slab is expected to be very weak. Therefore, the SPM effect, at least, is not the main pulse shaping mechanism. Instead, we observe a correlation between the onset of the modulated pulse spectrum and a tuning of the modulator driving frequency. At a certain modulator driving frequency, the laser generates pulses (~ 20 ps) which yield a smooth bell-shaped pulse spectrum with a 2.7 Å bandwidth. When the modulator driving frequency is tuned about 1KHz above the cavity resonance frequency, the pulse spectrum broadens and the modulated structure appears. This suggests that some phase modulation is introduced through the detuning in the modulation process and that this phase modulation is involved in the pulse shaping. In fact, for the case of mode-locking by FM modulation [26] when the pulse repetition frequency (twice the modulator driving frequency) is detuned above the cavity resonance frequency, the laser pulse width is actually shortened. The short pulse generation mechanism in our experiment is not yet fully understood, and work on this effect is continuing.

Also, we have observed a directional asymmetry of laser oscillation in our actively mode-locked ring laser oscillator. With the acousto-optic modulator driving power off, cw laser oscillation occurs in both counter propagating directions with nearly equal intensity. However, with the modulator driving power on and with the

(8)

Nd glass laser aligned to give short pulses, the oscillation intensity in one direction is much greater ($\gtrsim$ 20 times) than that in the other direction. The laser power drop-off in one direction is usually accompanied by an increase in power in the counter propagating beam. By adjusting the acousto-optic modulator elevation angle (around the Bragg angle), we can flip the dominant laser oscillation from one direction to the other direction. Mandel and Abraham [30] and Lett et al. [31] have studied the stability of a bidirectional homogeneously broadened ring laser. For a single longitudinal mode oscillation in two directional modes, they found that the symmetric solution is always unstable above threshold, whereas the asymmetric solution has a finite domain of stability. Destabilization of this asymmetric solution causes spontaneous and random switching between the zero-intensity mode and the oscillating mode. However, for multi-mode lasers, especially mode-locked ring lasers, no theoretical or experimental results of such directional asymmetry of oscillation have been reported. In fact, colliding pulse mode-locking of a ring laser [32] requires two equally intense beams in the two counter propagating directions. Tomov et al. [33] reported a unidirectional traveling wave operation of their mode-locked Nd glass ring laser. But in their set-up a saturable absorber cell was placed near one end of the laser medium to generate directional discrimination, and the unidirectional oscillation is unique. In our experiment, no discriminative element is deliberately inserted inside the ring cavity, and the modulator is placed a quarter of the cavity length away from the laser medium. Since the fluorescence lifetime of the Nd glass ($\approx$ 300µs) is much longer than the cavity round trip time (10 ns), cross saturation effects should be negligible. The mechanism of this previously unreported asymmetric directional oscillation in an actively mode-locked Nd glass ring laser is not well understood. However, we can again correlate the asymmetric oscillation to the pulse narrowing via the gain level increase since the gain in one direction will be enhanced if an asymmetric oscillation favors that direction.

(9)

We have also studied the Nd glass laser behavior when a mechanical chopper is used to chop (at a rate between 200 to 500 Hz) either the IR laser beam inside the cavity or the argon-ion laser pump beam outside the cavity. In both cases, simultaneous mode-locking of individual pulses and envelope relaxation oscillation occur as shown in Fig. 6. The period of the envelope relaxation peaks is about $50 \sim 60$ μs, and the width of the initial spike is about 1μs. After about 600 μs, the envelope of the mode-locked pulses reaches its steady state value. Similar phenomena have been observed before [34,35] in the prelase stage of actively mode-locked and Q-switched Nd:YAG lasers, and the envelope relaxation oscillation is the well known result of the transient interplay among the population inversion, the intracavity photon flux and the photon decay time [36].

The pulse energy at the peak of the initial spike is increased 40 times over the pulse energy at the steady state when we chop the infrared beam inside the cavity while we cw pump the Nd phosphate glass. The pulse energy increases at the expense of an increase in pulse width. Autocorrelation traces of pulses from this mode-locking and relaxation oscillation show the characteristic of a spike on a broader (80 to 100 ps) shoulder.

Regenerative Amplifier

We have also developed a linear cw-pumped Nd phosphate glass regenerative amplifier as shown in Fig. 7. (Like the oscillator, the amplifier is also cw pumped which allows operation at high repetition rates.) The resonator is constructed from two high-reflection (1.06μm) coated plane parallel mirrors and a f = 85 mm focusing lens. This resonator is similar to the oscillator ring resonator except that a different focusing lens and resonator length have been used. A 2 x 15 x 20 mm

(10)

Nd phosphate glass slab (Schott LG 760) provides the gain. The cooling scheme for the laser glass slab is the same as that used in the oscillator. A single intracavity Pockels cell [Medox 0690-KDP] is used in the regenerative amplifier. During the on stage, the Pockels cell introduces a quarter wave retardation and during the off stage it introduces a full wave retardation. The Pockels cell, combined with a quarter-wave plate and a thin film polarizer, traps the injected pulse and later dumps it out of the regenerative amplifier. Phase locking of the regenerative amplifier with the injected mode-locked pulse is maintained by driving the Pockels cell at 500 Hz down-shifted from the 50 MHz driving frequency of the laser oscillator acousto-optic modulator. To minimize loss, all intracavity elements are anti-reflection coated at $1.06\mu m$

To isolate the regenerative amplifier from the oscillator and extract the amplified pulses from the amplifier we use a $R = 10\%$ beam splitter. The beam waist of the oscillator is imaged by a lens to match the larger amplifier waist so that the diffraction loss of the injected pulse energy can be minimized. This approach maintains a high energy contrast ratio of the initial injected pulse to the spontaneous emission from the amplifier and thereby minimizes the amplified spontaneous emission.

A portion (~20 pJ) of the 20 ps output pulse train from the cw mode-locked Nd phosphate glass laser oscillator is injected into the regenerative amplifier When the regenerative amplifier is pumped with 1.8 watts of argon ion laser power, the injected pulse is amplified to maximum energy after about 300 round trip passes and then is dumped out from the amplifier. An amplified pulse energy of $1\mu J$ (5×10^{4} amplification) has been realized with this regenerative amplifier (When thermal birefringence is compensated for, then 5µJ output pulses can be

(11)

produced. This is discussed later.) The 500 Hz repetition rate is presently limited by the Pockels cell. However, the cw pump scheme should allow a 2 KHz repetition rate operation ultimately limited by upper level lifetime.

Preliminary streak camera measurements of the amplified pulse width show a primary peak 50 ~ 60 ps in width (Fig 8) and smaller satellites about 1 ns away. Two causes for this long pulse width are possible. One is the gain saturation which can cause the line-narrowing of the gain medium. However, because of the much broader linewidth of Nd glass than the pulse bandwidth, this line-narrowing will not affect the pulse bandwidth until the amplification is near its peak. Another possible cause could be the SPM which might occur in the later stage of the amplification process. Although we believe that self-phase modulation is not occurring in the oscillator because of the low power density, we should note that the pulse energy can be 40 times greater inside the regenerative amplifier than inside the oscillator. Thus, strong self-phase modulation may occur leading to the pulse broadening observed. Such pulse broadening could be eliminated by compressing the amplifier output with a grating pair. Considering the broad linewidth of Nd glass, one could expect amplification of pulses as short as 200 fs. (A low repetition rate Nd glass chirped pulse amplifier and compression system produced 2 ps pulses with the possibility of subpicosecond pulse performance [37, 38].)

Even when the regenerative amplifier is aligned to have a net gain greater than one, the relatively long amplification process (~ 300 round trips) indicates that the unsaturated net gain of the regenerative amplifier is small. We find that this small unsaturated net gain is caused by thermal birefringence. Thermal birefringence and thermal lensing effects are well known for high power Nd YAG and Nd glass lasers [39] Our experimental studies [40], in accordance with theory, show that under tight focusing even a few watts of absorbed heat can cause strong thermal

lensing and thermal birefringence. Using a mechanical chopper to chop the argon-ion laser pump beam, we observe the effect of the thermal birefringence loss. The laser leakage output from one end mirror is monitored by a pin-diode detector which is calibrated by a caloric power meter. With a polarizer inside the cavity and with the pump beam chopped at a 50 percent duty cycle, the laser output monotonically decreases after the initial relaxation oscillations (about 600 μs) during the lasing period. The laser output about 600 μs after lasing begins is compared with the laser output when cw pumping is used. Similar experiments are done with the polarizer removed. Fig 9 summarizes our results. Although the laser alignment has not been optimized, the dramatic difference between cw pumping and chopped pumping with and without the intracavity polarizer clearly reflects the effect of the thermal birefringence loss.

There are several possible solutions to the thermal problem. One can use a semiconductor diode laser or diode laser array as the pump source. The diode laser pump at ~ 800 nm has a better quantum efficiency and probably a better branching ratio than the argon-ion laser pump at 514 nm. Thus, for a given gain level the residual heat can be reduced by a factor of more than 3 as compared with argon-ion laser pumping. Recent experiments with diode-laser-array-pumped solid state lasers have shown high efficiency [41, 42], and the development of high power diode-laser-array pumping shows a promising future [43].

To avoid unnecessary heat generation, synchronous pumping up to 2 KHz can replace cw pumping, since one does not have to pump longer than the 300 μ sec fluorescence lifetime of Nd^{3+}. The unnecessary heat generated between each period of energy storage and amplification can thus be removed. High repetition

(13)

rate periodic pumping can be achieved either by using a quasi-cw diode laser array or by simply chopping the pump laser beam at a high repetition rate.

An alternative solution to the thermal problem is a thermal-birefringence-compensated resonator [44]. Fig. 10 is the schematic of a variant. It is designed specifically to accommodate the symmetric double end-pumping of two Nd glass slabs. The 90 crystal quartz polarization rotator, placed between the two Nd glass slabs, flips the radial and tangential field components at every point in the transverse beam profile. Thus, the difference between the radial index and the tangential index caused by thermal stress in one Nd glass slab is compensated for in the second Nd glass slab because the field components have been switched. With this thermal-birefringence-compensated regenerative amplifier, we have amplified the pulse energy to 5 µJ in about 110 round trips at the same 1.8 watt pump power used to pump the previously-configured regenerative amplifier. (We have end-pumped each phosphate glass slab with 0 9 watts.) This represents a factor of 5 increase in the amplified pulse energy and a reduction of about 3 in the build-up time.

(14)

Summary

We have described the performance of a cw actively mode-locked Nd phosphate glass laser oscillator and a high repetition rate Nd phosphate glass regenerative amplifier. A 100 MHz pulse train at 1.054 μm has been generated with 7 ps pulse widths and an average output power of >20 mW. By mechanically chopping the Nd glass laser beam in the cavity we increased the pulse energy 40 times at the expense of broadening the pulse width. Moreover, we found that the gain level of the Nd phosphate glass laser is important in generating short and coherent laser pulses. At moderate pumping levels a pulse width ~ 20 ps is produced which agrees with the value expected from a theory for the actively mode-locked homogeneous laser. At high pump levels even shorter pulses are generated, and phase modulation, introduced through the detuning in the modulation process, is involved in the pulse shaping. By compensating for the thermal birefringence, we designed a regenerative amplifier which amplified the laser pulses from the cw actively mode-locked Nd phosphate glass oscillator to 5 μJ at a 500 Hz repetition rate. In addition, only a single argon-ion laser pumped both the oscillator and the regenerative amplifier. Furthermore, the Nd glass medium has the potential for amplifying pulses as short as 200 fs at a high repetition rate.

Acknowlegement

We would like to thank T.J. McIlrath, U. Hochuli and C. Alley for lending us instruments and D. Cooper and Y.H. Shih for technical assistance. This work was supported in part by the Air Force Office of Scientific Research.

References:

[1]   G.R. Fleming and A.E. Siegman, Eds. *Ultrafast Phenomena V*, New York: Springer Verlag, Berlin, 1986.

[2]   D.H. Auston and K.B. Eisenthal, Eds. *Ultrafast Phenomena IV*, New York: Springer Verlag, Berlin, 1984.

[3]   M.J. Weber, Ed., *Handbook of Laser Science and Technology* Vol. 1 *Lasers and Masers*, CRC Press, 1982.

[4]   A.A. Kaminskii, *Laser Crystals*, New York: Springer Verlag, Berlin, 1981.

[5]   A.M. Johnson, R.H. Stolen, and W.M. Simpson, "80 x single stage compression of frequency doubled Nd:Yttrium aluminium garnet laser pulses, " *Appl. Phys. Lett.*, Vol. 44, pp. 729-731, 1984.

[6]   J.D. Kafka, B.H.Kolner, T. Baer and D.M. Bloom, "Compression of pulses from a continuous-wave mode-locked Nd.YAG laser, "*Opt. Lett.*, Vol 9, pp. 505-506, 1984.

[7]   S. De Silvestri, P. Laporta, and V. Magni, "14-W continuous-wave mode-locked Nd:YAG laser," *Opt. Lett.*, vol. 11, pp. 785-787, 1986.

[8]   A. Laubereau and W. Kaiser, "Generation and applications of passively mode-locked picosecond light pulses," *Opto-Electron.*, Vol. 6, pp. 1-24, 1974.

[9]   H. Al-Obaidi, R.J. Dewhurst, D. Jacoby, G.A. Oldershaw, and S.A. Ramsden, *Opt. Commum.*, Vol. 14, pp. 219-222, 1975

[10]   H. Vanherzeele, J.L. Van Eck, and A.E. Siegman, "Colliding pulse mode locking of a Nd:YAG laser with an antiresonant ring structure, "*Appl. Optics*, *Vol.* 20, pp. 3484-3486, 1981.

[11]   J.R. Taylor, W. Sibbett, and A.J. Cormier, "Bandwidth-limited picosecond pulses from a neodymium-phosphate glass oscillator," *Appl. Phys. Lett.*, Vol. 31, pp. 184-186, 1977.

[12]   T.R. Royt, "Passive mode-locking of the Nd-glass oscillator at high repetition rate with thermally compensated phosphate glasses," *Opt. Commun.*, Vol. 35, pp.271-276, 1980.

[13]   C. Kolmeder and W. Zinth, "Theoretical and experimental investigations of a passively mode-locked Nd glass laser," *Appl. Phys.*, Vol. 24, pp. 341-348, 1981.

[14]   L.S. Goldberg, P.E. Schoen, and M.J. Marrone, "Repetitively pulsed mode-locked Nd phosphate glass laser oscillator-amplifier system," *Appl. Optics*, Vol. 21, pp. 1474-1477, 1982.

[15]   L.S. Goldberg and P.E. Schoen, "Active-Passive mode-locking of a Nd phosphate glass laser using #5 saturable dye," *IEEE J. Quantum Electron.*, Vol. QE-20, pp. 628-630, 1984.

[16]   T. Tomie, "Picosecond pulse generation by self-phase modulation in an actively mode-locked and Q-switched phosphate glass laser," *Japan J. Appl. Phys.*, Vol. 24, pp. 1008-1017, 1985

[17]   S. Kishida, K. Washio, and S. Yoshikawa, "cw oscillation in a Nd phosphate glass laser," *Appl. Phys. Lett.*, Vol. 34, pp. 273-275, 1979.

[18]   S.A. Strobel, P.-T. Ho, C. H. Lee, and G.L. Burdge," Continuous wave mode-locked neodymium phosphate glass laser," *Appl. Phys. Lett.*, Vol. 45, pp. 1171-1172, 1984

[19]   L. Yan, J.D Ling, P -T Ho, and C.H. Lee, "Picosecond-pulse generation from a continuous-wave neodymium phosphate glass laser," *Opt Lett.*, Vol. 11, pp 502-503, 1986.

[20]   A.S.L. Gomes, W Sibbett, and J R Taylor, "Compression of Q-switched and mode-locked cw Nd YAG laser pulses," *IEEE J. Quantum Electron.*, Vol. QE-21, pp. 1157-1158, 1985.

[21] B. Zysset, W. Hodel, P. Beaud, and H.P. Weber, "200-femtosecond pulses at 1.06μm generated with a double-stage pulse compressor," *Opt. Lett.*, Vol. 11, pp. 156-158, 1986.

[22] I.N. Duling III, T. Norris, T. Sizer II, P. Bado, and G. Mourou, "Kilohertz synchronous amplification of 85-femtosecond optical pulses", *J. Opt. Soc. Am.*, Vol. B2, pp. 616-618, 1985.

[23] We are grateful to the Shanghai Institute of Optics and Fine Mechanics for the Nd phosphate glass slab

[24] E.P. Ippen and C V Shank, *"Techniques for Measurements,"* in *Ultrafast Light Pulses: Picosecond Techniques and Applications,* S. L. Shapiro, ed., New York: Springer Verlag, Berlin, pp. 85-88, 1977.

[25] D.W. Hall and M J. Weber, "Modeling gain saturation in neodymium laser glasses, "*IEEE J. Quantum Electron.*, Vol. QE-20, pp. 831-834, 1984.

[26] D.J. Kuizenga and A.E Siegman, "FM and AM mode-locking of the homogeneous laser - Parts I and II," *IEEE J. Quantum Electron.*, Vol QE-6, pp 694-715, 1970.

[27] A.E Siegman and D J Kuizenga, "Active mode-coupling phenomena in pulsed and continuous lasers," *Opto-Electron.*, Vol. 6, pp 43-66, 1974

[28] M.B Morris and T.J. McIlrath, "Portable high-resolution laser monochromator-interferometer with multichannel electronic readout," *Appl. Optics*, Vol. 18, pp 4145-4151, 1979.

[29] R.C. Eckardt, C.H. Lee, and J.N. Bradford, "Temporal and spectral development of mode locking in a ring-cavity Nd glass laser," *Appl. Phys Lett.*, Vol. 19, pp. 420-423, 1971.

[30] P. Mandel and N.B. Abraham, "Stability analysis of a bidirectional homogeneously broadened ring laser, "*Opt. Commun.*, Vol. 51 pp. 87-90, 1984

[31]   P. Lett, W. Christian, S. Singh, and L. Mandel, "Macroscopic quantum
        fluctuations and first-order phase transition in a laser," *Phys. Rev. Lett.*, Vol.
        47, pp. 1892-1895, 1981.

[32]   R.L. Fork, B.I. Greene, and C.V. Shank, "Generation of optical pulses shorter
        than 0.1 psec by colliding pulse mode locking," *Appl. Phys. Lett.*, Vol. 38, pp.
        671-672, 1981.

[33]   I.V. Tomov, R. Fedosejevs, and M.C. Richardson, "Unidirectional traveling
        wave operation of a mode-locking Nd glass ring laser," *Opt. Commum.*, Vol.
        21, pp. 327-331, 1977.

[34]   D.J. Kuizenga, *"Short-pulse oscillator development for the Nd:glass laser-
        fusion systems,"* IEEE J. Quantum Electron., Vol. QE-17, pp. 1694-1708, 1981.

[35]   G.F. Albrecht, M.T. Grune-sen, and D. Smith, *"An active mode-locked Q-
        switched oscillator using Nd^{3+} doped glass as the active medium,"* IEEE J.
        Quantum Electron., Vol QE-21, pp. 1189-1194, 1985.

[36]   See A. Yariv, *Quantum Electronics*, 2nd Ed. New York. John Wiley and Sons,
        1975 and references therein.

[37]   D. Strickland, P. Maine, M. Bowier, S. Williamson, and G. Mourou,
        "Picosecond Pulse Amplification Using Pulse Compression Techniques",
        Ultrafast Phenomena V, G.R. Fleming and A.E. Siegman, ed., New York
        Springer-Verlag, Berlin, pp. 38-42, 1986

[38]   P. Maime, D. Strickland, M. Bouvier, and G. Mourou, "Amplification of
        picosecond pulses to the terawatt level by chirped pulse amplification and
        compression", in *Digest of conference on Lasers and Electro-Optics*, Optical
        Society of America, Washington, D.C., 1987, paper FR2.

[39]   See W. Koechner, *Solid-State Laser Engineering*, New York: Spring Verlag,
        1976 and references therein

[40]   Unpublished.

[41] B. Zhou, T.J. Kane, G.J. Dixon, and R L. Byer, "Efficient, frequency-stable laser-diode-pumped Nd:YAG laser," *Opt. Lett.*, Vol. 10, pp. 62-64, 1985.

[42] W.J. Kozlovsky, T.Y. Fan, and R.L. Byer, "Diode-pumped continuous-wave Nd glass laser," *Opt. Lett.*, vol. 11, pp. 788-790, 1986.

[43] See "Digest of Conference on Lasers and Electro-Optics" (Optical Society of America, Washington, D.C., 1987).

[44] W.C. Scott and M. de Wit, "Birefringence compensation and TEM_{00} mode enhancement in a Nd:YAG laser," *Appl. Phys. Lett.*, Vol. 18, pp. 3-4, 1971

Figure Captions:

Figure 1:   Schematic of the cw actively mode-locked Nd phosphate glass laser
             oscillator. M1 - dichroic-coated plano-concave mirror with R ≈ 30 cm.
             M2 - R = 30 cm plano-concave mirror with HR coating. M3, M5 - plano
             mirrors with HR coating. M4 - plano mirror with a reflectance of 97%.

Figure 2:   Pulse widths observed at different pump powers. The solid squares
             are measured by a sampling oscilloscope; the circles are measured by
             autocorrelation.

Figure 3:   Sampling oscillogram of the cw mode-locked pulses. The combined
             response time of the detector and the sampling oscilloscope is 73 ps
             (FWHM).

Figure 4:   Autocorrelation trace of pulses from the cw mode-locked
             Nd phosphate glass laser. A Gaussian pulse shape is assumed. The 3 to
             1 ratio indicates that pulses are coherent.

Figure 5.   Spectrum of pulses of 7 psec pulse width. FWHM ≈ 5.5 A. The
             spectrometer has a resolution of 0.156 A/diode at 1µm.

Figure 6   Simultaneous mode-locking and relaxation oscillations when the pump
             beam outside the cavity is chopped. Although the individual mode-
             locked pulses cannot be resolved, the envelope relaxation oscillations
             can be seen clearly

Figure 7   Schematic of the linear Nd phosphate glass regenerative amplifier. M1
             - plano mirror with dichroic coatings. M2 - plano mirror with HR
             coating. L - lens with f = 8 5 cm. BS1 - beam splitter with reflectance
             of ~10% at 1 054 µm. BS2 - beam splitter with reflectance of ~50% at 514
             nm

Figure 8   Streak camera picture of the amplified pulse. The pulse width is 50 ps
             (FWHM).

Figure 9:   Laser output as observed through mirror M2 of the linear cavity. The
             Pockels cell and the quarter-wave plate are removed. Outputs for four
             cases are observed with or without the intracavity polarizer for either
             chopped or cw pumping. For the chopped pumping case the plotted
             power was measured about 600 µs after initial lasing.

Figure 10:   Schematic of the thermal birefringence compensated Nd phosphate
             glass regenerative amplifier. The two Nd phosphate glass slabs are the
             same (Schott LG 760). M1 - dichroic-coated plano-concave mirror with
             R = 10 cm. M2 - dichroic-coated plano-concave mirror with R = 30 cm
             M3 - plano mirror with HR coating. BS1 - beam splitter with R~10% at
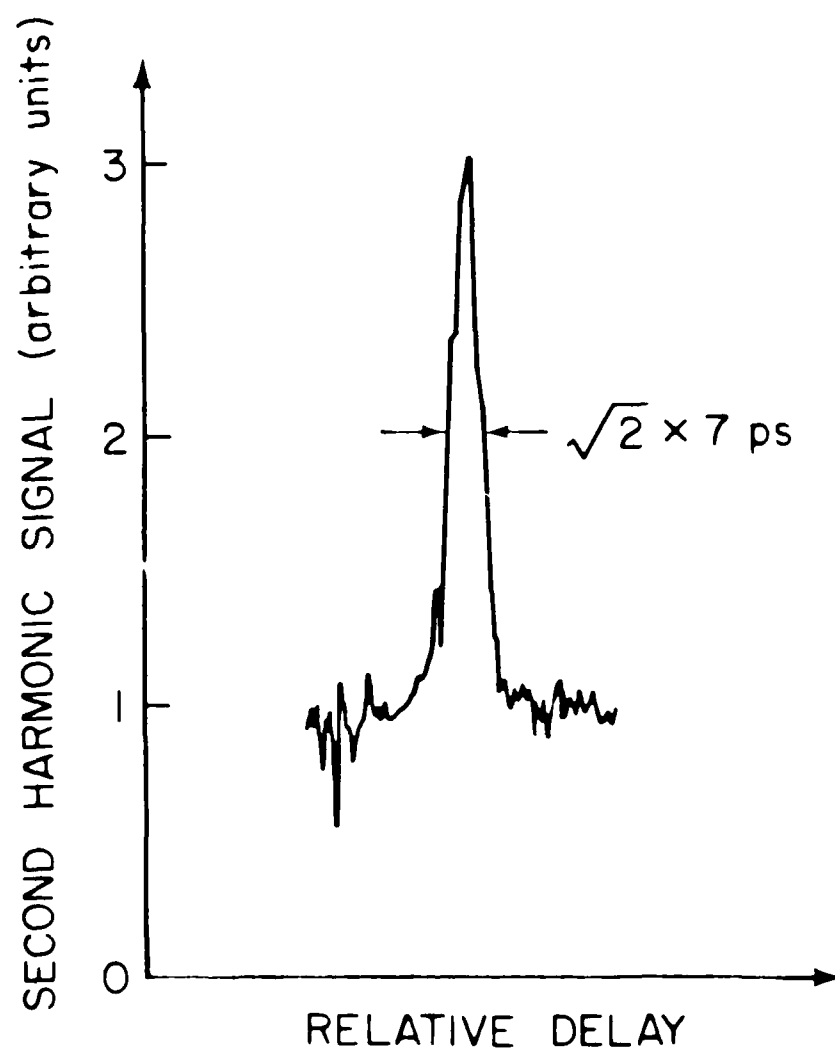   1 054 µm and R~50% at 514 nm.
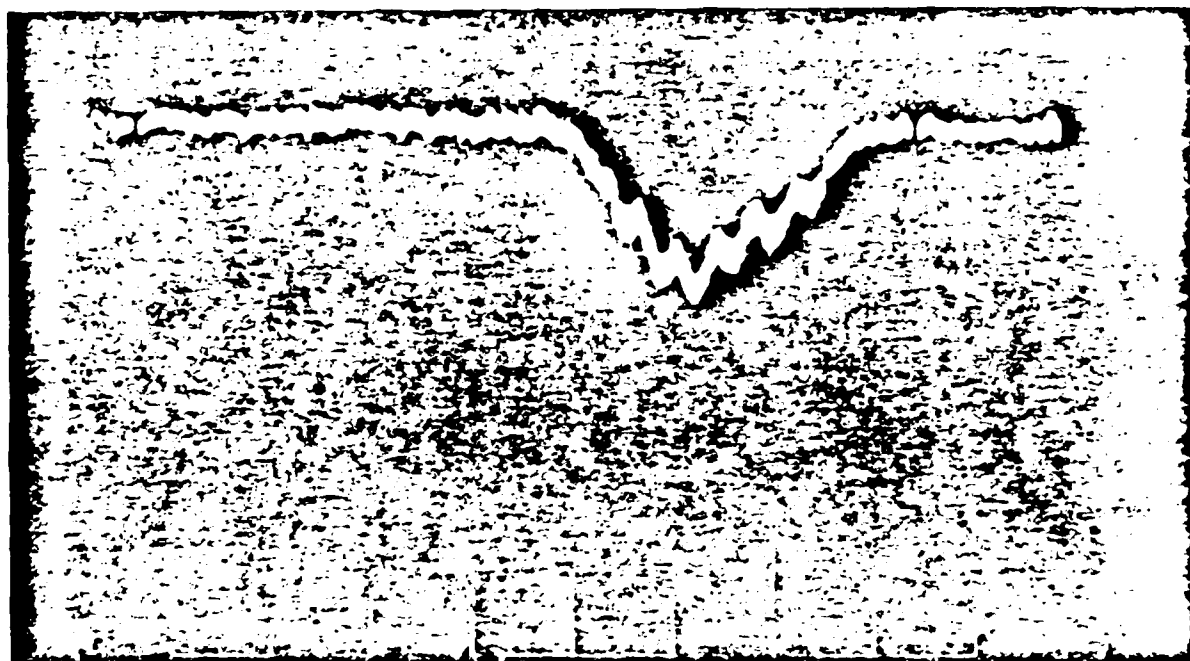
M5

M4

1054 nm

Acousto-optic Modulator

Nd:Phosphate Glass Slab

M2

M1

M3

CW Ar⁺ Laser

514 nm

Figure 1

Figure 3

├──────────── 33 Å ────────────┤

FWHM ≈ 5.5 Å

Figure 6

514 nm CW Ar$^+$ Laser

CW Mode-Locked Nd:Phosphate Glass Laser

BS 2

Amplified Pulses

$\frac{\lambda}{2}$ Plate

BS 1

M1 L M2

Nd:Phosphate Glass   Polarizer $\frac{\lambda}{4}$ Plate   Pockels Cell

50 ps

514 nm
Pump Beam

BS 2

Nd — Nd:Phosphate
Glass

M2

Nd

Nd

MI

Quartz Rotator   Polarizer $\frac{\lambda}{4}$ Plate   Pockels Cell

BS1

Amplified
Pulses

M3

CW Mode-Locked
Nd:Phosphate Glass Laser

$\frac{\lambda}{2}$ Plate

APPENDIX 7
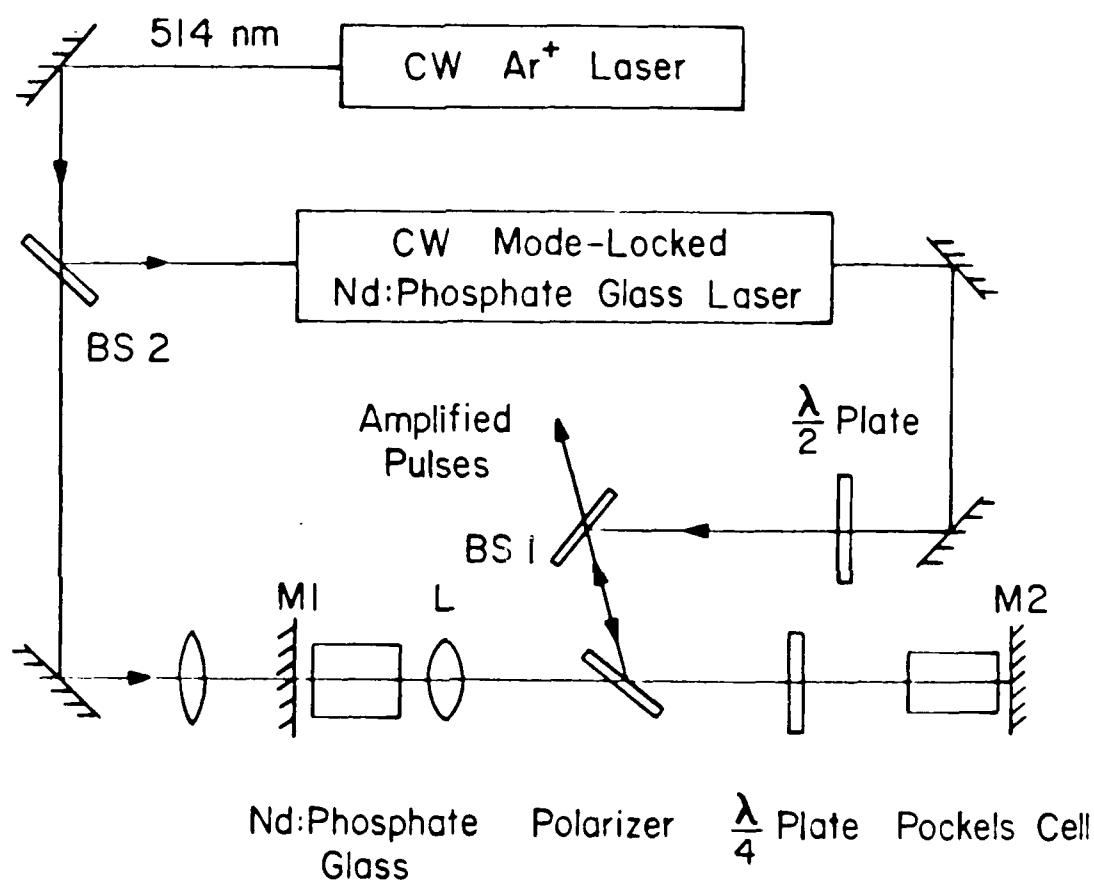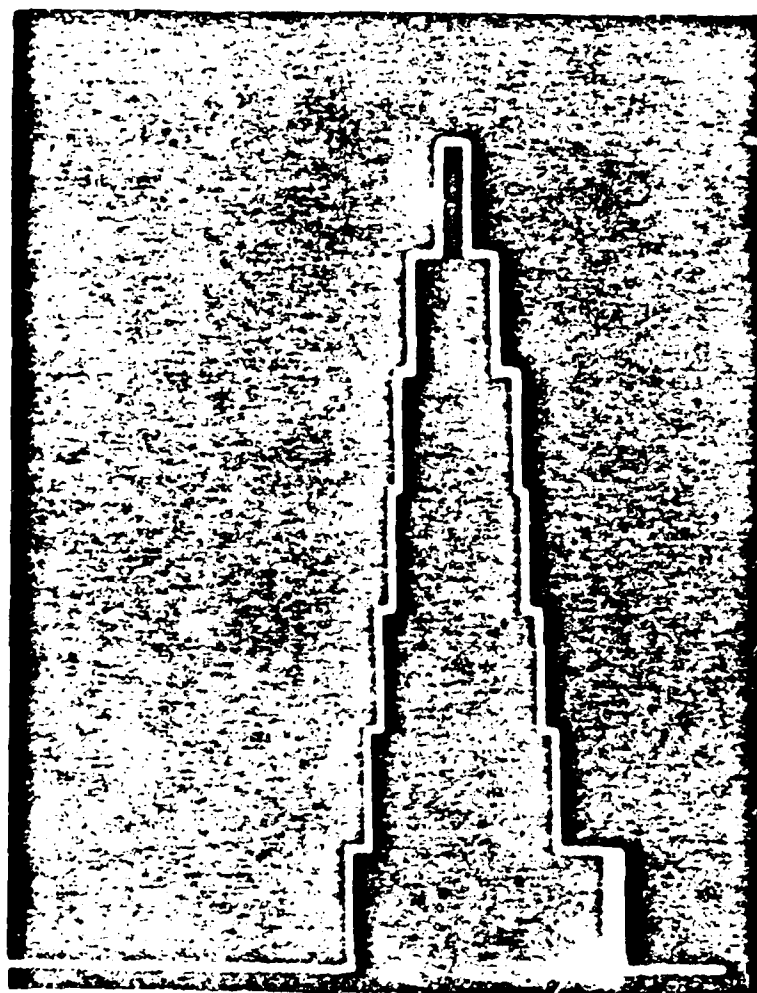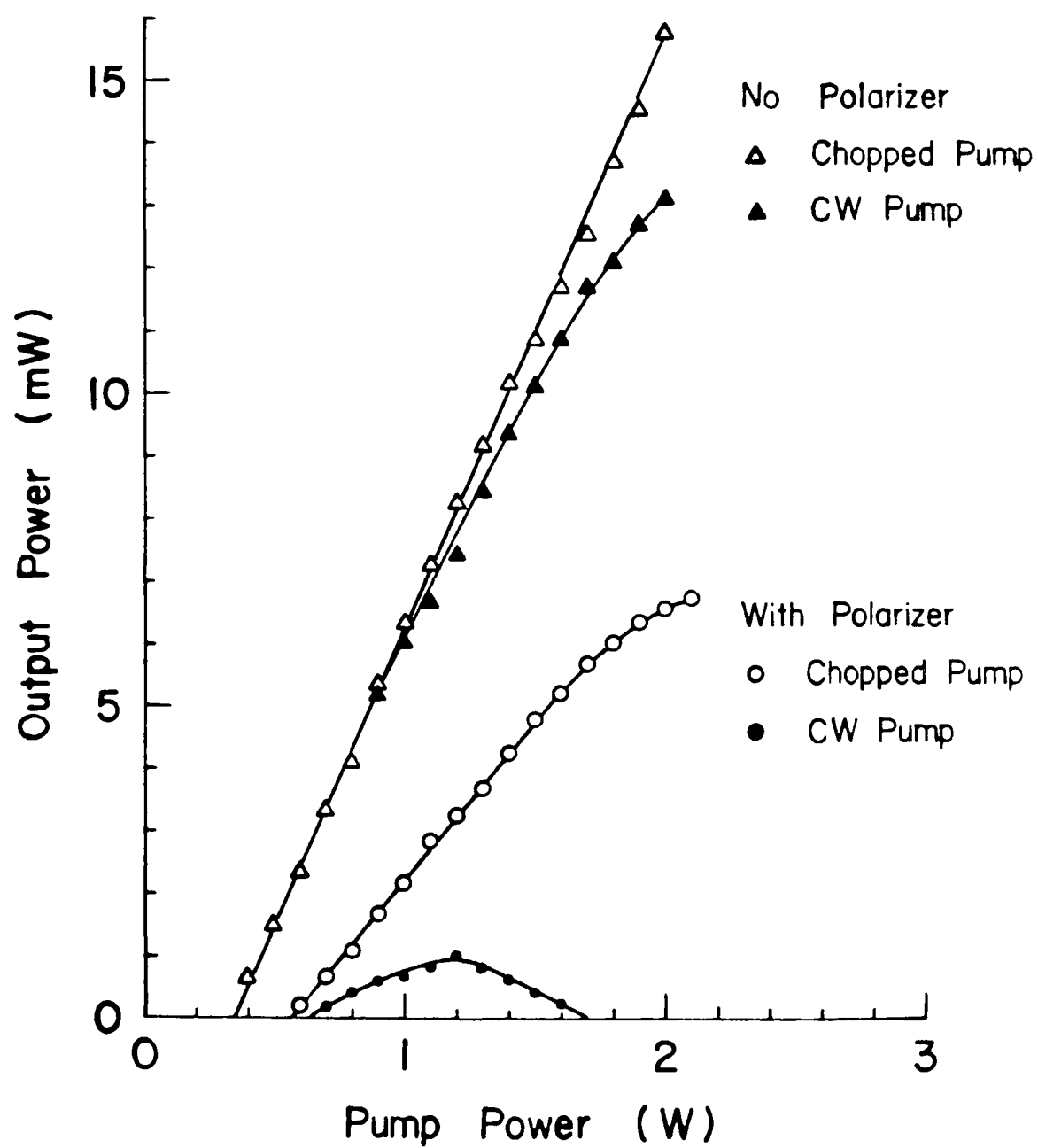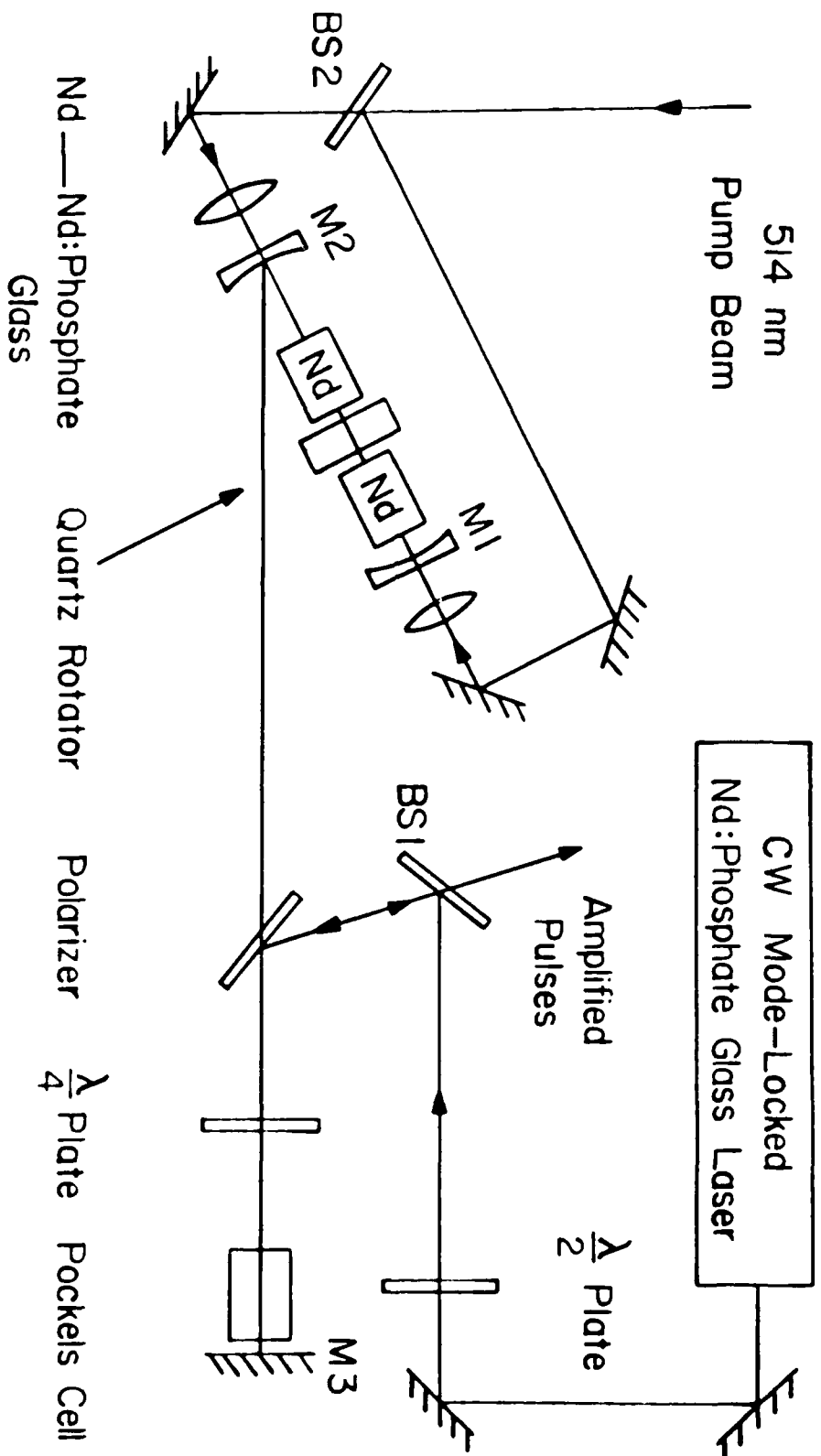
Investigation of a New Optoelectronic CW Microwave Source

CHRISTOPHER J. CLARK, EVE A. CHAUCHARD, KEVIN J. WEBB, MEMBER, IEEE,
KAWTHAR A. ZAKI, CHI H. LEE, SENIOR MEMBER, IEEE, PENELOPE POLAK-DINGLES,
HING-LOI A. HUNG, AND HO C. HUANG

Abstract—A new 10-GHz microwave source which utilizes picosecond photoconductors is presented. Experimental results are given, including details of a comprehensive noise study. Such a source can be extended to millimeter-wave frequencies, with application to monolithic active phased array antenna elements, high speed data processing, and transceivers.

INTRODUCTION

THE PRECISE generation and control of microwave and millimeter-wave signals using integrated technology is essential for the next generation of high-speed broad-band systems. It is desirable to utilize optoelectronic components where possible for such applications as microwave and millimeter-wave signal processing, receivers/transmitters, and phased array antennas. We now have at our disposal optoelectronic devices that work in the picosecond time domain. The trend is toward a class of devices which integrate optics into electronic functions. We classify this class of devices into the category of picosecond optical electronics, which combines the fields of optics and electronics [1]–[3]. The link for these two fields is picosecond photoconductivity [1].

The picosecond photoconductivity effect is the generation of an ultrashort photo-current signal in a photoconductor when it is illuminated by an ultrashort optical pulse. For example, 8-femtosecond (fs) optical pulses have been observed [2]. The unique feature of the picosecond optical device is its ability to generate low-noise electronic pulses synchronized with the optical pulses. For frequencies through Ka-band, a high-speed microelectronic amplifier, utilizing high electron mobility transistors (HEMT's), may be integrated with the photoconductor switch. Dispersion in microstrip interconnects will degrade the pulse shape. Therefore, for relatively large distances, it is necessary to convert the electrical signals back

into the optical form. Thus, a technology for conversion between optical and electrical waveforms and vice-versa is needed. Electrical pulses can be converted into optical pulses by: 1) electrooptic modulation in an optical channel waveguide, or 2) direct modulation of a laser diode by the pulse current.

The general class of switching devices based on the picosecond photoconductivity effect has received considerable attention recently [1]. The photoconductivity effect is the long wavelength limit of a more general phenomena in which the complex dielectric constant of the semiconducting medium is modified by the introduction of an optically induced electron-hole plasma. When the dimension of the plasma region is much smaller than the wavelength of the electrical signals to be controlled, the plasma region may be regarded as a lumped circuit element. Most semiconductor switches are in this category and they are regarded as conductive mode switches.

Ultrafast optoelectronic switching is an important application for conductive switches. The devices can be categorized into low and high voltage applications. In the low voltage application, the device is used as a high speed optical detector or fast sampler. The important characteristics are fast rise and decay times for the electrical signal. This generally necessitates a short carrier lifetime, even though this results in the disadvantage of low mobility. In the high voltage application the device is used as a jitter-free switch with extremely fast (a few picoseconds) turn-on time [3]. We have demonstrated the high voltage switching using $Cr:GaAs$, $CdS_{0.5}Se_{0.5}$, and insulating diamond.

The rise time of the photoconductive signal can approach the rise time of the optical pulse, which can be on the order of 10 fs (terahertz spectral components). The electrical pulse fall time is primarily determined by the carrier lifetime, which can be engineered to be as short as 1 ps.

There are a large number of devices which can be based on the picosecond photoconductivity effect. They include switches, gates, samplers, electronic pulse function correlators, A/D converters, optical detectors, dc to RF converters and coherent microwave/millimeter-wave generators. Such fast photoconductors can handle high power, are scalable (large and submicron sizes), have a large dynamic range, and can be monolithically integrated with
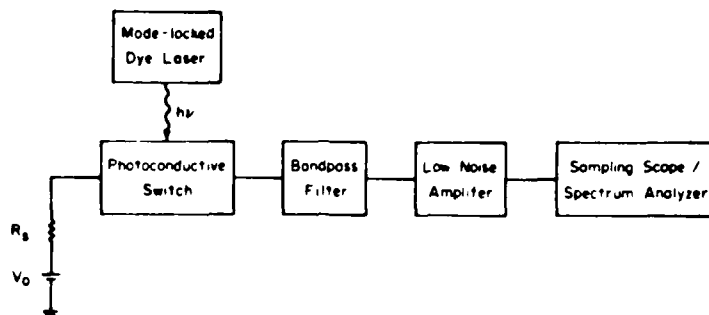
Fig 1. Basic experimental setup for generating CW microwave signals
from a mode-locked laser.

microelectronic devices. These features lend the device to applications such as: high data rate signal processing, high speed detectors, streak camera triggering, millimeter-wave phase shifting and modulating, ultra-short high power pulse generation, microwave and millimeter-wave sources, and on-chip picosecond diagnostics. A potentially powerful application for the device when used as a coherent CW source is in a phased array antenna. Optical techniques for feeding arrays have received considerable attention recently [4]-[7]. The central issue is to provide the correct phase and amplitude excitation at each element of the array in a manner which allows rapid scanning. A photoconductive switch with an appropriate filter and amplifier could be placed at each element in the array. The phase of excitation can then be controlled optically. Such an array of active elements can be monolithically integrated. The picosecond photoconductor can also be used to realize a pulse code modulator (PCM) by switching a microwave/millimeter-wave signal at appropriate intervals. Such a system permits very high modulation rates.

We have demonstrated earlier the generation of 3-GHz CW signals by the pulse excitation of a resonant cavity [8]. The generation of short pulses of microwave signals has been reported [9]-[11]. Also, a 3-GHz CW signal has been generated by using a mode-locked krypton-ion laser with both an avalanche photodiode and an optoelectronic switch [12]. In [13], a technique involving the FM sideband injection locking of a laser diode has been used to generate a 35-GHz CW signal. This was done by beating two longitudinal modes of a diode laser in a high-speed p-i-n detector. This technique requires accurate temperature stabilization of the lasers and provides a signal level of −53 dBm.

This paper will elaborate on the realization of a 10-GHz CW microwave source using the photoconductivity effect. An advantage of this technique is that the components required are relatively easy to obtain and use. The technique requires a minimum number of components: a source of short optical pulses (a mode-locked laser), a picosecond optical switch, a microwave filter, and an amplifier. Each of these components have the flexibility of being reduced in size so that the entire configuration may be integrated onto a single substrate. This will enhance the overall performance by minimizing the detrimental effects of disper-

sion, connectors, and cables. The output power and stability of the signal generated by this technique are the most critical factors in determining its applicability. The short term stability of the source is of particular importance and has not previously been considered in detail for this application. Methods for increasing the power level and improving the amplitude and frequency stability of the output signal are discussed.

EXPERIMENTAL SETUP

The experimental configuration for the generation of CW microwave signals with picosecond photoconductors is shown in Fig. 1. A synchronously pumped dye laser operating at 590 nm is used to obtain 3-ps FWHM optical pulses at a repetition rate of 100 MHz. These pulses are applied to a biased photoconductive switch. The switch may be designed such that the output electrical pulses have rise times that are limited by the rise time of the optical pulse. The spectral components produced at the switch output extend up to tens of gigahertz and are spaced every 100 MHz, corresponding to the harmonics of the pulse train generated. The switch is matched to 50 Ω and fed to a narrow-band bandpass filter. The passband of this filter is narrow enough so that only a single spectral component will be present at the output. The low noise amplifier provides the signal with gain so that the signal may be analyzed on a sampling oscilloscope.

This setup is also used to measure the frequency stability of the CW signal generated. This is done by measuring the phase noise on the spectral components with the spectrum analyzer. The noise on the CW signal generated results primarily from the jitter of the optical pulses generated by the mode-locked laser. Since the picosecond switch introduces negligible jitter in comparison, this setup may be used as a diagnostic tool for the operation of the laser system. Both AM and FM noise in the optical pulse train appear as noise sidebands on each spectral component. The large number of spectral components permit the observation of the relative amount of AM and FM noise produced by the laser system as a function of the harmonic number. Each spectral component may be considered as a signal obtained by frequency multiplying the fundamental component by its corresponding harmonic number. The AM noise remains constant with har-

monic number but FM noise is proportional to the square of the harmonic number [14]. This statement is correct for an ideal frequency multiplication process where the harmonic number is considered as the multiplication factor. The AM and FM noise produced by the laser will correspond to amplitude and phase fluctuations in the CW signal generated.

THE PICOSECOND PHOTOCONDUCTIVE SWITCH

The basic photoconductive switch is shown in Fig. 2. It consists of a microstrip transmission line structure with a small gap which separates the input from the output. The structure is fabricated on a semi-insulating photoconductive substrate. In this work a Cr-doped GaAs substrate with a 100-μm gap was used. When the gap is in the dark state (no optical illumination), the high resistivity of the semi-insulating substrate will provide a path of extremely low conductance. This high impedance state gives the switch excellent noise rejection properties since the dark current generated by the bias voltage is extremely low. When an optical pulse is focused on the switch gap, a temporary electron-hole plasma is formed, connecting the input to the output. This action produces an electrical pulse with a rise time approaching the optical pulse rise time and a fall time related primarily to the carrier recombination time. The microstrip transmission line has a characteristic impedance of 50 Ω, which allows for standard SMA input and output connections which minimize reflections and pulse broadening.

The photoconductive switch has been modeled by Auston [15] in terms of macroscopic circuit elements. The model consists of a conductance $G(t)$ in parallel with a capacitance C, which are embedded in a transmission line structure. Noting that this simplified model has an inherent RC time constant, the geometry and dimensions of the gap are critical for high speed switch operation. The capacitance of a 100-μm gap embedded in a 50-Ω microstrip line with a relative permittivity of 10 is approximately 25 fF [16].

A general expression for the switch conductance $G(t)$ was obtained in [15] by considering the dissipated power in the photoconductor and using Ohm's law. The conductance consists of two parts: the constant dark conductivity G_0, and a time varying conductance $g(t)$. To obtain an expression for $g(t)$, the electric field distribution in the gap must be known. The field distribution in the gap is a function of both the switch electrode geometry and the distribution of the optically induced charged carriers. When low level optical illumination is applied to the gap, the carrier concentration is low compared to the equilibrium concentration so that $0 < g \ll G_0$ and the field distribution is basically unchanged. An expression for the case of low level optical injection is given by [15]:

$$G(t) = G_0 + g(t)$$

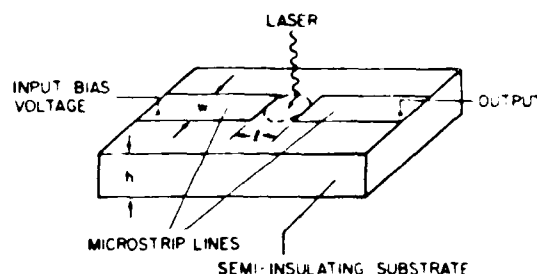$$g(t) = (1 - R) \frac{e}{h\omega} \frac{n(t)\mu_n + p(t)\mu_p}{l^2} W_p \quad (1)$$

Fig. 2 Picosecond photoconductive switch

where R is the reflectivity of the semiconductor surface, e is the charge of an electron, ω is the optical angular frequency, $n(t)$ and $p(t)$ are the time varying electron and hole concentrations, μ_n and μ_p are the electron and hole mobilities, l is the width of the gap, and W_p is the total energy in the optical pulse. When high level optical illumination is applied to the gap, the induced carrier concentrations are much higher than the equilibrium concentrations, so that $g \gg G_0$. A large space charge field is created as the generated electrons and holes drift apart. The addition of this space charge field completely alters the equilibrium electric field distribution. The distribution of the field may be calculated by solving Poisson's equation if the charge distribution and dynamics are known.

If the dimensions of the gap are selected to achieve the rise time desired, a simpler model may be used to predict the switch response. Neglecting the gap capacitance, the *equivalent circuit reduces to a simple time varying conductance inserted in a transmission line of characteristic impedance Z_0*. Transmission line analysis may be applied to obtain the solution for the transmitted voltage wave as

$$V_{out} = \frac{Z_0 V_{in}}{2Z_0 + 1/G(t)} \quad (2)$$

where V_{in} is the input bias voltage. If we assume constant carrier mobilities, $G(t)$ is proportional to the carrier concentrations, $n(t)$ and $p(t)$. Then for small concentration carrier values, V_{out} is proportional to $G(t)$. When the carrier concentration becomes large, V_{out} will saturate at $V_{in}/2$. An electron-hole pair is generated almost simultaneously with the absorption of a photon from the optical beam. Assuming the carrier concentration is low, the output waveform will emulate the leading edge of the optical pulse. Slow carrier recombination times cause an extended fall time in the output waveform. When a laser pulse with a duration which is much shorter than the carrier recombination time is applied to the switch, the output will resemble a single sided exponential pulse. Fig. 3 shows the output of the 100-μm Cr:GaAs switch with an input bias voltage of 15 V. The gap of the switch was illuminated with 3-ps FWHM pulses with an average power of 280 mW. The pulses occur every 10 ns, corresponding to the 100-MHz optical pulse repetition rate of the laser. The measured pulse fall time is approximately 1 ns.

Fourier analysis may be used to show that the band-

Fig. 3. Output waveform from a Cr:GaAs switch with a 100-μm gap and a 15-V bias when illuminated with 6 ps FWHM optical pulses with an average power of 280 mW.
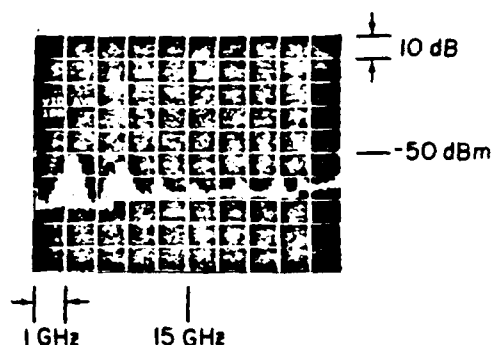

Fig. 4. Averaged power spectrum of the waveform shown in Fig. 3.

Fig. 5. Circular waveguide coupled cavity filter

width of the power spectrum of a pulse train is extended by decreasing the pulse rise and fall times. The rise time of the electrical pulse generated by the switch is limited by the laser's optical pulse rise time (approximately 3 ps). To achieve a short pulse fall time, it is necessary to use semiconductor materials which have a fast carrier recombination time. The length of the microstrip line must be kept to a minimum in order to prevent the degradation of the pulse rise time that results from dispersion. Fig. 4 shows the averaged output power spectrum produced by the waveform shown in Fig. 3. The spectral components are spaced every 100 MHz, corresponding to the Fourier series representation of the periodic pulse train. The envelope of the discrete spectrum is the Fourier transform of the pulse shape. The 1.6-GHz oscillatory nature of the envelope is most likely due to resonance effects caused by the photoconductor packaging and is being investigated further. Fig. 4 shows that the power spectrum extends to at least 20 GHz.

THE COUPLED CAVITY FILTER

A single frequency 10-GHz signal may be obtained if a bandpass filter is used to select only the 10-GHz spectral component from the switch output spectrum. The specifications for this filter are stringent in terms of the required rejection of the adjacent harmonics and low passband insertion loss. A filter with at least 30 dB of stopband insertion loss is required to sufficiently reject the two adjacent harmonics which are 100-MHz offset from the 10-GHz spectral component. The passband insertion loss of the filter must be kept to a minimum since the power level of the 10-GHz harmonic is approximately −50 dBm.
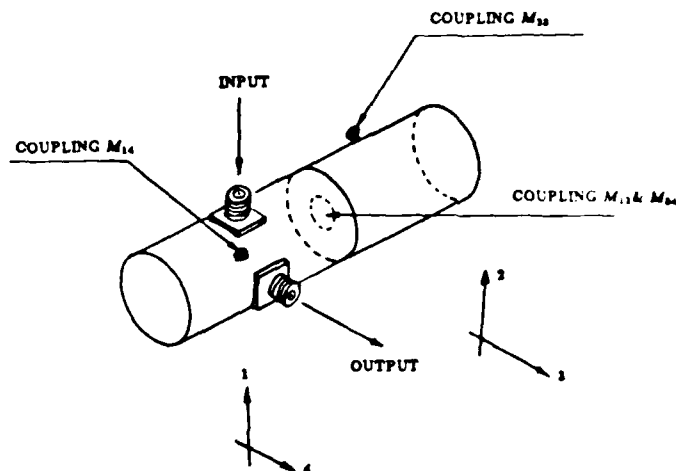
These requirements are most effectively met through the use of a narrow-band coupled waveguide filter with sharp selectivity [17].

The filter designed for this experiment is shown in Fig. 5. It consists of two cylindrical cavities which are magnetically coupled through a hole in their common wall. Input and output coupling for the filter is accomplished by using probes which are located to excite and detect the dominant TE_{111} mode. By introducing a screw at a 45° angle to the excited mode, each cavity will support two independent modes with orthogonal polarizations. The second mode is forced to resonate so that the electric field boundary condition on the conducting screw is met. The degree of coupling between these orthogonal modes is determined by the depth of the coupling screw. Two additional screws are used in each cavity to provide tuning of the resonant frequency of each mode. Each resonant mode in the cavity represents an equivalent single tuned circuit. Since each cavity resonates with two independently tunable modes, this filter may realize a four pole elliptic function response.

The filter was constructed with brass and tuned to have a center frequency of 9.78 GHz and a 3-dB bandwidth of 135 MHz. The maximum passband insertion loss was measured to be 1 dB and the stopband attenuation at the first harmonic to be rejected was approximately 30 dB. A large spurious response was measured at 10.88 GHz. Calculations have verified that this response corresponds to a resonance of the TM_{110} mode. The use of a cylindrical cavity mode chart [18] shows that this is the first mode that will resonate after the desired TE_{111} mode.

The instantaneous power spectrum of the switch output and the coupled cavity filter output is shown in Fig. 6. It was necessary to utilize a low-pass filter with a cutoff frequency of 10.3 GHz to attenuate signals passed by the spurious response.

THE LOW NOISE MESFET AMPLIFIER

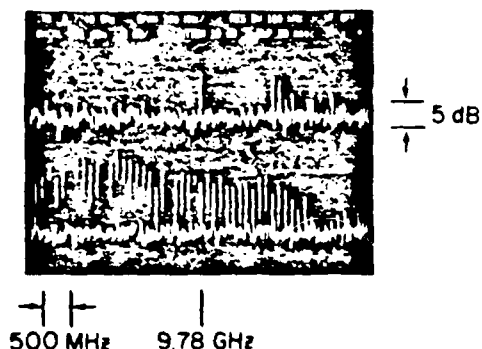Since the level of the 9.78-GHz component is −50 dBm, amplification is necessary to detect the waveform

Fig. 6. Instantaneous power spectrum of the switch output (bottom trace), and coupled cavity filter output prior to low-pass filtering (top trace)

Fig. 7. Output of the GaAs MESFET amplifier when using both the coupled cavity and low pass filters. Vertical scale: 10 mV/larger div, horizontal scale: 50 ps/larger div.

with a conventional sampling oscilloscope. In the experiment, a three-stage GaAs MESFET amplifier was used. At 9.78 GHz the amplifier provides a power gain of 30 dB, a 1-dB compression point of +7 dBm, and a noise figure of 2.2 dB. The 1-dB compression point can be improved by adjusting the bias of the last stage. The amplifier is broad-band, providing at least 20 dB of gain from 8.5 to 11.5 GHz. Isolators were used at the input and output of the amplifier to minimize termination effects. The sampling oscilloscope display of the 9.78-GHz CW signal obtained is shown in Fig. 7. This waveform indicates that the jitter of the microwave signal is very small.

FREQUENCY STABILITY CHARACTERIZATION

The 10-GHz signal generated by this technique must satisfy general stability requirements so that it may be used in the applications discussed in the introduction. We may apply classical frequency stability measurement techniques [20] to obtain a quantitative measure of the signal's short term stability. The short term stability is most easily evaluated by using the frequency domain description of the signal. This is done by representing the signal output as a carrier modulated by AM and FM noise. The discrete noise processes cause discrete spurious noise sidebands while random noise processes create a continuous noise pedestal. For most oscillators, the AM noise sidebands are negligible in comparison to the FM sidebands. This assumption may be validated by using a square law detector and measuring the power translated to baseband [21]. We are particularly interested in calculating the rms time jitter by considering the FM noise.

Extreme care must be exercised when calculating the total rms phase or timing jitter in an oscillator's output signal. The most common method for determining the rms jitter is to use the signal's RF power spectrum. Since there are possible pitfalls in the use of this method, a thorough analysis of the power spectral density of an angle-modulated carrier is provided. The RF power spectrum of a carrier which is angle-modulated by both continuous and discrete signals is obtained by Middleton [22]. Application of Middleton's results to noise in microwave transmitters is discussed by Ashley et al. [23]. The relationships given in these references are used as an aid in

understanding the validity of the RF spectrum method of calculating the total rms jitter.

When the AM noise is negligible, the oscillator output may be written in terms of an angle-modulated carrier

$$v(t) = A_0 \cos\left(2\pi f_c t - \Phi(t)\right) \qquad (3)$$

where A_0 is the peak carrier amplitude, f_c is the carrier frequency, and $\Phi(t)$ is the instantaneous phase fluctuation, sometimes referred to as phase noise. For most oscillators, $\Phi(t)$ is a combination of both discrete, deterministic noise processes and continuous, random noise processes. For sinusoidal modulation, the instantaneous phase fluctuation is

$$\Phi(t) = \mu_{\phi m} \cos\left(2\pi f_m t\right) \qquad (4)$$

where $\mu_{\phi m}$ is the modulation index (or peak phase deviation) and f_m is the frequency of the sinusoidal noise process. Middleton [22] has derived the power spectral density for sinusoidal phase modulation as

$$S_{RF}(f) = \frac{A_0^2}{2} \sum_{p=0}^{\infty} J_p^2(\mu_{\phi m}) \left\{ \delta[f - (f_c + pf_m)] \right. $$
$$\left. + \delta[f - (f_c - pf_m)] \right\} \qquad (5)$$

where J_p is the pth order Bessel function of the first kind. The spectrum obtained for sinusoidal angle modulation at a frequency f_m may be recognized as consisting of discrete sidebands spaced at multiples of f_m about the carrier. The power in the carrier and each of the sidebands is determined by the value of $\mu_{\phi m}$. Since $\mu_{\phi m}$ is the argument of the Bessel functions in this expression, angle modulation is a nonlinear process. The nonlinearity of the angle-modulation process may also be seen by computing the power spectral density of a multitone angle-modulated carrier. When more than one sinusoid simultaneously angle-modulates a carrier, sidebands of different amplitudes are produced from the case of the superposition of separate sinusoidal modulation signals. Additional sidebands are also produced at offset frequencies corresponding to the beat frequencies of the modulating tones. To obtain the rms jitter of the signal, it is desired to compute $S_{\phi m}(f)$, the baseband power spectral density of the modulating process. The nonlinear behavior of the angle modulation process creates difficulties in computing $S_{\phi m}(f)$ from $S_{RF}(f)$.

The computation of $S_{\phi m}(f)$ from $S_{RF}(f)$ can be simplified when the modulation index is very small. The approximations

$$J_0(\mu_{\phi m}) \approx 1$$

$$J_1(\mu_{\phi m}) \approx \frac{\mu_{\phi m}}{2}$$

$$J_2(\mu_{\phi m}),\ J_3(\mu_{\phi m}),\ J_4(\mu_{\phi m}) \cdots \approx 0 \qquad (6)$$

are valid for $\mu_{\phi m} \ll 1$. These approximations allow us to treat angle modulation as a linear process when $\mu_{\phi m}$ is extremely small. For this case, the power spectral density can be approximated as [23]

$$S_{RF}(f) \simeq \frac{A_0^2}{2}\delta(f - f_c) + \frac{A_0^2}{4}S_{\phi m}(f - f_c). \qquad (7)$$

Therefore, for small $\mu_{\phi m}$, the power spectral density of an angle-modulated carrier will consist of a discrete spike representing the carrier along with $S_{\phi m}(f)$ which is translated from baseband to the carrier frequency f_c.

An HP 8566B Spectrum Analyzer was used to accurately measure $S_{RF}(f)$ for each of the spectral components shown in Fig. 4. We found that (7) was valid for computing $S_{\phi m}(f)$ at frequencies as low as 30 Hz for the spectral components between 1 and 4 GHz. To compute the rms jitter, the single sideband phase noise spectral density $L(f)$ is used since it may be measured directly with the spectrum analyzer. $L(f)$ is defined as

$$L(f) = \frac{P_{ssb}(f)}{P_c} \qquad (8)$$

where $P_{ssb}(f)$ is the single sideband phase noise power in a 1-Hz bandwidth at a frequency f offset from the carrier and P_c is the carrier power. For the small modulation index case, (6) and (7) may be used to obtain

$$L(f) = \tfrac{1}{2}S_{\phi m}(f) = \tfrac{1}{2}\Delta\theta_{rms}^2(f) \qquad (9)$$

where the rms phase deviation $\Delta\theta_{rms}$ is obtained from the peak phase deviation $\mu_{\phi m}$. The rms time jitter due to modulating noise at an offset frequency f_m can be written in terms of the carrier and sideband signal powers measured in a 1-Hz bandwidth as

$$\Delta t_{rms}(f_m) = \frac{1}{\pi f_c}\sqrt{\frac{P_{ssb}(f_m)}{2P_c}}. \qquad (10)$$

In order to calculate the total rms jitter in the output signal, it is helpful to consider the continuous noise pedestal as a large number of sections of bandwidth B_N [21]. The small angle-modulation index approximation allows each section to be treated as an equivalent noise source with its mean frequency located at the center of its noise band. When the small modulation index approximation holds, angle-modulation may be treated as a linear process so that the principle of superposition may be applied. This allows the computation of the total rms time jitter in

the signal $\Delta t_{rms T}$ by making a summation of the equivalent noise sources on a power basis. The total rms time jitter calculated over the sideband frequency span between f_1 and f_2 is

$$\Delta t_{rms T} = \sqrt{\sum_{f_m = f_1}^{f_2}\left[\Delta t_{rms}(f_m)\right]^2}. \qquad (11)$$

For the continuous noise process case, this summation becomes an integral. The frequency span must be specified when using this method for calculating the total timing jitter, since the answer will depend on the amount of sideband power included. In our measurements, the resolution bandwidth and phase noise of the spectrum analyzer limited the lower frequency bound f_1 to 30 Hz. The upper frequency bound f_2 was limited to approximately 5 kHz.

It is now possible to discuss results obtained for signals produced by the optoelectronic source. The first measurements made were used to check if (7) could be applied to the spectral components of the switch output. Using the fact that the Δt_{rms} is a constant for each spectral component, the phase-noise to carrier power ratio for a given sinusoidal component of the noise is given by

$$\frac{P_{ssb}(f_m)}{P_c} = 2\left[\pi n f_0 \Delta t_{rms}(f_m)\right]^2 \qquad (12)$$

where n is the harmonic number and f_0 is the fundamental frequency (the pulse repetition rate). Phase-noise to carrier power ratio measurements were made for several harmonics of the switch output spectrum at an offset frequency of 150 Hz from the carrier. Fig. 8 shows these results plotted on a log–log graph, compared to a line with a slope of 2. The square-law dependence of the phase noise power to carrier power ratio for a pulse train can be shown by applying results obtained in [24] for pulse position modulation with a sinusoidal modulation signal. The large deviation from the theory below 1 GHz provides evidence that a large amount of AM noise is present on the output signal. The large amount of AM noise is most likely due to the Dye laser jet. To decrease the amount of AM noise, a compressed Nd:YAG laser such as the type described in [25] should be used as the source of the picosecond optical pulses. The compressed Nd:YAG laser system also has better frequency stability than a synchronously pumped Dye laser system because there is only one laser contributing to the FM noise. Further AM noise suppression may be obtained by applying AM stabilization (commercially available) to the Nd:YAG laser.

The total rms time jitter may be computed despite the presence of AM noise. Fig. 8 shows that for the harmonics above 1 GHz, the phase noise dominates over the AM noise. This allows us to use (11) to compute the total rms time jitter of the source. Fig. 9 shows the close in phase noise of the 9.78-GHz component as measured by the spectrum analyzer. Note that there is a continuous noise pedestal as well as discrete sidebands located at multiples of the 60-Hz power line frequency. Both types of noise
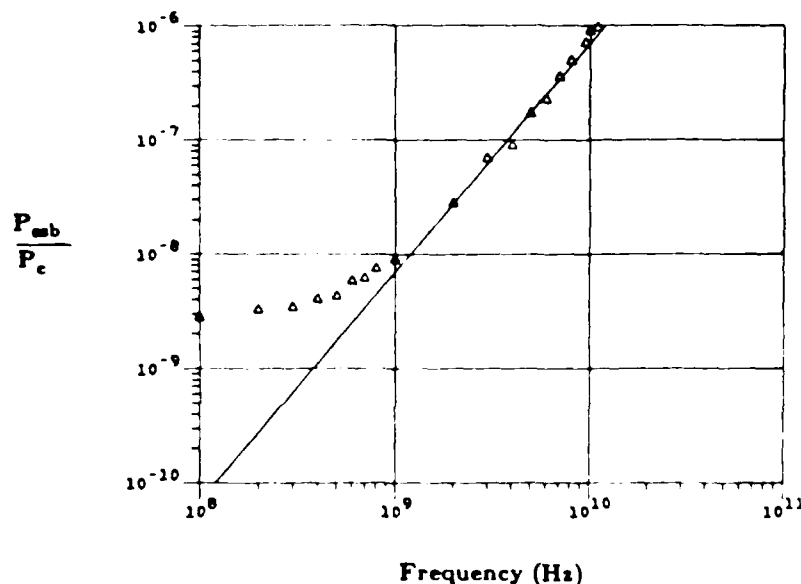
Frequency (Hz)

Fig 8 Square-law dependence of phase noise to carrier power ratio for n = 1 to 110 These measurements were made at a frequency offset of 150 Hz from the carrier.

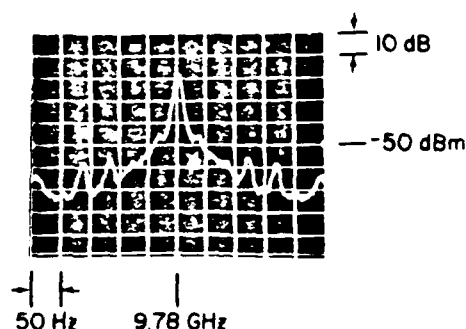

Fig 9. Power spectrum showing close-in phase noise of the 9.78-GHz spectral component. Both continuous and discrete noise processes may be measured.

processes contribute to the total rms time jitter and must be computed separately. To compute the contribution of jitter due to the continuous noise pedestal, the phase noise to carrier power ratio was measured for several offset frequencies and plotted for the 4-GHz spectral component as shown in Fig. 10. The data seems to follow a $1/f^2$ and a $1/f^3$ dependence as indicated by the lines drawn through the data. This data was integrated with f_1 = 30 Hz and f_2 = 5 kHz to obtain a value of Δt_{rms} of 1.81 ps. As a check on the validity of the small modulation index approximation, Hewlett Packard [19] suggests using a 10-dB/decade line with a y-axis intercept of -30 dB as shown above the data points in Fig. 10. The small modulation index approximation is valid for measured phase noise to carrier power ratio data below this line as it indicates a maximum peak phase deviation 0.2 rad when integrated over any one decade of frequency. The contribution from the deterministic noise processes was computed to be 3.03 ps giving a total rms time jitter of 3.53 ps for a CW signal produced by any of the spectral components. Most of these discrete noise processes could be

detected at the output of the RF source driving the Nd:YAG mode-locker unit. These undesired spurious responses may be reduced by utilizing a more stable RF source for the mode-locker. The total rms time jitter could not be computed accurately at 9.78 GHz because the phase noise data plotted above the validity line as suggested by HP.

Kolner et al. [25] have measured the rms timing jitter of a mode-locked and compressed Nd:YAG laser by utilizing an electrooptic sampling technique. They have calculated an upper limit of 11 ps rms jitter for fluctuation frequencies above 10 Hz. Currently the most effective method of decreasing the time fluctuations in the output of a mode-locked laser is phase locking the output of the laser to the reference RF source driving the mode-locker unit. Rodwell et al. [26] have reduced the total time fluctuations of a compressed mode-locked Nd:YAG laser from 2.9 to 0.9 ps rms with this method.

CONCLUSION

We have described a new technique of producing CW microwave signals which are phase coherent to a mode-locked laser source. Extensive measurements have been made to calculate the frequency stability of the CW signal generated. The total rms time jitter of the 10-GHz signal produced in our experiment is approximately 3.53 ps. This number has been computed by the RF spectrum method from the sideband phase noise power between 30 Hz and 5 kHz. Methods of improving both the AM noise fluctuations and the rms timing jitter have been discussed. It is presently assumed that the jitter in the microwave CW signals generated by this technique is mainly due to laser jitter. We are currently working on a technique that will allow us to measure the small amount of additional jitter contributed by the switch. Stabilization of the YAG laser
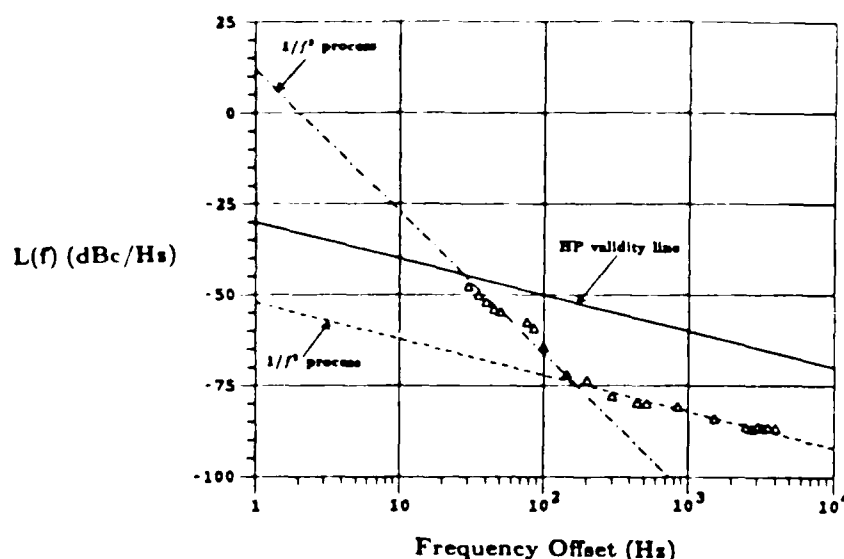
Fig 10 Single sideband phase noise spectral density for the 4-GHz spectral component. Discrete noise data is not included.

using a phase locked loop may be necessary for more comprehensive noise evaluations and certain applications.

Higher output power can be obtained by using photoconductor arrays or higher gain amplifiers. Materials with faster switching speeds than Cr:GaAs may also be used, enabling higher power to be obtained at frequencies in the millimeter-wave band. The width of the photoconductive switch gap may be increased to allow for larger bias voltages and increased power handling capabilities. Although 10-GHz operation has been reported here, a 100-GHz source is feasible, as a femtosecond laser and photoconductors with picosecond carrier lifetime are currently available. The filtering operation becomes more demanding at the higher frequencies. It is therefore desirable to increase the effective repetition rate of the laser. This can be done by using optical or electrical delays. With the optical technique, the repetition rate can be multiplied by 8 or 16 without difficulty [12]. The integrated filter currently being studied will be necessary for higher frequency operation. The ultimate goal is to integrate the laser, photoconductive switch, filter, and amplifier. This will result in a compact, robust, high performance system which can be employed for many high frequency sources, high speed data processing, and antenna applications.

REFERENCES

[1] C. H. Lee, "Introduction A historical overview," in *Picosecond Optoelectronic Devices*, C. H. Lee, Ed. Orlando, FL: Academic, 1984, pp 1-9

[2] C. V. Shank, "The role of ultrashort optical pulses in high-speed electronics," in *Picosecond Electronics and Optoelectronics*, G. A. Mourou, D. M. Bloom and C. H. Lee, Eds. New York: Springer-Verlag, 1985, pp 18-22

[3] C. H. Lee and V. K. Mathur, "Picosecond photoconductivity and its applications," *IEEE J. Quantum Electron.*, vol. QE17, pp 2098-2111, 1981.

[4] G. A. Koepf, "Optical processor for phased array antenna beam formation," *Proc. SPIE*, vol 477, pp 75-81, 1984.

[5] P. G. Sheehan and J. R. Forrest, "The use of optical techniques for beamforming in phased arrays," *Proc. SPIE*, vol. 477, pp 82-89, 1984.

[6] P. D. Stilwell and W. C. Collins, "Fiber optically fed phased arrays," presented at SPIE Tech. Symp. on Optical Technology for Microwave Applications II, 1985.

[7] R. Forrer, H. W. Yen, and R. A. Peters, "Optoelectronic switch arrays for microwave networks," presented at SPIE Tech. Symp on Optical Technology for Microwave Applications II, 1985.

[8] M. G. Li, C. H. Lee, A. Caroglanian, E. A. Greene, C. Y. She, P. Polak-Dingles, and A. Rosen, in *Picosecond Electronics and Optoelectronics*, G. A. Mourou, D. M. Bloom, and C. H. Lee, Eds. New York: Springer-Verlag, 1985, pp. 216-219.

[9] G. Mourou, C. V. Stancampiano, and D. Blumenthal, "Picosecond microwave pulse generation," *Appl. Phys. Lett.*, vol. 38, no. 6, pp 470-472, 1981.

[10] C. S. Chang, M. J. Rhee, C. H. Lee, A. Rosen, and H. Davis, in *Picosecond Electronics and Optoelectronics*, G. A. Mourou, D. M. Bloom, and C. H. Lee, Eds. New York: Springer-Verlag, 1985, pp 220-223.

[11] P. Paulus, W. Brinker, and D. Jager, "Generation of microwave pulses by optoelectronically switched resonators," *IEEE J. Quantum Electron.*, vol. QE-22, no. 1, pp 108-111, Jan 1986.

[12] A. Mooradian, "Use of spatial time-division repetition rate multiplication of mode-locked laser pulses to generate microwave radiation from optoelectronic switches," *Appl. Phys. Lett.*, vol 45, no. 5, pp 494-496, 1984.

[13] L. Goldberg, A. M. Yurek, H. F. Taylor, and J. F. Weller, "35-GHz signal generation with an injection locked laser diode," *Electron. Lett.*, vol 21, no. 18, pp 814-815, 1985

[14] W. P. Robins, *Phase Noise in Signal Sources*. England: Peregrinus, 1982

[15] D. H. Auston, "Picosecond photoconductors Physical properties and applications," in *Picosecond Optoelectronic Devices*, C. H. Lee, ed New York: Academic, 1984.

[16] M. Maeda, "An analysis of gap in microstrip transmission lines," *IEEE Trans. Microwave Theory Tech.*, vol MTT-20, pp 390-396, 1972

[17] A. E. Atia and A. E. Williams, "Narrow-bandpass waveguide filters," *IEEE Trans Microwave Theory Tech.*, vol MTT-20, pp 258-265, Apr 1972

[18] G. L. Matthaei, L. Young, and E. M. T. Jones, *Microwave Filters, Impedance-Matching Networks, and Coupling Structures*. New York: McGraw-Hill, 1964

[19] "Phase noise characterization of microwave oscillators," Product Note 117296, Hewlett Packard, 1985

[20] V F Kroupa, Ed, *Frequency Stability Fundamentals and Measurements* New York IEEE, 1983

[21] J G Ondria, "A microwave system for measurements of AM and FM noise spectra," *IEEE Trans Microwave Theory Tech*, vol MTT-16, pp 767-781, Sept 1968

[22] D Middleton, *Introduction to Statistical Communication Theory* New York McGraw-Hill, 1960

[23] J R Ashley, T A Barley, and G J Rast, Jr, "The measurement of noise in microwave transmitters," *IEEE Trans Microwave Theory Tech*, vol MTT 25, pp 294-318, Apr 1977

[24] M Schwartz, W R Bennett, and S Stein, *Communication Systems and Techniques* New York McGraw-Hill, 1966

[25] B H Kolner and D M Bloom, "Electrooptic sampling in GaAs integrated circuits," *IEEE J Quantum Electron*, vol QE-22, no 1, pp 79-93, 1986

[26] M J Rodwell, K J Weingarten, D M Bloom, T Baer, and B H Kolner, "Reduction of timing fluctuations in a mode-locked Nd YAG laser by electronic feedback," to be published

*

Christopher J. Clark received the B S and M S degrees from the University of Maryland, College Park, in 1983 and 1986, respectively, both in electrical engineering

From 1984 to 1986, he was a Member of the Technical Staff at Watkins-Johnson Company, where he was engaged in the design of RF and microwave receiving systems. In September 1986, he joined TRW Inc., and is currently with the RF Electronics Laboratory, which is responsible for the design and development of microwave, millimeter-wave, and electrooptical subsystems and circuits

Mr Clark is a member of Eta Kappa Nu and Tau Beta Pi

*

Eve A. Chauchard was born in Boulogne-Billancourt, France in 1958 She received the Doctorat degree in physics from the University of Paris, Orsay, France, in 1984

She is currently a Research Associate at the University of Maryland, College Park Her research interests are optical semiconductor switching and applications, and nonlinear optics

*

Kevin J. Webb (S'80-M'84) was born in Stawell, Victoria, Australia, on July 7, 1956 He received the B Eng and M Eng degrees in communication and electronic engineering from the Royal Melbourne Institute of Technology, Australia, in 1978 and 1983, respectively, the M S E E degree from the University of California, Santa Barbara, in 1981, and the Ph D degree in electrical engineering from the University of Illinois, Urbana, in 1984

Since 1984, he has been an Assistant Professor in the Electrical Engineering Department at the University of Maryland, College Park Current research interests include electromagnetics, millimeter-wave and microwave integrated circuits, numerical methods, and related computer software

Dr Webb is a member of Tau Beta Pi, Eta Kappa Nu, and Phi Kappa Phi

Kawthar A. Zaki received the B S degree with honors from Ain Shams University, Cairo, Egypt in 1962, and the M S and Ph D degrees from the University of California, Berkeley, in 1966 and 1969, respectively, all in electrical engineering

From 1962 to 1964, she was a Lecturer in the Department of Electrical Engineering Ain Shams University From 1965 to 1969, she held the position of Research Assistant in the Electronic Research Laboratory, University of California, Berkeley She joined the Electrical Engineering Department, University of Maryland, College Park, MD, in 1970, where she is presently an Associate Professor Her research interests are in the areas of electromagnetics, microwave circuits, optimization, and computer-aided design

Dr Zaki is a member of Tau Beta Pi

*

Chi H. Lee (M'79, SM'86) received the B S degree in electrical engineering from the National Taiwan University, Taipei, Taiwan, and the M S and Ph D degrees in applied physics from Harvard University, Cambridge, MA, in 1959, 1962, and 1968, respectively

He was with the IBM San Jose Research Laboratory from 1967 to 1968 Since 1968 he has been with the University of Maryland, College Park, MD, where he is now a Professor of Electrical Engineering His areas of research include optical-microwave interactions, picosecond optical electronics, nonlinear optical effects, and millimeter-wave devices

Dr Lee is a Fellow of the American Optical Society and a member of the American Physical Society He currently serves as the chairman of the technical committee on lightwave technology of the IEEE Microwave Theory and Techniques Society

*

Penelope Polak-Dingles received the B S in 1969 from the University of Illinois at Urbana After graduation, she worked in the undergraduate chemistry program at the University of Illinois in Chicago until 1974 and then returned to graduate school at that campus, completing the requirements for a Ph D in physical chemistry in 1979

She has held postdoctoral appointments at the Chemistry Department of the University of Maryland and the Laser Physics Branch of the Naval Research Lab Currently, she is a Research Associate at the Laboratory for Physical Sciences, her research interests are in ultrafast phenomena and the kinetics of optoelectronic processes in semiconductor materials

*

Hing-loi A. Hung received the S B degree in electrical engineering from M I T in 1968 and the M S and Ph D degrees from Cornell University, in 1970 and 1974, respectively

While at Cornell, he studied microwave avalanche devices After a short teaching assignment at the University Electrical Engineering Department, he joined COMSAT Laboratories in 1974 He worked on the 28 GHz IMPATT amplifier for the COMSTAR Beacon and participated in the transponder design for INTELSAT V, VI, and STC satellites His research interest has been in the areas of thermoelectrically cooled low-noise techniques, low frequency noise of MESFET's, nonlinearities of solid-state power amplifiers, and automated RF measurements Presently, he is the Manager of the Monolithic Microwave Techniques Department of the Microelectronics Division, pursuing GaAs FET and MMIC developments for satellite and broad-band applications He has been a Professorial Lecturer in Engineering at the George Washington University since 1978

Dr Hung was Vice-Chairman and Chairman of the IEEE Electrical Devices Society, Washington Section, from 1980 to 1982

Ho C. Huang received the B S degree from the National Taiwan University, Taipei, Taiwan, and the M S and Ph D degrees from Cornell University, all in electrical engineering, in 1959, 1965, and 1967, respectively.

He is the Director of the Microelectronics Division at COMSAT Laboratories His responsibilities include research in III-V compound semiconductor materials, microwave device and circuit design, MIC and MMIC fabrication technology, and physical/chemical analysis These areas are vertically integrated to ensure efficiency in the research and development of microwave devices and components Prior to joining COMSAT in December 1983, he was with RCA Laboratories, where he was responsible for the development of MMIC GaAs FET's, silicon millimeter wave IMPATT diodes and p-i-n diodes, and flight-qualified components for space applications

Dr Huang has served as Session Chairman for many IEEE technical conferences He has been awarded seven U S patents and has published numerous papers on GaAs FET's, transferred electron effect devices, IMPATT's, TRAPATT's, electron-beam semiconductors, and acoustic delay lines. In 1983, he was granted the David Sarnoff Award for Outstanding Technical Achievement for a team effort leading to the first commercial microwave solid-state power amplifier in space

MICROCOPY RESOLUTION TEST CHART
NATIONAL BUREAU OF STANDARDS-1963 A

APPENDIX 8

Fe:InGaAs Picosecond Optoelectronic Switches

E. A. Chauchard and Chi H. Lee

Electrical Engineering Department

University of Maryland

College Park, Maryland 20742

V. Diadiuk and G. W. Turner
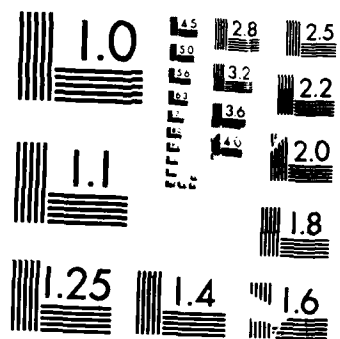
Massachusetts Institute of Technology – Lincoln Laboratory

Lexington, Massachusetts 02173-9973

ABSTRACT

The different phenomena which contribute to the time response of Fe:InGaAs

photoconductive switches were studied with picosecond resolution. Electrode

fabrication process can modify drastically the device performance. Screening of

the applied electric field by the photogenerated carriers was found to be very

large.

Fe:InGaAs Picosecond Optoelectronic Switches

E.A. Chauchard and Chi H. Lee

Electrical Engineering Department

University of Maryland

College Park, Maryland 20742

V. Diadiuk and G.W. Turner

Massachusetts Institute of Technology-Lincoln Laboratory

Lexington, MA 02173-0073

Since the discovery of picosecond photoconductivity , optoelectronic switches made of a variety of materials have been studied[1]. A great number of applications have already been recognized and many new techniques depend on the availability of ultrafast (picosecond) devices. The switches studied in this work are Fe doped InGaAs grown on InP substrates. The semi-insulating character of the Fe:InGaAs epilayer makes it a very attractive material for fabrication of integrated devices such as PIN photodetectors and FET.[2] This material also exhibits a very high mobility (10000 cm^2/Vs) and a light sensitivity extending up to 1.65 μm. The fabrication of a switch by deposition of metallic electrodes allows us to assess the switch characteristics as well as to test the material optical properties for other applications. Studying the speed of a device often reveals several phenomena which can appear as distinct time constants in the observed time waveform. The attribution of each of these different time constants to a particular cause is difficult and often inaccurate. The phenomena contributing to the device speed can be classified into two main categories: carrier recombination times (bulk recombination, surface recombination, Auger recombination, etc.) and effects related to the applied electric field (carrier sweep-out). In addition, two other effects can contribute to the observed time

2

waveform: contact fabrication which plays a role because of the formation of a Schottky barrier at the metal-semiconductor interface and optical intensity which can saturate the switch and lead to slower response times.

This paper presents a study of the effect of the applied electric field on the speed of different devices. We point out the distinction between the carrier recombination time, the carrier sweep-out effect due to the field-induced movement of the carriers and the effects due to Schottky barriers at the electrodes. This last effect was investigated by comparing the responses of switches made of the same material but with different electrode fabrication techniques. Two types of contacts were used: e-beam evaporated gold which was not alloyed, and e-beam evaporated NiGeAu which was alloyed for 20 sec. at 420 °C. Table 1 summarizes the characteristics of the switches. Two different gap geometries-straight gap and interdigitated- were also compared. The light source used in this work was a CW mode-locked dye laser synchronously pumped by Nd:YAG laser, producing 3 ps pulses at a repetition rate of 100 MHz. The observations were made with a Tektronix sampling scope. Fig. 1 shows some examples of waveforms observed for switch #3.

Switch response time was studied for an applied voltage varying between 0.2 V and 10 V. The output waveforms were analysed by digitizing by computer and displaying on a semi-logarithmic scale. It could then be noticed that the waveform decay was of single or double exponential shape. The decay time constants were determined by fitting one or two straight lines to the display. Figure 2 a and b are plots of the observed decay time-constants for switches with gold and alloyed electrodes respectively. When two components of the time constant could be resolved on the oscilloscope trace, the slower component was represented on Figure 2 by a solid line, while the faster component was represented by a dotted line. It can be seen that the slower component of the switches with gold

3

electrodes varied drastically with applied bias voltage. This strong effect was not observed with any of the alloyed electrode switches (for clarity, only three sets of data were plotted although a greater number of devices were studied). We interpret this fact as follows. The non-alloyed electrodes create a potential barrier at the metal-semiconductor interface where the photogenerated carriers can be trapped. Increasing the electric field lowers the barrier and allows the carriers to flow, increasing the speed of the device. For the switches with alloyed electrodes, the barrier is much lower so the device is faster and there is little effect of the applied field. For one of the alloyed electrodes switches (#5), a slight dependence of the slower decay time constant on the bias voltage is visible. This may be due to an unsuccessful step in the alloying process for this particular device. The results of Fig. 2 show that in order to obtain a fast device even at low bias voltage, alloyed electrodes are required.

The faster component of the decay probably reflects the actual carrier recombination time of the material, although this cannot be assured for the following reason. When a voltage is applied across the gap, the electric field sweeps out the carriers, increasing the speed of the device[3,4]. When determined by sweep-out, the device response time is expected to vary linearly with the applied field. However, the results of Fig. 2 show that the decay time of these switches does not decrease further than 150 ps. The gap capacitance is too small to explain this value. This effect could be due to the fact that the carrier mobility saturates at high fields, so a saturated value of velocity should be expected. However, if one makes the simple assumptions that the device response time corresponds to the time needed by the carriers to cross the gap and that the electric field in the gap equals the bias voltage divided by the gap length, the reported mobility data[5] yield a device response time much faster than the observed one. This would indicate that the electric field in the gap is much smaller than the value expected from the applied voltage. For instance, with

4

10 V bias in the 3 µm switch (#3), the device response time leads to a carrier velocity of 12 x 10⁵ cm/s, corresponding to an effective field 270 times smaller than the field expected from the applied voltage. Thus, screening of the field by the photogenerated carriers[6] seems to be very important at this relatively high injection level. The existence of trap states in the material, which could be responsible of a long component in the device response, has been tested by illuminating the device with an HeNe laser beam in addition to the picosecond dye laser pulses. No change was observed in the time response of the devices, implying that significant density of traps is not present.

The switch response time was also a function of the intensity of the illumination. As the light intensity was increased, the device response became slower and the output pulse exhibited a flat top. This saturation phenomenan has been explained in ref. 7. At low light level, the devices were in general slightly faster than shown on Fig. 2. This shows that the effective electric field in the gap was slightly higher since less photogenerated carriers provide less screening of the applied field. Little differences were observed in the time responses of the straight gap switches and the interdigitated switches.

The study of a number Fe:InGaAs switches with different design parameters (gap size and geometry, electrode fabrication process) by varying the applied electric field and light intensity led to the observation of several distinct phenomena which contribute to the time response of the device. In particular, electrode fabrication process can modify drastically the switch performance. Gold electrodes deposited on the surface were found to increase the response time, particularly at low bias voltages. Alloyed NiGeAu electrodes are more suitable for obtaining faster devices. The screening of the field by the carriers can be estimated by the method presented here and was found to decrease the effective field in the switch by a very large factor.

5

ACKNOWLEDGEMENTS

REFERENCES

1. <u>Picosecond Optoelectronic Devices</u>. Chi H. Lee (Ed.), Academic Press, (1984).

2. V. Diadiuk and S.H. Groves, Appl. Phys. Lett. <u>46</u>, 2, pp. 157-158.

3. G.G. Shahidi, E.P. Ippen and J. Melngailis, in <u>Picosecond Electronics and Optoelectronics</u>. G.A. Mourou, D.M. Bloom and Chi H. Lee (Eds.), Springer-Verlag, (1985).

4. K. Kaede, Y. Arakawa, P. Derry, J. Paslaski and A. Yariv, Appl. Phys. Lett. <u>38</u>, 16, pp. 1096-1097, (1986).

5. J.R. Hayes, A.R. Adams and P.D. Greene, in <u>GaInAsP Alloy Semiconductors</u>, T.P. Pearsall (Ed.), John Wiley & Sons, Ltd., pp. 189, (1982).

6. D.H. Auston, in <u>Picosecond Optoelectronic Devices</u>. Chi H. Lee (Ed.), Academic Press, (1984).

7. Kenneth K. Li, John R. Whinnery and Andrew Dienes, <u>Proc. SPIE 322</u>, pp. 124-130, (1982).

FIGURE CAPTIONS

Fig. 1.   Waveform observed for switch #3 biased at different voltages.

a: 10 V, b: 7 V, c: 4 V, d: 2V, e: 1 V, f: 0.2 V.

Fig. 2.   Decay time constants versus bias voltage for Fe:InGaAs switches with:
(a) gold contacts, (b) NiGeAu alloyed contacts.   Points joint with
solid or dotted lines represent, respectively, the slowest and fastest
component of the decay.

(a):   □ : switch #1, Δ : switch #2, 0 : switch #3.

(b):   □ : switch #4, Δ : switch #5, 0 : switch #6.

Table 1. Description of devices

Switch #	Material	Gap Size (μm)	Gap Geometry	Electrode Type
1	Fe:InGaAs	20	straight	Au
2	Fe:InGaAs	10	straight	Au
3	Fe:InGaAs	3	straight	Au
4	Fe:InGaAs	10	straight	NiGeAu
5	Fe:InGaAs	6	fingers	NiGeAu
6	Fe:InGaAs	5	straight	NiGeAu
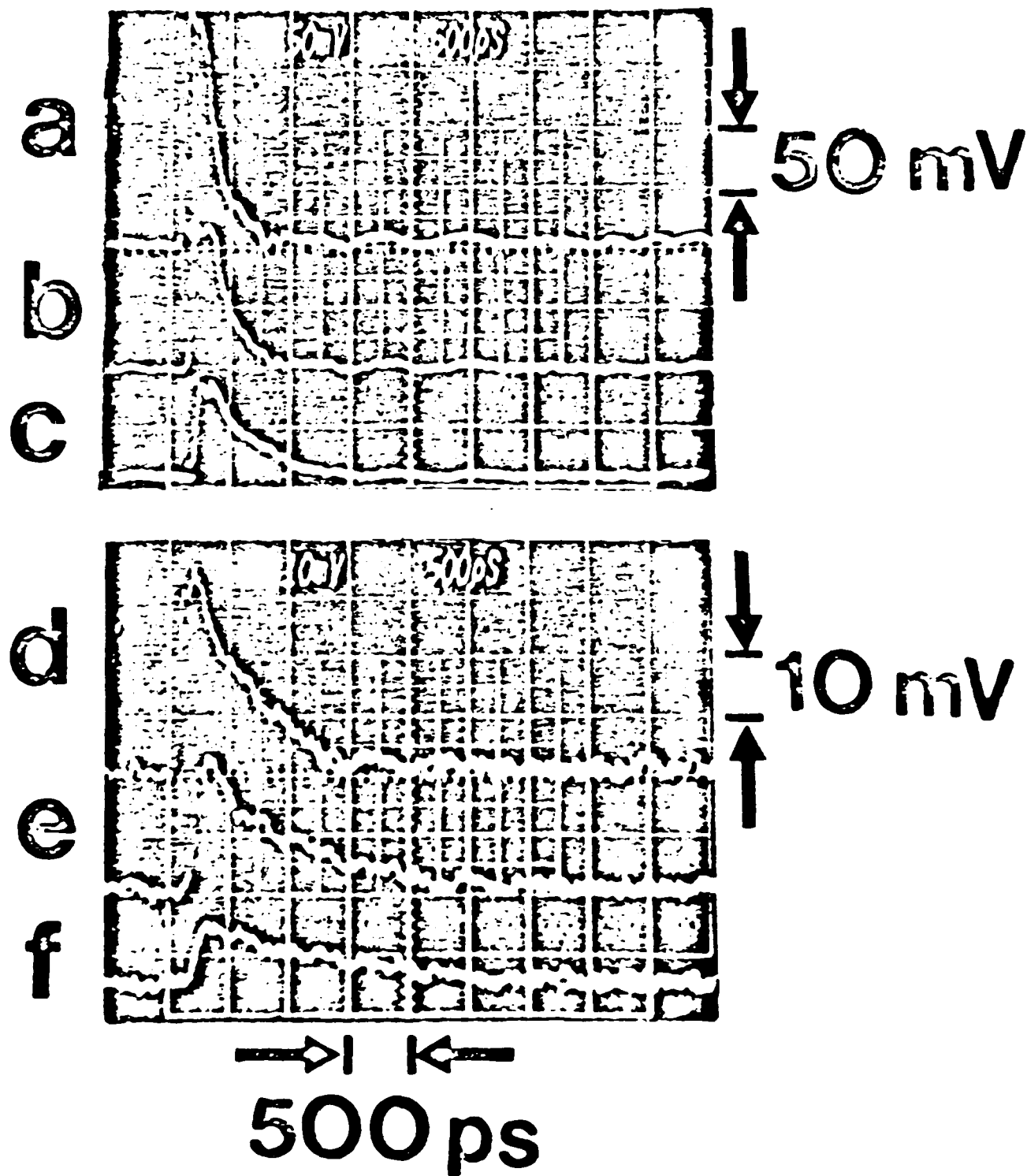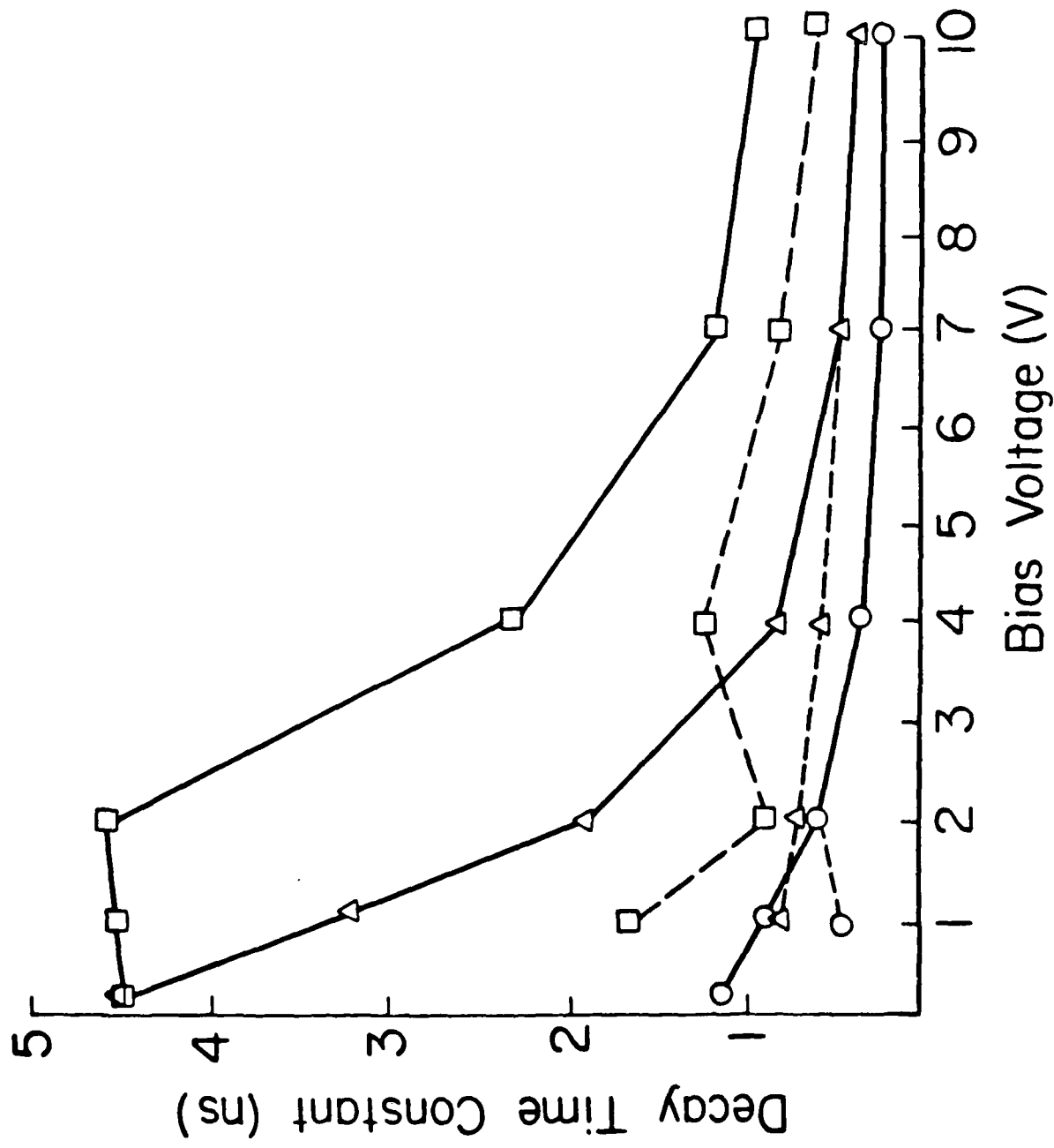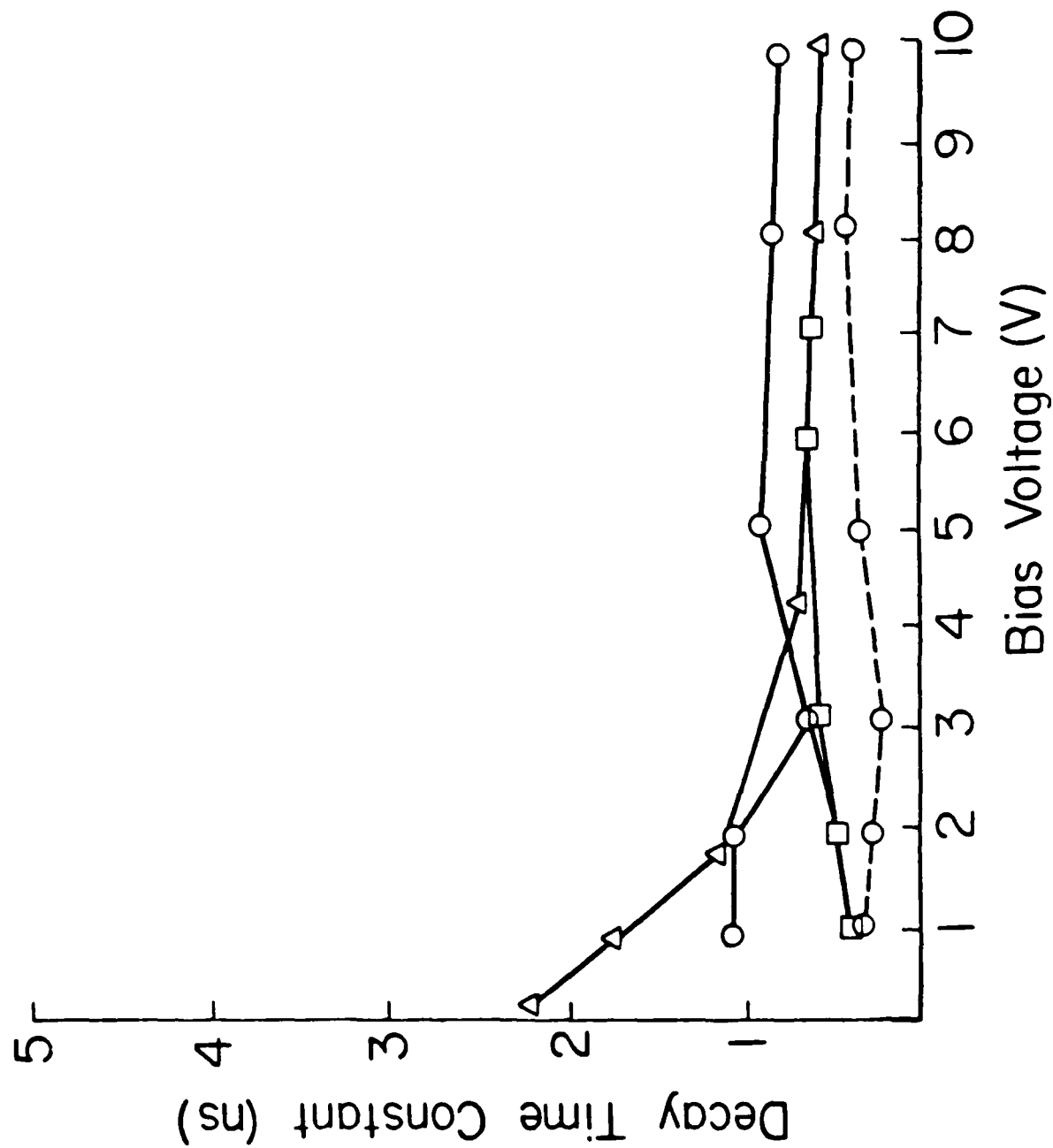
a

b

c

50 mV

d

e

f

10 mV

500 ps

FIG 1

FIG 2 a

Fig 2 b

Bias Voltage (V)

Decay Time Constant (ns)

Q-28

Generation of Kilowatt/Kilovolt Broadband
Micowave Bursts with a Single Picosecond
Photoconductive Switch

Hrayr A. Sayadian, M.G. Li, and Chi H. Lee
Department of Electrical Engineering
University of Maryland
College Park, Maryland 20742
301-454-6832, 6852

ABSTRACT

A single picosecond GaAs photoconductive
switch is used to pulse excite a microwave reso-
nant cavity, generating various microwave wave-
forms. The generation of over 7 kW, with peak to
peak voltage over 1.2 kV, of broadband microwave
bursts is demonstrated.

INTRODUCTION

In the last few years, there has been a great
interest in the generation of coherent microwave
pulses using ultrashort optical pulses (1-4).
These techniques use optical pulses to trigger
photoconductive switches, thus allowing picosecond
synchronization of the generated microwave pulses.
However, drawbacks of the exported methods are 1)
the low voltage and power outputs (1,2), and ii)
the large number of photoconductive switches to be
triggered (3,4). Earlier we demonstrated conver-
sion of DC energy to single frequency RF energy,
albeit at low voltage and power, using a single
switch and a coaxial resonant cavity (5). In this
paper we show the versatility of this technique.
Among the different waveforms generated, we have
produced over 7 kilowatts of broadband, single
cycle, microwave pulses of peak to peak voltage of
over 1.2 kV with over 50% energy conversion
efficiency.

EXPERIMENTAL SYSTEM

Schematic of the experimental arragement is
shown in Fig. 1. Coaxial slotted lines were used
as quarter wave resonant cavities. Specifically,
a 25 cm long HP slotted line cavity, resonating at
300 MHz, and 9 cm long homemade cavity, resonating
at 1 GHz, were used. These resonanant frequencies
are for high Q operation of the cavities. An
active-passive mode-locked Nd:YAG laser is used to
generate ~ 1 mJ of 1.06 um radiation, of 100 pico-
second pulsewidth, with repetition rate of 1 Hz,
to trigger the GaAs switch. The performance of
GaAs switches were tested, under DC bias of up to
4 kV, with 1.06 um pulses for several thousand
consecutive shots without any observable degrada-
tion in performance.

Activating the GaAs switch by the optical pulse
generates a rectangular electric pulse of at most
half the DC charged voltage. The electric pulse
excites the resonant cavity through coupling ele-
ment A_1. Coupling element A_2 allows the extrac-
tion of the generated microwaves from the excited
cavity, to be observed by a 1 ns risetime storage
scope. Two important and useful parameters that
control the waveform, and hence the frequency
distribution, of the generated microwaves are i)
strength of the coupling provided by A_1 and
A_2, and ii) length of the coaxial line C_2
connecting the GaAs switch to A_1.

In Fig. 2 we show a typical electric pulse
(~1.25 kV in magnitude and 2 ns in duration) used
to excite the cavities. The width of the pulse is
determined by the length of the charged coaxial
line C_1. The rise time is determined by that of
the optical trigger pulse.

RESULTS

In Fig. 3 we show the effects of coupling (A_1
and A_2) and the length of C_2. The generated wave-
form using the 300 MHz cavity, is due to "strong"
couplings at A_1 and A_2. A strong coupling is
obtained by directly connecting the center wire of
an input/output coaxial line to the center wire of
the coaxial resonant cavity. The generated wave-
form can be explained as follows; some of the
incident voltage pulse on A_1 excites the cavity,
while some is reflected with a change in sign
(since the effective impedance of A_1 is less than
the characteristic impedance of C_2). The
reflected pulse suffers an open circuit reflection
at the switch (thus keeping the same sign) and is
incident on A_1 repeating the above process. The
ratio of the magnitudes of successive pulses is
constant, and depends on the coupling strength.
The time between successive pulse excitations is
given by twice the travel time in the length of C_2
(20 ns round trip time in this case). Note that
the first cycle has a peak to beak voltage of
~1.2 kV, and that the peak power is over 7 kWatts.
The energy conversion efficiency, including all the
reflected pulses, is over 50%.

In Fig. 4 we show the affect of changing the
couplings and the length of C_2. Intermediate
connection for A_2) is used to excite the 1 GHz
cavity, together with a 5 ns (double travel time)
long C_2. Note the relatively larger voltages of
the reflected pulses due to the weak coupling at
A_1.

In Fig. 5 we show the waveform generated by
the 1 GHz cavity with stong couplings and with a
≈ 0.5 ns (double travel time) long C_2. Note that
the width of the generated single cycle pulse is
larger than the period of the resonance frequency.
There are several reasons for this, the most
important of which are; 1) the nonzero (0.5 ns)
time shift between the (successive) added
microwave pulses, 11) the loading of the cavity,
and 111) the finite risetime of the scope. The
waveform generated by the 300 MHz cavity with
strong couplings and with a 0.5 ns long C_2 is
shown in Fig. 6.

Finally, a relatively high Q factor is
obtained for the cavity when the coupling is weak
(loop antennae for A_1 and A_2). In this case the
triggered electrical pulse excites the cavity at
its resonant frequency through A_1, while A_2
allowes the extraction of the generated narrow
band microwaves. In Fig. 7 we show the observed
waveform for the 1 GHz cavity when C_2 is ≈ 5 ns
long. Note that over 100 mW of 1 GHz RF is
generated, with an estimated bandwidth of less
than 10 MHz. The modulated envelope is due to
beating between the cavity resonant frequency and
the length of C_2. The nonzero dip of the envelope
is caused by the relatively long lifetime of the
switch (few ns) when excited by a 1.06μm trigger
pulse. This "smears" the effective length of C_2
and hence affects the beating with the cavity
resonance frequency. Indeed we have observed a
zero dip in the envelope when a short lifetime
switch is used (e.g. Cr doped GaAs or 0.53μm
trigger pulse.). Unfortunately the use of 0.53μm
to trigger high voltage pulses is not practical
(6).

The use of spectrum analysers, to examine the
frequency distribution of the high voltage high
power microwave bursts (Figs. 3-6), is not
feasable due to the short duration of the bursts
and their low repitition rate. However, more than
qualitative information can be obtained by theore-
tical methods (7). The calculated frequency
distribution of the power in single cycle (with
positive and negative parts, as in Figs. 5,6)
electrical pulses, with a period of τ, shows that
the main lobe extends up to 2/τ. The significance
of this is evident once one realizes that, similar
calculations for one sided electrical pulses (as
in Fig. 2) show that the main lobe extends up to
1/τ only. The frequency distribution for the
waveforms in Figs. 3,4 is given by that for a
single pulse divided by $\left[1+a^2-2a\ \cos(2\pi ft_s)\right]$
where a is negative of the ratio of magnitudes of
successive pulses (this depends on the coupling
strength) and t_s is the separation between sec-
cessive pulses (round trip length of C_2).

CONCLUSION

We have shown the versatility of microwave
generation, through the excitation of a resonant
cavity with a single high voltage pulse, triggered
by a photoconductive switch. The high power
microwave bursts generated may find important
applications in high resolution phased array radar
operation.

REFERENCES

1. G. Mourou, C.V. Stemcampiano, A. Antonetti
and A. Orszag, Appl. Phys. Lett. 38, 470
(1981),also C. Mourou, C.V. Stemcampiano, and D.
Blumenthal, ibid, 39, 295 (1981).

2. R.Heidemann, T. Pfiffer and D. Jager,
Elect. Lett., 19, 316 (1983).

3. A. Mooradian, Appl. Pjys. Lett. 45, 49-
(1984).

4. C.S. Chang, M.C. Jeng, M.J. Rhee, Chi H.
Lee, A. Rosen, and H. Davis, IEEE MTT-S
International Microwave Symposium Digest (1984),
pp. 540-541.

5. M.G. Li, C.H. Lee, A. Caroglanian, E.A.
Greene, C.Y. She, P. Polak-Dingles, and A. Rosen,
in Picosecond Electronics and Opto-electronics,
Proceedings Topical Meeting, Nevada, 1985, Eds.
Mourou, Bloom, and Lee, pp. 216-219.

6. H.A. Sayadian, S.T. Feng, J. Goldhar, and
C.H. Lee, in Picosecond of Electronics and
Optoelectronics, Proceedings of second Topical
Meeting, Nevada, 1987, Eds. Lee, Leonerger,
Capasso, and Morkoc.

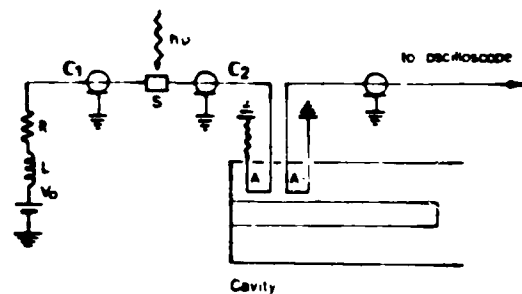7. H.A. Sayadian, M.G. Li, And C.H. Lee (to be
published).

Fig. 1 Schematic of the experimental arrangement. S is GaAs photoconduc-
        tive switch, A_1 and A_2 are input/output cavity coupling elements.
        C_1 and C_2 are coaxial cables. The resistance (R) and inductance (L)
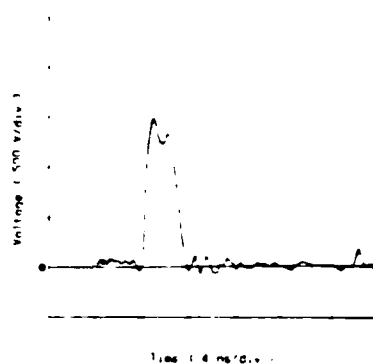   provide isolation between the DC power supply and the charged line
        C_1.

Fig. 2 Typical electric pulse, generated by optically triggering the photo-
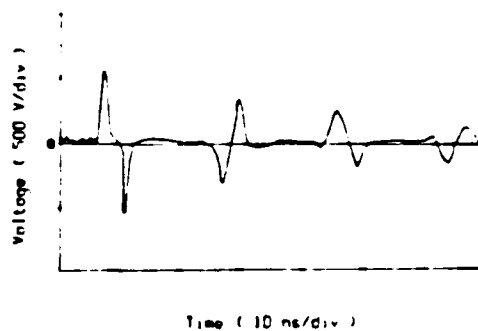   conductive switch, used to excite the cavities.

Fig. 3 Microwave pulse generated using the 300 MHz cavity with strongly
        coupled A_1 and A_2 (see text for definition of coupling strength) and
        20 ns (round trip) long C_2.

651

Fig. 4 Microwave pulse generated using the 1 GHz
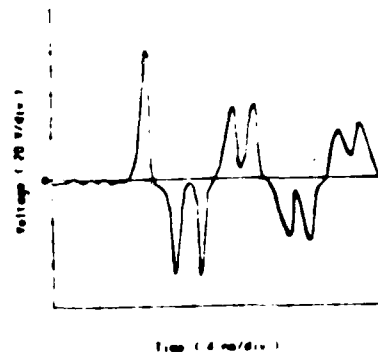cavity with intermediate coupling and 5 ns
long C_2.

Fig.5 Microwave pulse generated using the 1 GHz
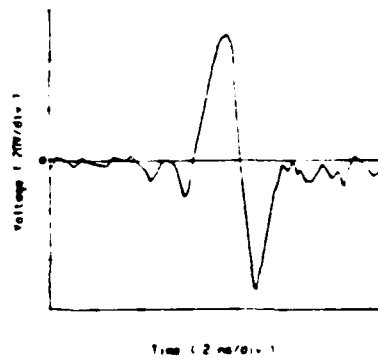cavity with strong coupling and ~0.5 ns
long C_2.

Fig. 6 Microwave pulse generated using the 300
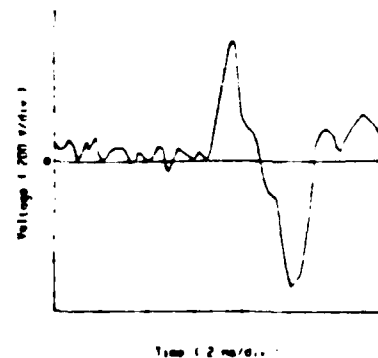MHz cavity with strong coupling and ~0.5 ns
long C_2.

Fig. 7 Microwave generation using the 1 GHz
cavity with weak coupling and ~5 ns long
C_2. (2V / vert. div. , 10 ns / hor. div.)

652

AIR FORCE OFFICE OF SCIENTIFIC RESEARCH (AFSC)
NOTICE OF TRANSMITTAL TO DTIC
This technical report has been reviewed and is
approved for public release IAW AFR 190-12.
Distribution is unlimited.
MATTHEW J. KERPER
Chief, Technical Information Division

END

Feb.

1988

DTIC